A NEW SECONDARY FLOW SOURCE MODEL FOR PREDICTING TURBULENT FLOW IN NON-CIRCULAR DUCTS

M.MEYYAPPAN

A thesis
presented to the University of Manitoba
in partial fulfillment of the
requirements for the degree of
Master of Science
in
Mechanical Engineering

Winnipeg,Manitoba
1991

ISBN 0-315-77836-9

A NEW SECONDARY FLOW SOURCE MODEL FOR PREDICTING TURBULENT FLOW IN NON-CIRCULAR DUCTS

BY

MANICKAM MEYYAPPAN

A thesis submitted to the Faculty of Graduate Studies of the University of Manitoba in partial fulfillment of the requirements of the degree of

MASTER OF SCIENCE

Abstract

A new model is proposed to predict turbulent flows in non-circular ducts. In such flows, the presence of sharp corners results in secondary flows. The present model is aimed at the simulation of the cause of these secondary flows in terms of the profile of wall shear stress. The developed model is tested using a finite difference numerical scheme based on primitive variables. The model predicts turbulent flows in a square duct and several rectangular ducts of various aspect ratios, all to within good accuracy.

Acknowledgement

I am really glad to use this opportunity to express my sincere thanks to Dr.A.C.Trupp for his invaluable guidance, constant encouragement and enterprising supervision.

I am grateful to the financial support provided through research and teaching assistantships by the Department of Mechanical Engineering during the course of this work. I thank the faculty and staff of the Department of Mechanical Engineering who helped me in many ways during my studies.

Finally I thank my family and my friends for supporting me emotionally and morally.

Contents

List of Figures

Nomenclature

a	Coefficients in the discretized equation
a_1,a_2,..	Constants used in the model developed
A_e, A_w, A_n, A_s	Areas of the control volume in the east,west, north and south directions respectively
A,B	Constants used in the wall function
b,b_i, b_s	Source terms in the discretized equations
c	Coefficients used in the pressure correction equation
C_1, C_2, C_6, C_1'	Turbulence model constants
D_h	Hydraulic diameter of the cross section used
f_1, f_2, f_3	Algebraic functions employed in the model formulation
$F_1, F_2,$ F_3, F_4	Expressions derived for the Reynold's stress terms in the octant B
$F_{1-A}, F_{2-A},$ F_{3-A}, F_{4-A}	Expressions derived for the Reynold's stress terms in the octant A
J	Total flux across the grid boundary
k	Turbulent kinetic energy $(u^2 + v^2 + w^2)^{1/2}/2$
k^+	Normalised turbulent kinetic energy(k/u_τ^2)
l_y	Distance of the surface of zero shear stress from the wall, parallel to the y coordinate
l_z	Distance of the surface of zero shear stress from the wall, parallel to the z coordinate
p	Fluctuating component of the pressure
P	Mean value of the pressure
Pe	Peclet number
P_t	Production of turbulent energy
Re	Reynolds number of flow

S_ϕ	Source of the partial differential equation for any given variable ϕ
S_1	Length of the wider side of the duct
S_2	Length of the smaller side of the duct
t	Time variable in the Navier-Stokes equation
u	Fluctuating component of velocity in the x-direction
$\overline{u_i u_j}$	Reynolds stress term in tensor notation
u_τ	Frictional velocity(τ_w/ρ)
U	Mean value of the velocity in the x-direction
U_B or U_b	Bulk velocity of flow
U_c	Mean velocity of flow at the centre of the duct
v,w	Fluctuating components of velocity in y and z directions respectively
V,W	Mean components of velocity in y and z directions respectively
x,y,z	Coordinate axes with x in the axis of flow
ϵ	Rate of turbulent dissipation
σ_k,σ_ϵ	Constants used in the transport equations of k and ϵ
ω	Vorticity of turbulent flow
μ	Absolute viscosity of the fluid
Γ	Diffusion coefficient used in the general conservation equation
ϕ	General variable
ν	Kinematic viscosity of the fluid
ρ	Density of the fluid
τ	Turbulent shear stress
τ_w	Wall shear stress
Δ_y, Δ_z	Grid width of the control volume in y and z directions respectively
Ψ	Stream function
ξ	Convergence criterion

Subscripts

i,j	Tensor notations
e,w,n,s	Represents eastern,western,northern and southern grid faces
E,W,N,S	Represents eastern,western,northern and southern neighbouring nodal faces
t	Denotes terms due to turbulence
x,y,z	Derivatives in the respective direction

Superscripts

-	Overbar indicates the mean value
'	Represents derivatives as well as instantaneous values
g	Guessed values
c	Corrected values

Chapter 1

Introduction

The field of Computational Fluid Mechanics revolves around the prediction of important fluid parameters for the given flow conditions. For flows in ducts of non-circular cross section, the nature of the flow is predominantly turbulent as can be seen in many engineering applications such as heat exchangers, ventilation and air conditioning systems, nuclear reactors, turbo machineries, open channels, canals and rivers. In the above-mentioned examples, designers are primarily interested in the overall pressure drop and heat transfer characteristics of the flows, as influenced by the parameters characterising the passage geometry. In many instances, details of the turbulence at the interface between adjoining tube-array passages is influential in determining the level of turbulent mixing which occurs between them. In all these types of flows, a secondary flow develops and superimposes itself upon the primary axial flow. This transverse flow has a pronounced effect on peripheral wall shear stress distributions and local heating rates in the corner region. The corner region is inherently a low wall shear stress region which is prone to flow separation and stall formation under adverse pressure gradients and for constant heat flux conditions at the wall, local temperature 'hot spots' can develop in the corner regions because convective heat transfer rates are inhibited in this region by virtue of the low wall shear stress condition. Hence it is important to predict accurately the turbulent characteristics and the internal flow structures to arrive at better and safer designs of the critical engineering applications.

The secondary flow results from imbalances in the Reynolds stresses over the cross sectional plane. Launder and Ying[1] were the first to develop a vorticity source model based on the gradients of the axial velocity. This model was subsequently modified and has been applied by numerous researchers including Nakayama et al.[2] to predict turbulent flow structure in non-circular ducts. Other secondary flow source models have been proposed and applied successfully; e.g. Seale[3] where linkage is made to the turbulent kinetic energy field. The idea of including the wall shear stress in the prediction of Reynolds stresses was originally discussed by Perkins[4].

In this thesis, three different new models(model I,model I A and model II) have been developed based on the wall shear stress to predict the secondary flows in non-circular ducts. These models were tested numerically in square and rectangular ducts of different aspect ratios, using two different numerical schemes, Vorticity Stream function method(VSM) and Primitive Variable method(PVM). Results of model II match fairly closely with the experimental data of Hoagland [5] and Leutheusser[6]. Out of these two numerical schemes, the Primitive Variable scheme using SIMPLE algorithm, performed better, and produced relatively accurate predictions.

Chapter 2

Literature Review

2.1 General

Fully developed flows in ducts of non-circular cross-section are quite common in engineering practice. There are examples involving laminar flow, like the lubricant supply passages for bearings, the extrusion ducts of polymer processing plants and the heat exchangers of the food processing industries. But compact heat exchangers often operate in turbulent flow, as do the regenerators employed for waste heat recovery in the glass making and other industries. Turbulent flows are also encountered in another important area of application involving regular arrays of parallel tubes, as found in boilers, condensers and nuclear reactors. In such flows, a transverse movement of fluid had been observed since the turn of the century. There is clear experimental evidence[7, 8] that cross stream motions always exist in turbulent flows in non-circular ducts, without the presence of any external driving mechanism. These cross stream motions are called the secondary motions. If the ducts are curved the centrifugal forces act at right angles to the main flow direction resulting in a secondary motion which is pressure induced and is said to be of Prandtl's first kind. This first kind also exists in curved circular ducts and for laminar flow. If the ducts are straight, the secondary motion is caused by turbulence and is called secondary motion of Prandtl's second kind.

The tendency of the flow, is for the core fluid to flow in towards narrow regions

such as corners of the triangular duct, then parallel to the walls and then finally back into the core in the wider regions. The magnitude of the secondary velocities is quite small, scarcely exceeding $1 - 2\%$ of the mean axial velocity. Still, they exert a significant influence on all aspects of the flow behaviour including the level and distribution of the wall shear [7] and heat transfer. Detailed investigations of the source of these motions reveal them to be due to a particular feature of the turbulent stress field, in which the cross stream stresses are connected to the axial strain rates.

2.2 Experimental Investigation

Nikuradse[9] was the first to observe the difference between the turbulent flow in circular pipes and square ducts. For the latter, lines of constant velocity are displaced towards the corner and away from the mid-points of the walls compared to those of the laminar flow. Prandtl[10] postulated that this behaviour is the result of the turbulent fluctuations along the isovels giving rise to a net flow normal to the isovel where a variation in the curvature occurs. In straight non- circular ducts or channels he envisaged a system of longitudinal spirals in the flow, conveying momentum into the corner regions. This required that the velocity fluctuations tangential to the isovels exceed those perpenticular to it, so that a centrifugal acceleration is induced in the regions of isovel curvature, propelling fluid radially outwards. Secondary currents, he concluded, must therefore be established in the direction of the isovel distortions and be supported by the anisotropy of the turbulent direct stresses. All subsequent secondary flow measurements in fully developed straight non- circular duct flows have substantiated this qualitative argument. Attempts at at a more rigorous explanation, by Einstein and Li [11] and Hinze[12], have shown that secondary currents of the second kind (as defined by Prandtl), are produced by the non uniformities in anisotropic wall turbulence.

However Townsend[13] appears to have been the first to formally locate the cause

of the secondary flow. He showed that for a boundary layer with a free edge, secondary flows would result from non-zero values of the term$(\overline{v^2} - \overline{u^2})$, where $\overline{v^2}$ and $\overline{u^2}$ are the transverse normal Reynolds stresses. He further stated that the inequality of the turbulent normal stresses that gives rise to the secondary cross flow in boundary layers of finite width is the cause of the secondary flows known to occur in channels of other than circular cross section.

Hoagland[5] measured complete mean flow velocity for fully developed turbulent flow in a square channel. He was the first to measure the secondary velocities by hot wire anemometer. Maximum secondary velocities were found to be about 1% to1.5% of the centre line axial velocity and occurred near the walls in the corner region. His rectangular duct had the aspect ratio of 1 : 1,2 : 1 and 3 : 1. The results indicate typical secondary flow velocities of the order of 1% of the maximum value of the mean axial velocity. They also showed that these secondary flows have a pronounced effect on isotach distribution. Hoagland also determined the local wall shear stress distribution in a square channel by direct measurements with a Preston tube. Subsequently Leutheusser[6] presented local wall shear stress distributions in a rectangular channel.

Later Brundrett and Baines[7] used the hot wire technique with a better accuracy, in a square duct to measure the secondary velocities as well as other turbulent quantities. They focussed on the secondary flows and the regions where the axial vorticity is created and destroyed. They concluded that the production of axial vorticity is associated with the relative proximity of an element of the fluid to the walls of the duct. In rectangular ducts the production of the vorticity is associated with the region near the corner bisector, and the corner bisector separates a pair of independent secondary circulations that have opposing sense of rotation. Brundrett and Baines [7] showed that the gradients in the plane of the cross section give rise to a source of stream vorticity. Their experimental works included hot wire measurements of all

six components of the Reynolds stress. From the data obtained they concluded that in rectangular sectioned ducts, it is predominantly the normal stress gradients which generate the velocities in the plane of the cross-section.

Gessner and Jones[14] used hot wire to examine the Reynolds number effect on secondary flow. They stated that the secondary flow decreases slightly with increasing Reynolds number when non-dimensionalised by the centre line axial velocity. They found that the greatest skewness of wall shear stress occurs in the immediate vicinity of the corners. For a rectangular channel, the skewness on the longer wall is greater than the skewness on the shorter wall, at points equidistant from the corner. They concluded that the differences between the Reynolds stresses and static pressure gradients in the plane of cross section cause secondary flow. In 1970, Perkins[4] in his detailed analysis of turbulent structure mechanism in a non-circular duct, concluded that the mean streamwise vorticity in turbulent flow arises both from mean flow skewing and from the inhomogenity of anisotropic wall turbulence.

Launder and Ying[15] used hot wire to measure secondary flow in rough and smooth square ducts. They found that the secondary velocities when normalized with average friction velocity are independent of duct roughness. They also contended that when normalized with friction velocity, secondary velocities are reasonably independent of Reynolds number. Square duct has been studied analytically by Launder and Singham[16], Wilson et al.[17], Launder and Ying[1] and Gerard[18]. Rectangular ducts have been additionally examined by Tracy[19] and Hinze[20].

Apart from experimental works in square and and rectangular ducts, measurements have also been reported from many ducts with other cross-sectional shapes such as in triangular array rod bundles by Kjellstrom[21] and Trupp and Azad[22], in a two square interconnected sub-channels by Lyall[23], in a circular duct containing two small rods by Kacker[24], in a duct containing rods in a square array by Rowe[25], in a duct simulating an interior subchannel of a triangular array by Carajilescov and

Todreas[26], in a single row of rods between two flat walls by Rehme[27], in an equilateral triangular duct by Aly et al.[8], in a simulated rod bundle by Seale[28], in closely spaced rod arrays by Hooper and Rehme[29] and in a trapezoidal duct by Khalifa[30].

Other than the fully developed turbulent flow, several experimental results have been reported on the developing flows in square and rectangular ducts. Experimenters include Ahmed and Brundrett[31], Po[32], Melling and Whitelaw[33] and Lund[34]. Many of these experiments were conducted in square ducts.

2.3 Numerical Prediction

2.3.1 Turbulence Modelling

The turbulence model is defined by Rodi[35] as a set of equations(algebraic or differential) which determine the turbulent transport terms in the mean flow equations and thus close the system of equations. It is based on the hypotheses about turbulent processes and require empirical input in the form of constants or functions. It does not simulate the details of the turbulent motion but only the effect of turbulence on the mean flow behaviour.

2.3.2 Time Averaged Models

The Navier-Stokes equations are accepted widely as the proper tool to describe the turbulent motion of fluid. But due to non-linearity of this equation and also due to the small scale of turbulence, the Navier-Stokes equation cannot be solved for any turbulent flow of practical interest, despite recent advances in computers. A ratio of the length scale of energy containing eddies to that of energy dissipating one is roughly proportional to $Re^{\frac{3}{4}}$. So, the number of grid points required in numerical calculation may be of the order of $Re^{\frac{9}{4}}$. This number of spatial grids and resultant time steps for Reynolds number of practical range are far beyond the scope and speed

of present day computers. But since, as such there is no practical need to know the details of the turbulent fluctuations, the governing equations are averaged over a time scale which is long enough compared with that of the turbulent motion. The resulting equations describe the time averaged distribution of the quantities such as velocity, temperature and shear stress. The models with this method are defined by Hirata et al.[36] as 'Time averaged models'.

2.3.3 Classification Of Time Averaged Models

Depending upon the nature of equations employed and the extent of approximations made, 'time averaged models' can be classified as:

1. Integral Method Model(I.M.): Models using ordinary differential equations obtained by integrating the 'pde'(partial differential equations) across a boundary layer.
2. Mixing Length Model(M.L.M.): Models to solve only the pde s for the mean flow velocity with the eddy viscosity given by the mixing length hypothesis; no pde s for the turbulent quantities.
3. Kinetic energy and Length scale Model(K.L.M.): Models involving one pde for the turbulent energy; the length scale is either assumed(one equation model) or calculated with another pde(two equation model).
4. Algebraic Stress Model(A.S.M.): Models consisting of two equation model and additional algebraic equations for Reynolds stress components.
5. Full Reynolds Stress Model(F.R.S.M.): Models using pde s for all significant shear and normal Reynolds stress components and usually one pde for the length scale.

There is another approach developed rather recently, in which the Navier-Stokes equations are first solved for energy containing eddies; then the obained velocity and

temperature profiles are averaged over a time interval to give the mean distributions of the velocity and temperature. This type of modelling is called 'Structural model'. The following model falls under this category.

- Large eddy simulation(L.E.S.): Computation of the three dimensional, time dependent, large eddy structure by use of a model for the small scale of turbulence.

2.3.4 Numerical Predictions History

Although the existence of the turbulence driven secondary motions and their origins in the Reynolds stress field have been known for sometime, the absence of the detailed models for the stresses led early workers such as Deissler and Taylor[37], Rapier and Redman[38], Bender et al.[39] and others to ignore the explicit appearance of secondary velocities in the equations of motion, thereby reducing them to single axial momentum equation and obtain the Reynolds stresses from empirical relations based on the Newtonian equation. Typically, turbulent viscosity was obtained from a mixing length or a similar formulation. But the predictions based on this concept were substantially in error, exhibiting for example, deviation from measured axial velocity distributions up to 100%. Attempts to improve matters led to 'second generation'methods such as those of Ibragimov et al. [40], Meyder[41] and Ramm and Johannasen[42]. These works tried to introduce secondary flow effects indirectly, either via measured data such as wall shear stress distributions or by causing the eddy viscosity to be anisotropic. Such methods gave improved agreement with the experiment, but leaned heavily on empirical input.

The same thing can be said of the third generation procedures of the kind devised by Nijsing[43] and Gerrard[18], in which the terms in the equations of motion containing the secondary velocities were retained, but the velocities themselves were specified empirically from the measurement rather than calculated. However the

agreement was better and was attributed to the realistic representation of secondary flow effects. It led to the the realisation that the turbulence model should be capable of calculating the secondary flows via their fundamental origins in the turbulent stress field. This, in turn, led to the next, contemporary generation of methods, in which the ad hoc stress-strain relation was abandoned and replaced by direct calculation of the stresses from their fundamental transport equations. These are called stress transport models.

This class of turbulence model has its origins in the basic equations of motion, which can be manipulated and time averaged to yield equations for the Reynolds stresses themselves. But this process does not by itself give closure, for it generates new unknowns. These unknown terms need to be defined in terms of calculable quantities; an exercise which has resulted in multiplicity of closures. Some of the important stress closures applied for fully developed duct flows are derived by Hanjelic and Launder[44], Launder and Ying[1], Naot et al.[45] and Reece[46]. These involved the development of a transport equation for the scalar turbulence kinetic energy, k. This modelling process has however given rise to one further unknown, namely the turbulence dissipation,ϵ. This can be found by linking ϵ to the local length scale or by another general approach of developing an additional transport equation for ϵ, obtained by operating on the Navier-Stokes equations. Naot et al.[45] and Reece[46] applied these stress transport equations to the present class of flow and both invoked only those simplifications allowed by the fully developed flow conditions. However the complexity and the costs engendered by such calculations provide a powerful incentive to exploit whatever further simplifications the applications allow.

Launder and Ying[1] were the first to recognise the smallness of the secondary velocities in fully developed duct flow. This provides the justification for ignoring the terms representing transport by convection and diffusion, in the stress transport equations. This is an important simplification, for it results in the removal of

all differential coefficients of the Reynolds stresses and the equations become algebraic in latter. Now the model deals with the algebraic terms and hence gets the name,'Algebraic stress model'. They used length scale to define ϵ.

This model known as LY model was later employed by Aly et al.[8] to predict turbulent flow in an equilateral triangular duct with success, after adjusting the empirical coefficients in the equations. But Carajilescov and Todreas[47] were not satisfied with this model when they applied it to axial flow in a rod bundle assembly. Later Tatchell [48] used LY model to predict flow in a square duct, replacing algebraic calculation of ϵ with its own differential transport equation.

The original LY model needs the solution of a set of implicit simultaneous algebraic equations for the individual stress components. Gessner and Emery[49] worked further algebraically on the model to reach an explicit set for the stresses which is more computationally convenient and physically informative.

Seale[3] noted that the use of algebraic stress models was unsatisfactory and gave inconsistent results in the sub-channels within a rod bundle. Based on the observation of Alshamani[50, 51] on the relationship between the fluctuating velocities(when normalised by the local friction velocity) in a number of pipe and two-dimensional channel flows, Seale formulated a vorticity source model in terms of the normalised turbulent kinetic energy. He found good agreement with the experimental results when he applied his model in square,triangular ducts and sub-channels within a rod bundle. However the model could not produce proper axial velocity distribution when applied to the duct used by Rehme[27]. Seale's model was later used by Khalifa[30] for a trapezoidal duct and the agreement with the experimental data is reasonable.

Later, Zhou[52] developed two vorticity source models,one based on the distribution of k and the other based on that of ϵ. These two models predicted results that are comparable to other vorticity source models.

2.3.5 Numerical Scheme

In order to test the models developed, the final expressions of the transport equations need to be solved numerically. It is to be noted that the numerical schemes should deal with the problem of defining the unknown pressure field. Keeping this in view, two different solution techniques, namely, Vorticity-Stream function method and the Primitive variable method(hereafter referred to as VSM and PVM respectively) were proposed and developed over a period of time by many researchers.

The VSM has an advantage in that there is no pressure term appearing in the transport equations. The elimination of pressure from the two momentum equations, by cross differentiation leads to a vorticity transport equation. This when combined with the definition of stream function for steady two-dimensional situations forms the basis of the VSM. This method is made easily accessible through the book by Gosman et al. [53]. This finite volume based procedure uses central differencing for all terms except those describing convection which are upwind-differenced. It employs point iteration with under- relaxation to solve the discretized equations in a sequential manner, i.e., alternating in turn between the vorticity,stream function and other variables. This scheme was used by various researchers. Notable examples are the works done in the square duct by Launder and Ying [1], in the triangular duct by Aly et al.[8], in the rod array bundles by Seale[28] and in trapezoidal ducts by Khalifa[30].

Many of the stress-models based calculations have been performed with variants of the finite volume solution procedure for the three- dimensional developing duct flows of Patankar and Spalding [54] or the recirculating flow version thereof described by Caretto et al.[55]. Since these procedures work with the primitive variables(i.e. components of velocity and pressure), this method is known as the Primitive Variables Method(PVM). This method uses staggered velocity and pressure grids and hybrid central- upwind differencing. It approaches the solution in a stepwise or iterative

fashion by obtaining estimates of the velocity field from the momentum equations and then inferring corrections to it and the pressure field via a continuity based pressure correction calculation. Tatchell[48] employed the developing-flow variant and improved the LY model in his calculations of square duct flow.Reece[46] used the same variant to solve the full differential stress equations of the Launder et al.[56] model for a similar application. This scheme demands under-relaxation and some other preconditions to produce predictions. Other notable examples of this scheme are the works done by Gosman and Rapley[57] in arbitrary cross sections and Nakayama et al.[2] in various non-circular ducts.

Chapter 3

Modelling

This section deals with the equations that govern the flow under specified conditions. The equations involved are the basic momentum equations for the axial and cross sectional velocities and the transport equations for the turbulent kinetic energy and the turbulent dissipation rate. For the PVM, the continuity equation has been reformulated as a pressure correction equation using the method of Patankar and Spalding [54]. A cartesian coordinate system, as shown in the Fig. 3.1, was adopted. The grid structure is described later in this thesis.

3.1 Governing Equations

Using tensor notation,the continuity equation which describes the mass conservation, is given as

$$\frac{\partial U_i'}{\partial x_i} = 0 \tag{3.1}$$

The axial momentum equation which describes momentum conservation of the flow in the axial flow direction is given by the Navier-Stokes equation as

$$\frac{\partial U_i'}{\partial t} + U_j' \frac{\partial U_i'}{\partial x_j} = -\frac{1}{\rho}\frac{\partial P'}{\partial x_i} + \nu \frac{\partial^2 U_j'}{\partial x_j \partial x_j} \tag{3.2}$$

where p' is the instantaneous static pressure.

For an incompressible flow under a steady state condition, equation(3.2) becomes

$$U_j' \frac{\partial U_i'}{\partial x_j} = -\frac{1}{\rho}\frac{\partial P'}{\partial x_i} + \nu \frac{\partial^2 U_j'}{\partial x_j \partial x_j} \tag{3.3}$$

Splitting the instantaneous values into mean values and fluctuating quantities and then taking the time average, results in:

$$U_i' = U_i + u_i \tag{3.4}$$

$$P' = P + p \tag{3.5}$$

Continuity equation:

$$\frac{\partial U_i}{\partial x_i} = 0 \tag{3.6}$$

and the axial momentum equation:

$$U_j \frac{\partial U_i}{\partial x_j} = -\frac{1}{\rho}\frac{\partial p}{\partial x_i} + \frac{\partial}{\partial x_j}(\nu \frac{\partial U_i}{\partial x_j} - \overline{u_i u_j}) \tag{3.7}$$

These equations are exact since no assumptions have been introduced in deriving them, but they no longer form a closed set. Due to non-linearity of the equations(3.2), and (3.3) the averaging process has introduced unknown correlations,$\overline{u_i u_j}$, between the fluctuating velocities. Physically these correlations multiplied by the density ρ, represent the transport of momentum due to the fluctuating motion. The term $-\rho\overline{u_i u_j}$ is the transport of x_i momentum in the direction of x_j or vice versa; it acts as a stress on the fluid and is therefore called a turbulent or Reynolds stress.

In equation(3.7) for fully developed flow conditions, changes in the axial flow direction are negligible. So $(\partial/\partial x) = 0$ for all the variables except for the pressure. Also $\nu = \mu/\rho$.

Expanding equation(3.7)in the x-direction,

$$U\frac{\partial U}{\partial x} + V\frac{\partial U}{\partial y} + W\frac{\partial U}{\partial z} = -\frac{1}{\rho}\frac{\partial p}{\partial x} + \frac{\partial}{\partial y}(\nu\frac{\partial U}{\partial y} - \overline{uv}) + \frac{\partial}{\partial z}(\nu\frac{\partial U}{\partial z} - \overline{uw}) \tag{3.8}$$

Applying the fully developed flow conditions and simplifying,

$$\rho V\frac{\partial U}{\partial y} + \rho W\frac{\partial U}{\partial z} = -\frac{\partial p}{\partial x} + \rho\frac{\partial}{\partial y}(\nu\frac{\partial U}{\partial y} - \overline{uv}) + \rho\frac{\partial}{\partial z}(\nu\frac{\partial U}{\partial z} - \overline{uw}) \tag{3.9}$$

From earlier literatures, $\overline{uv} = -\nu_t(\partial U/\partial y)$ and $\overline{uw} = -\nu_t(\partial U/\partial z)$.

Substituting and further simplifying,

$$\rho V\frac{\partial U}{\partial y} + \rho W\frac{\partial U}{\partial z} - \rho\frac{\partial}{\partial y}((\nu+\nu_t)\frac{\partial U}{\partial y}) - \rho\frac{\partial}{\partial z}((\nu+\nu_t)\frac{\partial U}{\partial z}) = -\frac{\partial p}{\partial x} \tag{3.10}$$

$$\frac{\partial}{\partial y}(\rho VU - (\mu+\mu_t)\frac{\partial U}{\partial y}) + \frac{\partial}{\partial z}(\rho WU - (\mu+\mu_t)\frac{\partial U}{\partial z}) = -\frac{\partial p}{\partial x} \tag{3.11}$$

Expanding the equation(3.7) in the y direction,

$$\rho V\frac{\partial V}{\partial y} + \rho W\frac{\partial V}{\partial z} = -\frac{\partial p}{\partial y} + \rho\frac{\partial}{\partial y}(\nu\frac{\partial V}{\partial y} - \overline{v^2}) + \rho\frac{\partial}{\partial z}(\nu\frac{\partial V}{\partial z} - \overline{vw}) \tag{3.12}$$

$$\frac{\partial}{\partial y}(\rho VV - (\mu)\frac{\partial V}{\partial y}) + \frac{\partial}{\partial z}(\rho WV - (\mu)\frac{\partial V}{\partial z}) = -\frac{\partial p}{\partial y} + \frac{\partial \tau_{yy}}{\partial y} + \frac{\partial \tau_{yz}}{\partial z} \tag{3.13}$$

Similarly for the z direction,

$$\rho V\frac{\partial W}{\partial y} + \rho W\frac{\partial W}{\partial z} = -\frac{\partial p}{\partial z} + \rho\frac{\partial}{\partial y}(\nu\frac{\partial W}{\partial y} - \overline{vw}) + \rho\frac{\partial}{\partial z}(\nu\frac{\partial W}{\partial z} - \overline{w^2}) \tag{3.14}$$

$$\frac{\partial}{\partial y}(\rho VW - (\mu)\frac{\partial W}{\partial y}) + \frac{\partial}{\partial z}(\rho WW - (\mu)\frac{\partial W}{\partial z}) = -\frac{\partial p}{\partial z} + \frac{\partial \tau_{yz}}{\partial y} + \frac{\partial \tau_{zz}}{\partial z} \tag{3.15}$$

The expressions for the transport equations for k and ϵ are taken in the same form as used by most of the previous researchers such as Zhou[52].

For the turbulent kinetic energy k:

$$\frac{\partial}{\partial y}(\rho Vk - \frac{(\mu+\mu_t)}{\sigma_k}\frac{\partial k}{\partial y}) + \frac{\partial}{\partial z}(\rho Wk - \frac{(\mu+\mu_t)}{\sigma_k}\frac{\partial k}{\partial z}) = \rho(P_t - \epsilon) \tag{3.16}$$

For the turbulent eddy dissipation rate, ϵ:

$$\frac{\partial}{\partial y}(\rho V\epsilon - \frac{(\mu+\mu_t)}{\sigma_\epsilon}\frac{\partial \epsilon}{\partial y}) + \frac{\partial}{\partial z}(\rho W\epsilon - \frac{(\mu+\mu_t)}{\sigma_\epsilon}\frac{\partial \epsilon}{\partial z}) = \frac{\rho\epsilon}{k}(C_1P_t - C_2\epsilon) \tag{3.17}$$

where P_t, the rate of production of turbulent kinetic energy, is given by,

$$P_t = \frac{\mu_t}{\rho}(\frac{\partial^2 U}{\partial y^2} + \frac{\partial^2 U}{\partial z^2}) \tag{3.18}$$

and μ_t, the turbulent viscosity,is given by,

$$\mu_t = C_D\rho\frac{k^2}{\epsilon} \tag{3.19}$$

The continuity equation becomes

$$\frac{\partial V}{\partial y} + \frac{\partial W}{\partial z} = 0 \tag{3.20}$$

3.2 Vorticity Stream Function Method(VSM)

As stated earlier, the Vorticity Source method involves the solution of the transport equations for the vorticity and stream functions apart from the momentum equation for axial velocity and the transport equations for turbulent kinetic energy and rate of turbulent dissipation. Derivation of vorticity and stream function equations are only mentioned briefly here. A detailed derivation is available in Zhou[52].

3.2.1 Axial Vorticity and Stream Function Equation

The stream function Ψ,and the axial vorticity ω, can be defined as

$$\rho V = \frac{\partial \Psi}{\partial z} \tag{3.21}$$

$$\rho W = -\frac{\partial \Psi}{\partial y} \tag{3.22}$$

$$\omega = \frac{\partial W}{\partial y} - \frac{\partial V}{\partial z} \tag{3.23}$$

The problem of defining the pressure terms in the equations(3.13) and (3.15) is avoided by cross differentiating these two equations and eliminating the pressure gradient terms in them. Simplification is made using the expressions for axial vorticity(3.23) and the continuity equation(3.20) to arrive at the transport equation for the axial vorticity.

$$V\frac{\partial \omega}{\partial y} + W\frac{\partial \omega}{\partial z} = \frac{\partial^2}{\partial y \partial z}(\overline{v^2} - \overline{w^2}) - (\frac{\partial^2}{\partial y^2}\overline{vw} - \frac{\partial^2}{\partial z^2}\overline{vw}) + \nu(\frac{\partial^2 \omega}{\partial y^2} + \frac{\partial^2 \omega}{\partial z^2}) \tag{3.24}$$

This equation as well as the expression for ω include only velocities and gradients in the y and z directions and exists only if the secondary velocities exist and vice versa.

Here the terms on the left hand side represent the convection of the streamwise vorticity by the mean motion. The first and the second terms on the right hand side express the influence of the turbulent stresses on the production or destruction of

streamwise vorticity. The last term on the right hand side represent the damping by viscosity.

Expression for the stream function equation is reached by the substitution of equation(3.21) and (3.22) into(3.23)

$$\frac{\partial}{\partial y}(\frac{\partial \Psi}{\partial y}) + \frac{\partial}{\partial z}(\frac{\partial \Psi}{\partial z}) + \rho\omega = 0 \tag{3.25}$$

The equations(3.11), (3.24), (3.16) and (3.17) are redefined in terms of the stream function, to get the following set of equations.

$$\frac{\partial}{\partial y}(U\frac{\partial \Psi}{\partial z}) - \frac{\partial}{\partial z}(U\frac{\partial \Psi}{\partial y}) - [\frac{\partial}{\partial y}(\mu+\mu_t)\frac{\partial U}{\partial y}] - [\frac{\partial}{\partial z}(\mu+\mu_t)\frac{\partial U}{\partial z}] + \frac{\partial P}{\partial x} = 0 \tag{3.26}$$

$$\begin{aligned}\frac{\partial}{\partial y}(\omega\frac{\partial \Psi}{\partial z}) - \frac{\partial}{\partial z}(\omega\frac{\partial \Psi}{\partial y}) - \frac{\partial}{\partial y}[\frac{\partial}{\partial y}(\mu\omega)] \;&-\; \frac{\partial}{\partial z}[\frac{\partial}{\partial z}(\mu\omega)] - \rho\frac{\partial^2}{\partial y \partial z}(\overline{v^2} - \overline{w^2}) \\ &+\; \rho(\frac{\partial^2}{\partial y^2}\overline{vw} - \frac{\partial^2}{\partial z^2}\overline{vw}) = 0\end{aligned} \tag{3.27}$$

$$\begin{aligned}\frac{\partial}{\partial y}(k\frac{\partial \Psi}{\partial z}) - \frac{\partial}{\partial z}(k\frac{\partial \Psi}{\partial y}) \;&-\; [\frac{\partial}{\partial y}(\mu+\frac{\mu_t}{\sigma_k})\frac{\partial k}{\partial y}] - [\frac{\partial}{\partial z}(\mu+\frac{\mu_t}{\sigma_k})\frac{\partial k}{\partial z}] \\ &-\; \mu_t[(\frac{\partial U}{\partial y})^2 + (\frac{\partial U}{\partial z})^2] + \rho\epsilon = 0\end{aligned} \tag{3.28}$$

$$\begin{aligned}\frac{\partial}{\partial y}(\epsilon\frac{\partial \Psi}{\partial z}) - \frac{\partial}{\partial z}(\epsilon\frac{\partial \Psi}{\partial y}) \;&-\; [\frac{\partial}{\partial y}(\mu+\frac{\mu_t}{\sigma_\epsilon})\frac{\partial \epsilon}{\partial y}] - [\frac{\partial}{\partial z}(\mu+\frac{\mu_t}{\sigma_\epsilon})\frac{\partial \epsilon}{\partial z}] \\ &-\; C_1\frac{\mu_t\epsilon}{k}[(\frac{\partial U}{\partial y})^2 + (\frac{\partial U}{\partial z})^2] + C_2\rho\frac{\epsilon^2}{k} = 0\end{aligned} \tag{3.29}$$

3.2.2 Boundary Conditions

The domain and coordinates are shown in the Fig. 3.2.

Stream Function(Ψ)

Since no net mass is transferred across all the boundaries,the stream function is constant along these boundaries. The constant was conveniently set to be zero.

Axial Vorticity(ω)

The vorticity boundary condition at the symmetric lines is derived from its definition. At $y = 0$ in Fig 3.2 from the symmetric property, it can be written that $(\partial W/\partial y) = 0$. Along $y = 0$, V is zero which results in $(\partial V/\partial z) = 0$.

Since

$$\omega = \frac{\partial W}{\partial y} - \frac{\partial V}{\partial z}$$

we get

$$\omega = 0 \quad at\ y = 0$$

It works the same way when $z = 0$. Therefore, the vorticity is zero at the two symmetry line boundaries. Near the wall, it was assumed(as per standard practice[53]) that the vorticity varies linearly with the normal distance from the wall.

U,k and ϵ

Along the symmetry lines due to the symmetric conditions, gradients of U, k and ϵ become zero. From Fig. 3.1 mathematically,

For $y = 0$, and $0 \leq z \leq S_2$

$$\frac{\partial U}{\partial y} = \frac{\partial k}{\partial y} = \frac{\partial \epsilon}{\partial y} = 0 \tag{3.30}$$

For $z = 0$,and $0 \leq y \leq S_1$

$$\frac{\partial U}{\partial z} = \frac{\partial k}{\partial z} = \frac{\partial \epsilon}{\partial z} = 0 \tag{3.31}$$

It is assumed that the universal law of the wall holds good in secondary flow problems and can be used to represent the velocity profile in the region close to the wall region. Therefore, a boundary condition was imposed on the nodes next to the wall. However care was taken in designing the grid such that these first string of nodes are located beyond the viscous sublayer for the Reynolds number involved. The boundary

condition is expressed as

$$U = u_\tau[A\ ln(\frac{\rho u_\tau |z_n - z_p|}{\mu}) + B] \tag{3.32}$$

where u_τ represents the local friction velocity and A and B are constants. The suffix p denotes the wall node whereas n stands for the node next to the wall, in the direction normal to the wall.

3.3 Primitive Variable Method(PVM)

In this method, the equations(3.11), (3.13), (3.15), (3.16) and (3.17) along with the continuity equation(3.20) can be put in a general form,for any general variable ϕ. For a cartesian coordinate system(x,y,z), with x in the axial flow direction, the general conservation equation may be written as:

$$(\rho V\phi - \Gamma\phi_y)_y + (\rho W\phi - \Gamma\phi_z)_z = S_\phi \tag{3.33}$$

where U, V and W are the mean velocity components in x, y and z directions respectively. For each governing equation, the general dependent variable ϕ, the diffusion coefficient Γ and the source term S_ϕ are as follows:

Continuity equation:

$$\phi = 1; \Gamma = 0; S_\phi = 0 \tag{3.34}$$

U momentum equation:

$$\phi = U; \Gamma = \mu + \mu_t; S_\phi = -p_x \tag{3.35}$$

V momentum equation:

$$\phi = V; \Gamma = \mu; S_\phi = (\tau_{yy} - p)_y + (\tau_{yz})_z \tag{3.36}$$

W momentum equation:

$$\phi = W; \Gamma = \mu; S_\phi = (\tau_{zz} - p)_z + (\tau_{yz})_y \tag{3.37}$$

k,turbulent kinetic energy equation:

$$\phi = k; \Gamma = \mu + \mu_t/\sigma_k; S_\phi = \rho(Pt - \epsilon) \tag{3.38}$$

ϵ,dissipation rate equation:

$$\phi = \epsilon; \Gamma = \mu + \mu_t/\sigma_\epsilon; S_\phi = \rho\epsilon(C_1 Pt - C_2\epsilon)/k \tag{3.39}$$

3.3.1 Boundary conditions

U,k and ϵ

Due to symmetric conditions, gradients of U, k and ϵ are zero, along the symmetry lines.

For $y = 0$, and $0 \leq z \leq S_2$(as in section 3.2.2):

$$\frac{\partial U}{\partial y} = \frac{\partial k}{\partial y} = \frac{\partial \epsilon}{\partial y} = 0 \tag{3.40}$$

For $z = 0$, and $0 \leq y \leq S_1$

$$\frac{\partial U}{\partial z} = \frac{\partial k}{\partial z} = \frac{\partial \epsilon}{\partial z} = 0 \tag{3.41}$$

For near wall flow, the universal law of the wall is applied. This is done again through equation(3.32).

V and W

Since there is no net mass flow across the boundary,

$$V = 0 \quad at \quad y = 0 \tag{3.42}$$

and

$$W = 0 \quad at \quad z = 0 \tag{3.43}$$

From symmetric conditions,

$$\frac{\partial W}{\partial y} = 0 \quad at \quad y = 0 \tag{3.44}$$

$$\frac{\partial V}{\partial z} = 0 \quad at \quad z = 0 \tag{3.45}$$

All along the walls, due to no-slip condition, both V and W are taken to be zero.

3.4 Model Development

3.4.1 Model I Vorticity Stream-Function Method Model

In the vorticity stream-function method, the terms containing the gradients of the Reynolds Stress in equation(3.27)are yet to be defined.

Launder and Ying[1] proposed the first vorticity stream-function model in terms of the cross planar gradients of the axial velocity. This is given by the expression:

$$(\overline{v^2} - \overline{w^2}) = C_1' \mu_t \frac{k}{\rho\epsilon}[(\frac{\partial U}{\partial z})^2 - (\frac{\partial U}{\partial y})^2] \tag{3.46}$$

The constant C_1' has a wide range of values among different investigators. Launder and Ying[1] used a value of 0.0185; Gessner and Po[60] used 0.101; Aly, Trupp and Gerrard[8] used 0.011.

Many researchers accept the fact that one of the effects of the secondary flow is to distribute wall shear stress uniformly along the walls of the duct. In other words, the secondary flow is the cause and one of its effects is the uniform distribution of the wall shear stress. Now using the guessed distribution of the effect,wall shear stress,an attempt is made to induce the cause, secondary flow. This way of linking secondary flow generation to the wall shear stress distribution,was introduced by Perkins [4], in the case of boundary layer shear flow using vorticity source term method. He suggested the idea of linking the cross planar gradients of the difference between the normal Reynolds stresses to the variation in the profile of wall shear stresses. From the experimental data he assumed a linear variation of the term $((\overline{v^2} - \overline{w^2})/u_\tau^2)$ with the normal distance from wall, expressed as a fraction of the distance of no-shear stress plane from the wall.

Using this idea a model was developed for the vorticity source term method and applied in square and rectangular ducts.

Consider the point P(y,z) in octant B of Fig. 3.2, where l is the distance of the plane of zero shear stress from the wall at the point P. For any point P(y,z), the parameter l depends only on y. Assuming the wall boundaries to lie along the coordinate axes y and z, one can write that the wall shear stress and hence the frictional velocity along the y-coordinate, depend on y, the distance from the corner. As per the assumptions made earlier,

$$\frac{(\overline{v^2} - \overline{w^2})}{u_\tau^2} = f(\frac{z}{l}) \tag{3.47}$$

where

$$f(\frac{z}{l}) = -(1 - \frac{z}{l}) \tag{3.48}$$

from Perkins[4].

Denoting the production of vorticity by the term P_3 and writing $f(z/l)$ as f,

$$\begin{aligned} P_3 &= \frac{\partial^2}{\partial y \partial z}(\overline{v}^2 - \overline{w}^2) \\ &= \frac{\partial^2}{\partial y \partial z}(u_\tau^2 f) \end{aligned} \tag{3.49}$$

For octant B,

$$u_\tau = f(y)$$

and

$$l = f(y)$$

Differentiating equation(3.49) partially with respect to y at first, and then to z,

$$\begin{aligned} P_3 &= \frac{\partial}{\partial z}(2u_\tau f \frac{\partial u_\tau}{\partial y} - u_\tau^2 \frac{z}{l^2}\frac{\partial l}{\partial y}) \\ &= 2u_\tau \frac{\partial u_\tau}{\partial y}\frac{1}{l} - u_\tau^2 \frac{1}{l^2}\frac{\partial l}{\partial y} \end{aligned} \tag{3.50}$$

Substituting for u_τ,

$$P_3 = \frac{1}{\rho}(\frac{2\tau_w^{1/2}}{l}\frac{\partial}{\partial y}(\tau_w^{1/2}) - \frac{\tau_w}{l^2}\frac{\partial l}{\partial y}) \tag{3.51}$$

or

$$P_3 = C_5(\frac{2\tau_w^{1/2}}{l}\frac{\partial}{\partial y}(\tau_w^{1/2}) - \frac{\tau_w}{l^2}\frac{\partial l}{\partial y}) \tag{3.52}$$

where C_5 is a constant introduced for tuning the model to suit the experimental data. This constant C_5 also takes care of the factor $1/\rho$.

Thus in the simplified form it is given as

$$\frac{\partial^2(\overline{v^2} - \overline{w^2})}{\partial y \partial z} = C_5(2\frac{\tau_w^{1/2}}{l}\frac{\partial \tau_w^{1/2}}{\partial y} - \frac{\tau_w}{l^2}\frac{\partial l}{\partial z}) \tag{3.53}$$

This expression is used to calculate the values of the source terms for all the nodes that are immediately adjacent to the boundary nodes.The rest of the solution methodology was the same as developed by Zhou[52].

As shown in Section 5, the model performed well for the square duct. However its predictions for rectangular ducts of various aspect ratios fell short of the experimental data particularly in the location and the shape of the secondary flow cells and in the wall shear stress distributions. Overall, although predictions were comparable to the other models including LY, Seale, Naot, k and ϵ using the VSM, efforts were continued to try and improve performance.

3.4.2 Model I A

One possible way of improving the performance of the model I is to extend the definition of the vorticity source term for grid points other than those lying immediately adjacent to the walls.

It is quite reasonable to assume that the Reynolds stresses, (both normal and shear) depend to a large extent on the distance from the solid surface. Non dimensionalizing the Reynolds stresses with u_τ, the local wall shear velocity, it should be possible for regions not too close to the wall, to write

$$(\bar{v}^2/u_\tau^2) = f_1(z/l)$$

$$(\bar{v}w/u_\tau^2) = f_2(z/l)$$

and

$$(\bar{w}^2/u_\tau^2) = f_3(z/l)$$

where z is the perpendicular distance from the solid surface.

With this view the experimental data of Brundrett and Baines[7] for a turbulent flow in a square duct, were analysed. The parameters $(\overline{v^2}/u_\tau^2)$,$(\overline{w^2}/u_\tau^2)$ and $(\overline{vw}/u_\tau^2)$ were each plotted as functions of (z/l). The resulting curves are shown in Figs. 3.4-3.6. As can be seen from the figures, these functions fall into smooth curves and thereby validate the assumptions made earlier. This enables us to define expressions for these functions in terms of (z/l) as:

$$f_1(z/l) = a_1(z/l)^3 + a_2(z/l)^2 + a_3(z/l) + a_4 \tag{3.54}$$

$$f_2(z/l) = a_5(z/l)^2 + a_6(z/l) + a_7 \tag{3.55}$$

$$f_3(z/l) = a_8(z/l)^3 + a_9(z/l)^2 + a_{10}(z/l) + a_{11} \tag{3.56}$$

From equations(3.54) to(3.56), it can be stated

$$\begin{aligned}(\overline{v^2} - \overline{w^2}) &= (f_1(z/l) - f_3(z/l))u_\tau^2 \\ &= f_4(z/l)u_\tau^2 \end{aligned} \tag{3.57}$$

where

$$\begin{aligned} f_4(z/l) &= f_1(z/l) - f_3(z/l) \\ &= a_{12}(z/l)^3 + a_{13}(z/l)^2 + a_{14}(z/l) + a_{15} \end{aligned} \tag{3.58}$$

Now the vorticity source term can be defined as

$$\frac{\partial^2(\overline{v^2} - \overline{w^2})}{\partial y \partial z} = \frac{\partial^2}{\partial y \partial z}(f_4(z/l)u_\tau^2) \tag{3.59}$$

For octant B, u_τ and l are functions of only y. Carrying out partial differentiation and simplifying further

$$\frac{\partial^2(\overline{v^2} - \overline{w^2})}{\partial y \partial z} = 2\tau_w^{1/2}\frac{\partial \tau_w^{1/2}}{\partial y}\frac{1}{\rho l}[3a_{12}(z/l)^2 - 2a_{13}(z/l) + a_{14}]$$

$$-\tau_w \frac{1}{\rho l^2}\frac{\partial l}{\partial y}[3a_{12}(z/l)^2 - 2a_{13}(z/l) + a_{14}]$$
$$-\tau_w \frac{z}{\rho l^3}\frac{\partial l}{\partial y}[6a_{12}(z/l) - 2a_{13}] \quad (3.60)$$

The expression thus obtained is discretized and numerically tried using the solution methodology of Zhou[52]. For octant A the vorticity source term definition is modified accordingly. Attempt was made to predict turbulent flow in a square a duct at Re=75,000. But the model produced an output that was not symmetrical. Additional work on this model may bring out predictions that are comparable to that of model I. But this attempt encouraged the idea of extending the definition of Reynolds stress terms over the whole flow domain.

3.4.3 Model II Primitive Variable Method Model

In an effort to improve performance, it was decided to test a different numerical scheme, viz, the Primitive variable method, as proposed by Patankar and Spalding[54]. It can be seen that in the corresponding equations(3.36)and(3.37), the terms containing the cross-sectional plane gradients of the Reynolds stress need to be defined. Gessner and Emery[49]modified the original LY model to give simplified expressions for these terms as given by:

$$\tau_{yy} = \rho[\frac{C'C_D k^3}{\epsilon^2}U_y^2 - C'_k k] \quad (3.61)$$

$$\tau_{zz} = \rho[\frac{C'C_D k^3}{\epsilon^2}U_z^2 - C'_k k] \quad (3.62)$$

$$\tau_{yz} = \rho[\frac{C'C_D k^3}{\epsilon^2}U_y U_z] \quad (3.63)$$

where C', C'_k are the empirical constants. Values for these constants are given later at the end of this chapter. Alternatively, as denoted next, these Reynolds stress terms can be defined in terms of the wall shear stress.

Next expressions are formulated for the gradients of the Reynolds stress terms.

Let

$$F_1 = \frac{\partial}{\partial y}(\tau_{yy}) \tag{3.64}$$

$$F_2 = \frac{\partial}{\partial z}(\tau_{yz}) \tag{3.65}$$

$$F_3 = \frac{\partial}{\partial z}(\tau_{zz}) \tag{3.66}$$

and

$$F_4 = \frac{\partial}{\partial y}(\tau_{yz}) \tag{3.67}$$

Defining these terms for the octant B shown in the Fig. 3.2, for which l and u_τ are functions of only y:

$$\begin{aligned} F_1 &= \frac{\partial}{\partial y}(-\rho\overline{v^2}) \\ &= \frac{\partial}{\partial y}(-\rho u_\tau^2 f_1) \\ &= -\rho\{f_1\frac{\partial u_\tau^2}{\partial y} + u_\tau^2\frac{\partial f_1}{\partial(z/l)}\frac{\partial(z/l)}{\partial y}\} \\ &= -\rho u_\tau^2 f_1' z(-\frac{1}{l^2})\frac{\partial l}{\partial y} - 2\rho f_1 u_\tau\frac{\partial u_\tau}{\partial y} \end{aligned} \tag{3.68}$$

where f_1' is the derivative of f_1 with respect to (z/l).

$$\begin{aligned} F_2 &= \frac{\partial}{\partial z}(-\rho\overline{vw}) \\ &= \frac{\partial}{\partial z}(-\rho u_\tau^2 f_2) \\ &= -\rho u_\tau^2\frac{\partial f_2}{\partial z} \\ &= -\rho u_\tau^2\frac{f_2'}{l} \end{aligned} \tag{3.69}$$

where f_2' is the derivative. of f_2 with respect to (z/l).

$$\begin{aligned} F_3 &= \frac{\partial}{\partial z}(-\rho\overline{w^2}) \\ &= \frac{\partial}{\partial z}(-\rho u_\tau^2 f_3) \\ &= -\rho u_\tau^2\frac{f_3'}{l} \end{aligned} \tag{3.70}$$

where f_3' is the derivative of f_3 with respect to (z/l). and

$$\begin{aligned} F_4 &= \frac{\partial}{\partial y}(-\rho u_\tau^2 f_2) \\ &= -\rho\{u_\tau^2 f_2' z(-\frac{1}{l^2})\frac{\partial l}{\partial y} + 2 f_2 u_\tau \frac{\partial u_\tau}{\partial y}\} \\ &= -2\rho u_\tau f_2 \frac{\partial u_\tau}{\partial y} + \rho u_\tau^2 f_2' \frac{z}{l^2}\frac{\partial l}{\partial y} \end{aligned} \tag{3.71}$$

For octant A, l and u_τ are functions of only z. For regions not too close to the wall,

$$(\bar{v}^2/u_\tau^2) = f_{1-A}(y/l)$$

$$(\bar{v}w/u_\tau^2) = f_{2-A}(y/l)$$

and

$$(\bar{w}^2/u_\tau^2) = f_{3-A}(y/l)$$

where y is the perpendicular distance from the solid surface. Rewriting the expressions for the octant A,

$$f_{1-A}(y/l) = a_8(y/l)^3 + a_9(y/l)^2 + a_{10}(y/l) + a_{11} \tag{3.72}$$

$$f_{2-A}(y/l) = a_5(y/l)^2 + a_6(y/l) + a_7 \tag{3.73}$$

$$f_{3-A}(y/l) = a_1(y/l)^3 + a_2(y/l)^2 + a_3(y/l) + a_4 \tag{3.74}$$

Denoting the corresponding gradients of Reynolds stresses for the octant A as F_{1-A},F_{2-A},F_{3-A} and F_{4-A} these expressions become

$$F_{1-A} = -\rho u_\tau^2 \frac{f_{1-A}'}{l} \tag{3.75}$$

$$F_{2-A} = -2\rho f_{2-A} u_\tau \frac{\partial u_\tau}{\partial z} + +\rho u_\tau^2 f_{2-A}' \frac{y}{l^2}\frac{\partial l}{\partial z} \tag{3.76}$$

$$F_{3-A} = -2\rho f_{3-A} u_\tau \frac{\partial u_\tau}{\partial z} + +\rho u_\tau^2 f_{3-A}' \frac{y}{l^2}\frac{\partial l}{\partial z} \tag{3.77}$$

$$F_{4-A} = -\rho u_\tau^2 \frac{f_{2-A}'}{l} \tag{3.78}$$

where f_{1-A}',f_{2-A}',f_{3-A}' and f_{4-A}' are derivatives of f_{1-A}, f_{2-A}, f_{3-A} and f_{4-A} with respect to (y/l).

Transforming these equations to suit the first quadrant test section for the corresponding octants A and B, $(S_2 - z)$ replaces z, and $(S_1 - y)$ replaces y. Simplifying further using the relation $u_\tau^2 = \tau_w/\rho$:

$$\begin{aligned}
F_1 &= -2C_6\tau_w^{1/2}\frac{\partial \tau_w^{1/2}}{\partial y}\{a_1(\frac{s_2-z}{l})^3 + a_2(\frac{s_2-z}{l})^2 + a_3(\frac{s_2-z}{l}) + a_4\} \\
&\quad +\tau_w C_6\frac{(s_2-z)}{l^2}\frac{\partial l}{\partial y}\{3a_1(\frac{s_2-z}{l})^2 + 2a_2(\frac{s_2-z}{l}) + a_3\} \qquad (3.79)\\
F_2 &= -C_6\frac{\tau_w}{l}\{2a_5(\frac{s_2-z}{l}) + a_6\} \qquad (3.80)\\
F_3 &= -C_6\frac{\tau_w}{l}\{3a_8(\frac{s_2-z}{l})^2 + 2a_9(\frac{s_2-z}{l}) + a_{10}\} \qquad (3.81)\\
F_4 &= -2C_6\tau_w^{1/2}\frac{\partial \tau_w^{1/2}}{\partial y}\{a_5(\frac{s_2-z}{l})^2 + a_6(\frac{s_2-z}{l}) + a_7\} \\
&\quad +\tau_w C_6\frac{(s_2-z)}{l^2}\frac{\partial l}{\partial y}\{2a_5(\frac{s_2-z}{l}) + a_6\} \qquad (3.82)\\
F_{1-A} &= -C_6\frac{\tau_w}{l}\{3a_8(\frac{s_1-y}{l})^2 + 2a_9(\frac{s_1-y}{l}) + a_{10}\} \qquad (3.83)\\
F_{2-A} &= -2C_6\tau_w^{1/2}\frac{\partial \tau_w^{1/2}}{\partial z}\{a_5(\frac{s_1-y}{l})^2 + a_6(\frac{s_1-y}{l}) + a_7\} \\
&\quad +\tau_w C_6\frac{(s_1-y)}{l^2}\frac{\partial l}{\partial z}\{2a_5(\frac{s_1-y}{l}) + a_6\} \qquad (3.84)\\
F_{3-A} &= -2C_6\tau_w^{1/2}\frac{\partial \tau_w^{1/2}}{\partial z}\{a_1(\frac{s_1-y}{l})^3 + a_2(\frac{s_1-y}{l})^2 a_3(\frac{s_1-y}{l}) + a_4\} \\
&\quad +\tau_w C_6\frac{(s_1-y)}{l^2}\frac{\partial l}{\partial z}\{3a_1(\frac{s_1-y}{l})^2 + 2a_2(\frac{s_1-y}{l}) + a_3\} \qquad (3.85)\\
F_{4-A} &= -C_6\frac{\tau_w}{l}\{2a_5(\frac{s_1-y}{l}) + a_6\} \qquad (3.86)
\end{aligned}$$

where C_6 is a constant introduced for tuning the model to suit the experimental data.

Thus the Reynolds stress terms are defined algebraically by the expressions F_1, F_2, F_3 and F_4 for the octant(B) and F_{1-A}, F_{2-A}, F_{3-A} and F_{4-A} for the octant(A).

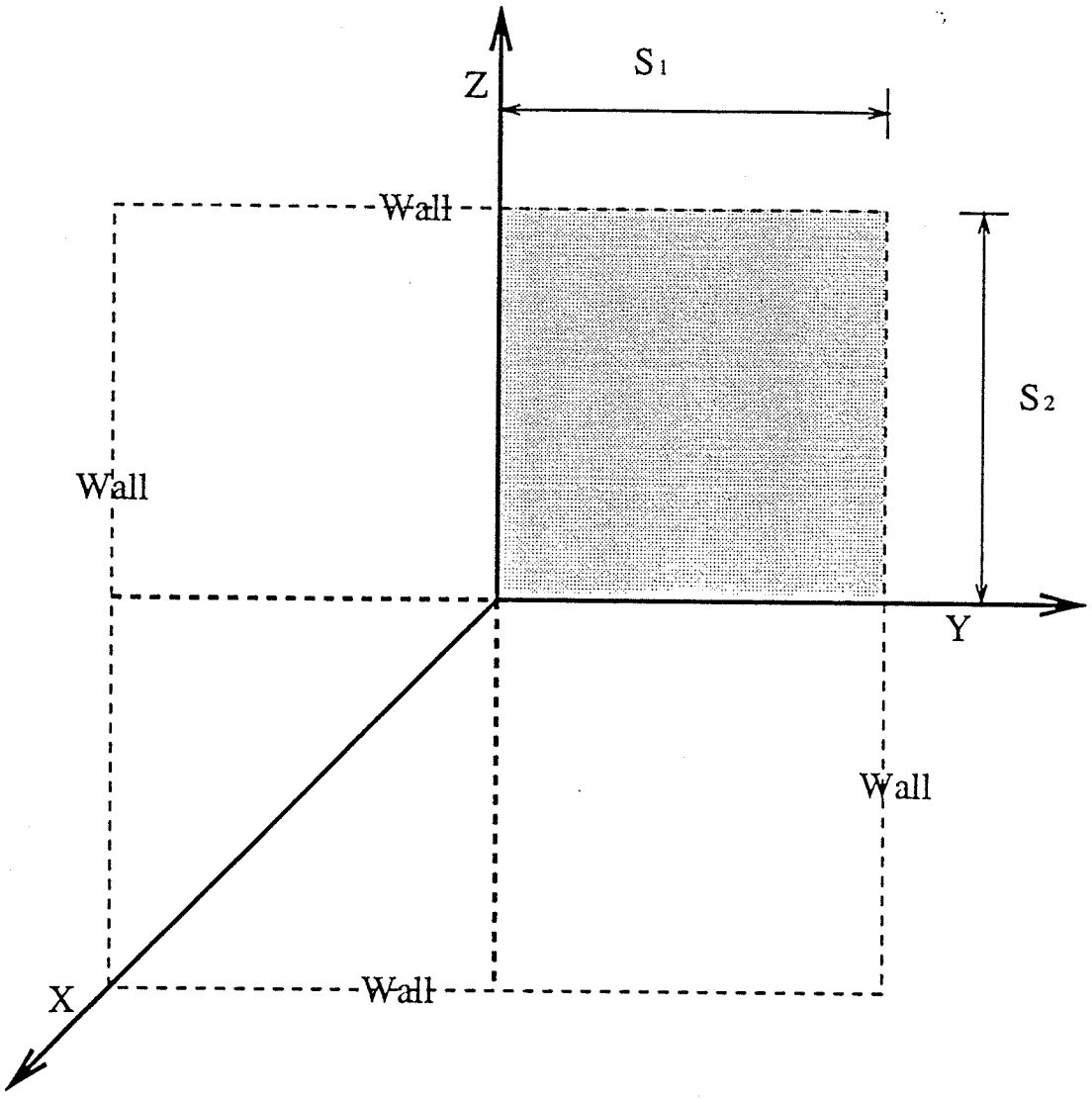

Figure 3.1: Coordinate system adopted and the symmetric quadrant where the developed model has been tested.

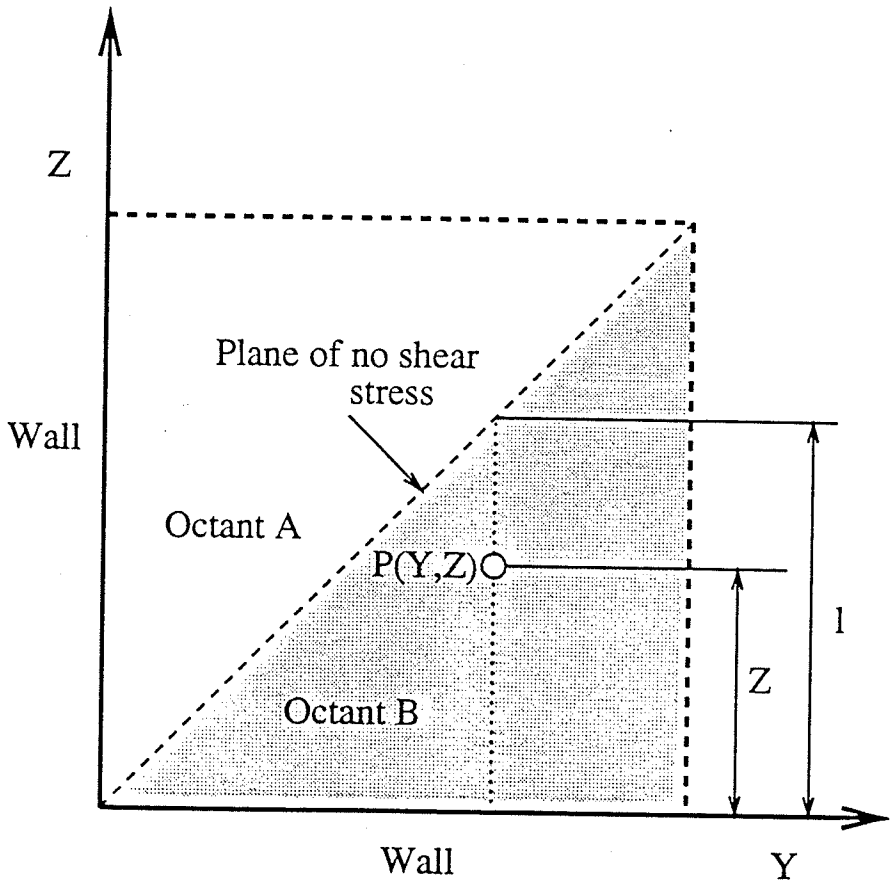

Figure 3.2: Quadrant used for deriving the model.

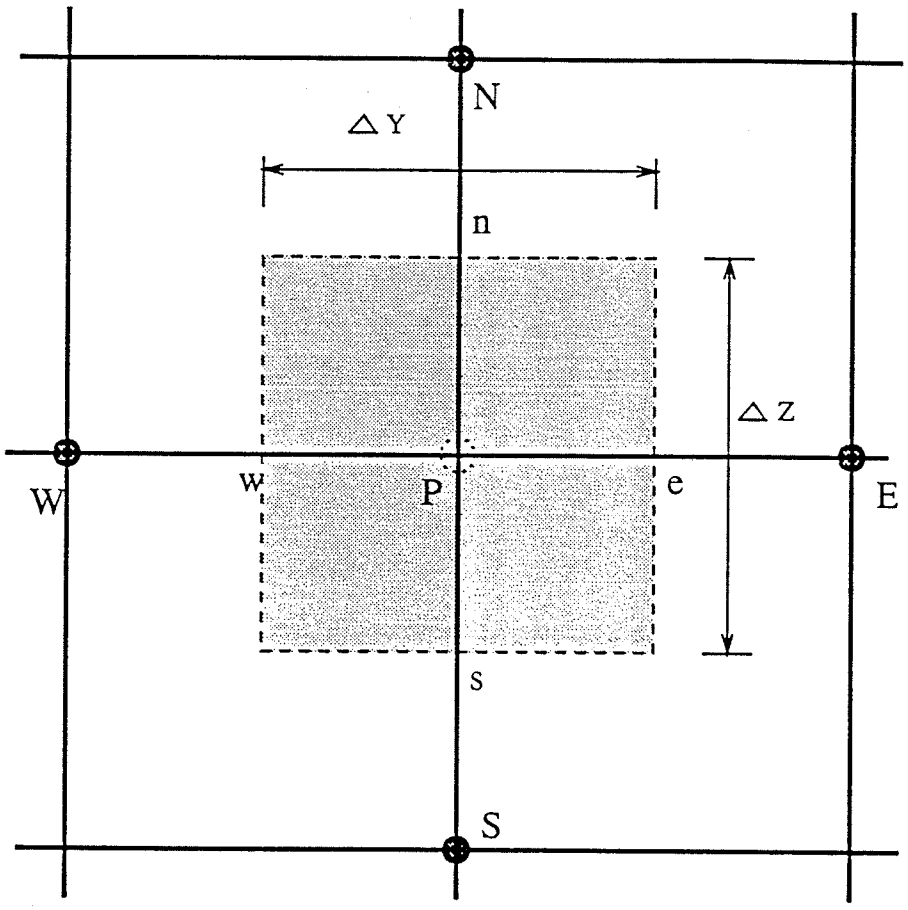

Figure 3.3: Control volume used for discretizing the general conservation equation.

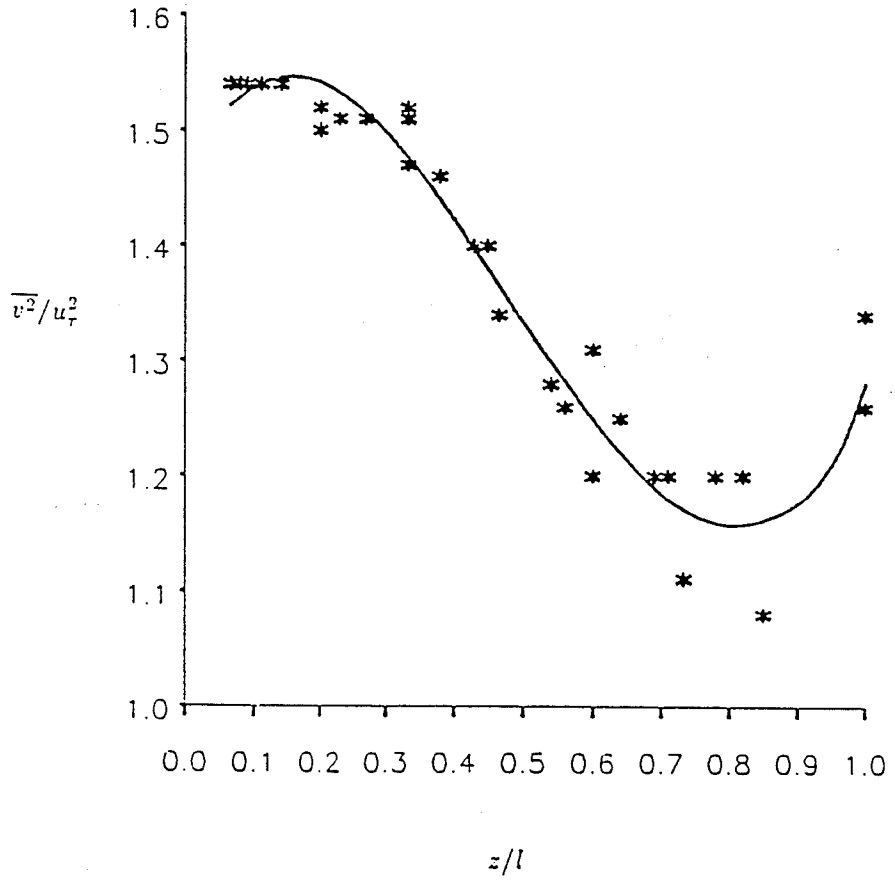

Figure 3.4: Plot of $(\overline{v^2}/u_\tau^2)$ from the experimental data of Brundrett and Baines(7)

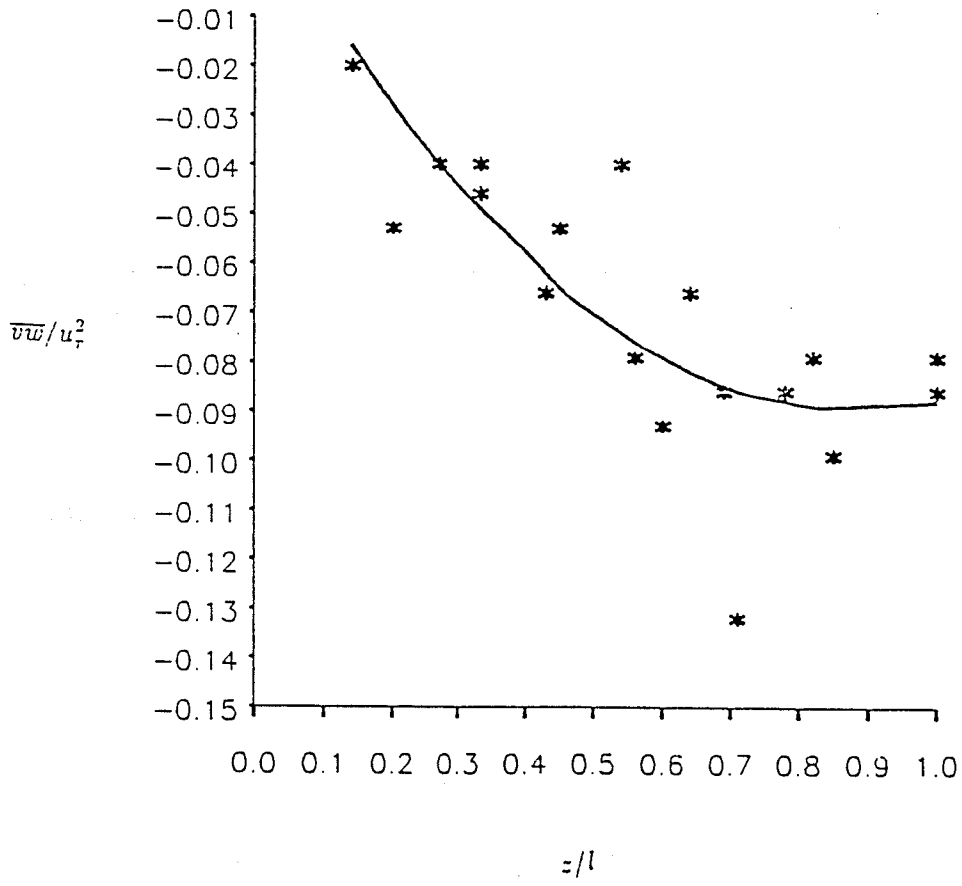

Figure 3.5: Plot of $(\overline{vw}/u_\tau^2)$ from the experimental data of Brundrett and Baines(7)

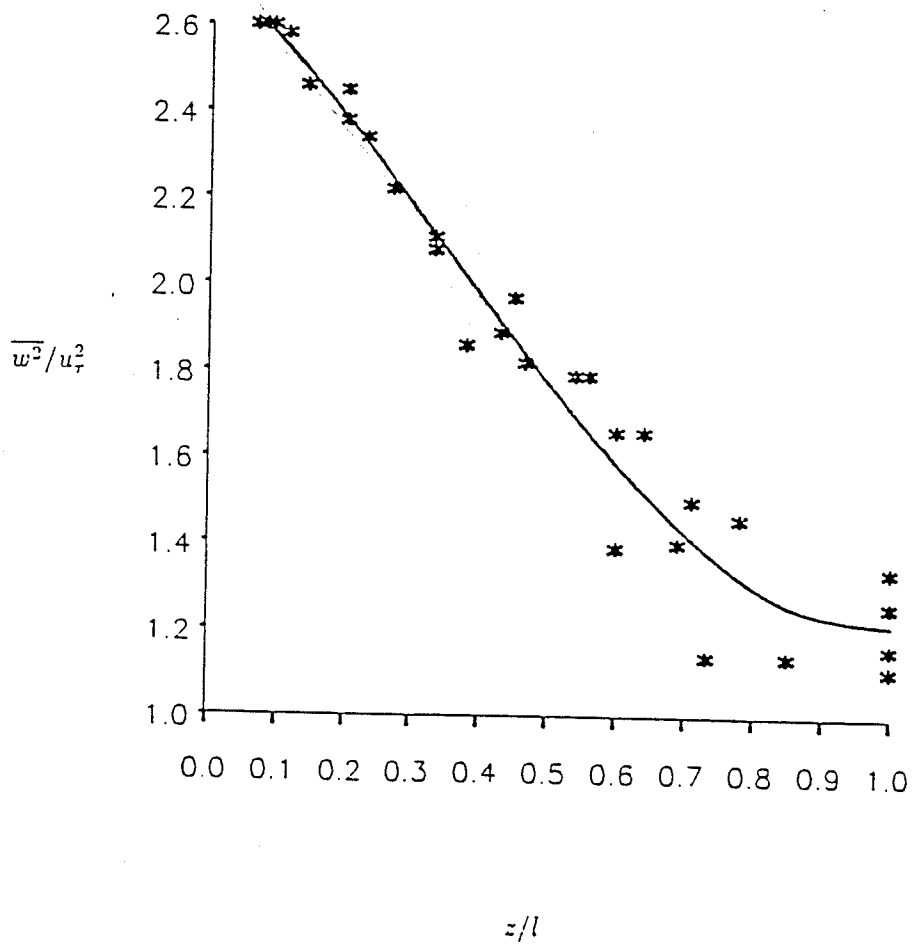

Figure 3.6: Plot of $(\overline{w^2}/u_\tau^2)$ from the experimental data of Brundrett and Baines(7)

Chapter 4

Numerical Programming

So far we have defined the partial differential equations needed to determine the values for various parameters involved. The necessary algebraic formulations are also derived. In order to verify the model developed,we need to solve these equations numerically after discretizing them. For model I and model I A using VSM, discretization and numerical solution are carried out as described in Zhou[52]. For model II using PVM, this can be done by discretizing the general conservation equation,

$$(\rho V\phi - \Gamma\phi_y)_y + (\rho W\phi - \Gamma\phi_z)_z = S_\phi$$

4.1 Discretization of the General Equation

The control volume on which the discretization is carried out is shown in the Fig. 3.3. P is the nodal point under consideration. Points E, W, N and S are the neighbouring points of the nodal point P. Similarly e, w, n and s are the grid boundaries in the east, west, north and south directions.

In the derivation of the discretization equation the following assumptions are made:

- The variable ϕ is assumed to remain uniform over the control volume chosen.
- The flow is assumed to be incompressible and hence the density ρ remains constant

- Viscosity of the fluid is assumed to remain constant for the flow domain

Replacing the convective and diffusive fluxes with total flux J, the equation may be written as

$$(J_2)_y + (J_3)_z = S_\phi \tag{4.1}$$

where J_2 and J_3 are the total fluxes in the y and z direction respectively. They are defined as

$$J_2 = \rho V \phi - \Gamma \phi_y \tag{4.2}$$

$$J_3 = \rho W \phi - \Gamma \phi_z \tag{4.3}$$

Integrating Eqn.(4.1) over the control volume shown in Fig. 3.3,

$$(J_2)_e - (J_2)_w + (J_3)_n - (J_3)_s = b_s \tag{4.4}$$

Here $(J_2)_e$, $(J_2)_w$, $(J_3)_n$ and $(J_3)_s$ denote the total flux across the eastern, western, northern and southern grid boundaries respectively. b_s, the integrated value of the source term over the grid volume is given by

$$b_s = S_\phi \Delta y \Delta z \tag{4.5}$$

In order to solve this let us consider a simple case of one dimensional flow without any source term. The flow is along the x direction, with a velocity U. The general conservation equation becomes,

$$(\rho U \phi - \Gamma \phi_x)_x = 0 \tag{4.6}$$

Let a domain $0 \leq x \leq L$ be used,with the boundary conditions,

at $x = 0,\ \phi = \phi_0$

and at $x = L,\ \phi = \phi_L$

The equation(4.5)can be solved exactly if Γ and ρ are taken to be constant. For this equation U is already a constant (from continuity equation). With these conditions

the exact solution is then obtained as shown in [59]. It is given as

$$\frac{\phi - \phi_0}{\phi_L - \phi_0} = \frac{exp(Pex/L) - 1}{exp(Pe) - 1}$$

where Pe is a Peclet number, defined by

$$Pe = \frac{\rho U L}{\Gamma}$$

Peclet number is a ratio of the convective flux and the diffusive flux. This exact solution enables ϕ to be more influenced by the upstream value ϕ_0, when the flow is in the positive x-direction and by the downstream value ϕ_L,when the flow is in the negative x-direction. The picture is reversed for negative values of Pe.

Now the exact solution can be used as a profile between points P and E, with ϕ_P and ϕ_E replacing ϕ_0 and ϕ_L and the distance $(\delta x)_e$ replacing L. This gives the expression for J_e, the total flux across the eastern grid face, as

$$J_e = F_e(\phi_P + \frac{\phi_P - \phi_E}{exp(Pe_e) - 1}) \tag{4.7}$$

where $F_e = \rho U_e$.

Similarly the expressions for J_w, J_n and J_s are obtained. Substituting these expressions in the equation(4.4), we get

$$F_e(\phi_P + \frac{\phi_P - \phi_E}{exp(P_e) - 1}) - F_w(\phi_W + \frac{\phi_W - \phi_P}{exp(P_w) - 1}) + F_n(\phi_P + \frac{\phi_P - \phi_N}{exp(P_n) - 1}) \tag{4.8}$$

$$- F_s s(\phi_S + \frac{\phi_S - \phi_P}{exp(P_s) - 1}) = b_s \tag{4.9}$$

(4.10)

Regrouping

$$a_P\phi_P = a_E\phi_E + a_W\phi_W + a_N\phi_N + a_S\phi_S + b_s \tag{4.11}$$

where

$$a_E = \frac{F_e}{exp(P_e) - 1} \tag{4.12}$$

$$a_W = \frac{F_w.exp(P_w)}{exp(P_w) - 1} \tag{4.13}$$

$$a_N = \frac{F_n}{exp(P_n) - 1} \tag{4.14}$$

$$a_S = \frac{F_s.exp(P_s)}{exp(P_s) - 1} \tag{4.15}$$

and

$$a_P = a_E + a_W + a_N + a_S + F_e - F_w + F_n - F_s \tag{4.16}$$

4.1.1 Pressure Correction Equation

As explained later in this thesis, a need was felt to solve the momentum equations for V and W in the staggered grids. For V, the grid was staggered in the y direction and for W, in the z direction. It can be noted that the source terms for cross sectional velocities have hidden pressure terms. These pressure terms are not defined as such and if taken out of the source terms present themselves as distinct driving forces on the control volume for cross-sectional velocities.

From the Fig. 3.3 for a velocity V_e, located at the eastern grid boundary of a main grid point P, the discretized equation can be written as

$$a_e V_e = \Sigma a_{nb} V_{nb} + b + (p_P - p_E) A_e \tag{4.17}$$

Here suffix nb refers to the neighbouring V grid points for the point at location e. The term $(p_P - p_E)A_e$ is the pressure force acting on the control volume and A_e is the area on which the pressure difference acts. Term b represents the source for that control volume.

A similar equation can be written for the W momentum equation as

$$a_n W_n = \Sigma a_{nb} W_{nb} + b + (p_P - p_N) A_n \tag{4.18}$$

To solve these equations pressure terms have to be estimated somehow. Unless the correct pressure field is employed, the resulting velocity field will not satisfy the continuity equation. This is tackled by assuming a guessed value for pressure p^g,

and correcting it later with the pressure correction value p^c. Thus the pressure p, is defined as

$$p = p^g + p^c \tag{4.19}$$

As the velocity components respond to this change in pressure, this in turn necessitates introducing corresponding velocity corrections in a similar way:

$$V = V^g + V^c \tag{4.20}$$

$$W = W^g + W^c \tag{4.21}$$

By solving the following discretized equations,

$$a_e V_e^g = \Sigma a_{nb} V_{nb}^g + b + (p_P^g - p_E^g) A_e \tag{4.22}$$

and

$$a_n W_n^g = \Sigma a_{nb} W_{nb}^g + b + (p_P^g - p_N^g) A_n, \tag{4.23}$$

one can get an imperfect velocity field based on guessed pressure field p^g. Subtracting equation(4.22) from (4.17) results in the expression

$$a_e V_e^c = \Sigma a_{nb} V_{nb}^c + (p_P^c - p_E^c) A_e \tag{4.24}$$

Now the influence of the neighbouring terms are eliminated by dropping the term $\Sigma a_{nb} V_{nb}^c$. This is done to simplify the solution procedure and justification for it lies in the proven fact that the final solution remains insensitive to the omission of this term. This point is dealt with in considerable length by Patankar[59]. Thus we get

$$V_e^c = \frac{A_e}{a_e}(p_P^c - p_E^c) \tag{4.25}$$

This equation is called the velocity correction equation for V. Substitution of the equation(4.25) in (4.20) leads to the final expression for V_e:

$$V_e = V_e^g + \frac{A_e}{a_e}(p_P^c - p_E^c) \tag{4.26}$$

The correction formula for the velocities in the other direction can be written similarly:

$$W_n = W_n^g + \frac{A_n}{a_n}(p_P^c - p_N^c) \tag{4.27}$$

Substituting for all the velocity components by the expressions obtained from the velocity correction equations and rearranging:

$$\begin{aligned}(V_e^g - V_w^g)\Delta z \quad &+ \quad (W_n^g - W_s^g)\Delta y + p_P^c[(\frac{A_e}{a_e} + \frac{A_w}{a_w})\Delta z + (\frac{A_n}{a_n} + \frac{A_s}{a_s})\Delta y] \\ &- \quad (\frac{A_e}{a_e}p_E^c + \frac{A_w}{a_w}p_W^c)\Delta z - (\frac{A_n}{a_n}p_N^c + \frac{A_s}{a_s}p_S^c)\Delta y = 0\end{aligned} \tag{4.28}$$

It can be put in a simple form as:

$$c_P p_P^c = c_E p_E^c + c_W p_W^c + c_N p_N^c + c_S p_S^c + bi \tag{4.29}$$

where

$$c_E = \frac{A_e}{a_e}\Delta z \tag{4.30}$$

$$c_W = \frac{A_w}{a_w}\Delta z \tag{4.31}$$

$$c_N = \frac{A_n}{a_n}\Delta y \tag{4.32}$$

$$c_S = \frac{A_s}{a_s}\Delta y \tag{4.33}$$

$$c_P = C_E + C_W + C_N + C_S \tag{4.34}$$

and

$$bi = (V_W^g - V_E^g)\Delta z + (W_S^g - W_N^g)\Delta y \tag{4.35}$$

Thus we obtain the discretized equation to evaluate the values for pressure corrections at the main grid points.

The boundary conditions for the pressure correction equation are somewhat different from those of other equations since it is different from the basic equation. The grid is designed in a way that the boundary coincides with a control volume face. Since the normal velocity at the control volume face V_e is known, there is no need

to use a guessed value V_e^g and then correct it later with V_e^c. Equation(4.26) then becomes,

$$p_P^c - p_E^c = 0 \tag{4.36}$$

In other words the pressure gradient at the control volume in a normal direction is zero. Numerically this can be effected by making the coefficient a_E equal to be zero. Thus for all the main grid points one step removed from the boundary,

$$a_E = 0 \tag{4.37}$$

Thus the boundary conditions for all the parameters involved are specified.

4.2 Grid Structure

Model I using VSM was applied in the third quadrant using the grid shown in Fig. 4.1. The density of grid points is high in the near wall zone. Up to a certain distance grid points are placed in an increasing geometric progression as one moves away from the walls. Model II is tested in a staggered grid system, to avoid any physically unrealistic predictions, based on the suggestions of Patankar[59]. In this system of grid structure,velocity field grid points are placed in between the pressure field grid points. This allows the direct evaluation of the velocities at the grid boundaries. Wherever cross sectional velocities are not available as such,they are found out from the average of the values in the adjacent grid points.

The advantage gained, however, comes with some strings attached by way of complexities involved in forming multiple grids, staggered and superimposed. But as argued by Patankar[59], this extra difficulty helps in bringing out some of the best numerical predictions. This method is definitely superior to the vorticity source method in terms of the accuracy in predictions. This is discussed in detail in Section 5. The modified grid system(in the first quadrant) is shown in Fig. 4.2. The distance between grid points is not uniform, the density of the grid points being high near

the corner regions. This is done to take care of the steep velocity gradients in these regions.

4.3 SIMPLE Algorithm

The procedure used for calculation of the flow field was developed by Patankar and Spalding[54]and given the name SIMPLE which stands for Semi Implicit Method for Pressure Linked Equations.

The important steps in this method of solving are mentioned below.

1. Initially the pressure field is guessed.
2. With the guessed pressure field the momentum equations for the cross sectional velocities V and W are solved. This gives the approximate cross sectional fields.
3. Since the pressure field is a guessed one and the velocity fields are approximate,these fields are to be corrected. In order to do this the pressure correction equation is solved giving out the values of the pressure corrections at various grid points.
4. These pressure corrections are then applied to the pressure values giving the corrected pressure values.
5. Cross sectional velocities are then corrected. Thus we get the corrected pressure and velocity fields.
6. With these values the momentum equation for the axial velocity, turbulent kinetic energy equation and equation for rate of diffusivity are solved in that order.
7. At this point all these parameters are checked for convergence. If all of them meet the criteria for convergence, it signals the overall convergence

of the program and the output gets printed. Failure to do so necessitates the repetition of the cycle from step 2 onwards till the program converges.

4.4 Initial Conditions

Initially the program was run with an assumption that there were no secondary flows. This was done by directing the program to solve only U,k and ϵ equations. To initiate this run some approximate average values were specified for U, k and ϵ. Initial values for axial pressure gradient and wall shear stresses were also assumed. This initial run gave the converged distributions for U, k and ϵ,without secondary flow. These distributions, along with zero initial values of the pressure and pressure correction, were treated as input to the main program. Since the program was run for a particular value of Reynolds number it is necessary that the final solution be bounded by this assigned value of the Reynolds number. This is done by multiplying the corrected values of the secondary velocities by a factor$((U_b)_{av}/U_b)$at each iteration. Here $(U_b)_{av}$ is the average bulk velocity obtained from the specified Reynolds number and U_b is the bulk velocity calculated from the predicted distribution of the axial velocity. The same factor is used for correcting the axial velocity distribution to yield the desired Reynolds number. Mathematically stating,

$$U_{i,j} = U_{i,j}(\frac{(U_b)_{av}}{U_b}) \tag{4.38}$$

$$V_{i,j} = V_{i,j}(\frac{(U_b)_{av}}{U_b}) \tag{4.39}$$

$$W_{i,j} = W_{i,j}(\frac{(U_b)_{av}}{U_b}) \tag{4.40}$$

4.5 Convergence criterion

Two different types of convergence criteria were used in this program. For axial velocity U,turbulent kinetic energy k,and rate of turbulent dissipation ϵ, the relative

change in the values with respect to the previous ones were compared with set values.

$$\frac{\phi_{new} - \phi_{old}}{\phi_{old}} \leq \xi \tag{4.41}$$

Here ξ, was set to be equal to 0.001.For pressure P, and cross sectional velocities V and W, the change in the successive values were compared with set values.

$$(\phi_{new} - \phi_{old}) \leq \xi \tag{4.42}$$

Here ξ was set to be equal to 0.0001.

4.6 Stability Criterion

The numerical program uses an iterative method for solving the coupled discretized equations. There are many methods for solving these equations out of which the simplest one, Gauss-Seidel point-by-point scheme, is selected. The present scheme satisfies the Scarborough[58] criterion to ensure stability.

The Scarborough criteria states that a *sufficient* condition for the convergence of the Gauss-Seidel method is

$$\frac{\Sigma|a_{nb}|}{|a_p|} \leq 1, for\ all\ equations \tag{4.43}$$

$$\frac{\Sigma|a_{nb}|}{|a_p|} < 1, for\ at\ least\ one\ equation \tag{4.44}$$

where a_{nb} refers to the coefficients of the neighbouring grid points and a_p refers to that of the point under consideration. Care was taken in satisfying these two conditions. The second condition is satisfied at nodes near the boundaries by specifying the boundary conditions.

4.7 Grid Size

As mentioned earlier,the model developed was tested in the first quadrant of a square duct and various rectangular ducts of different aspect ratios. A grid size of 14×14

was used for the square duct. For rectangular ducts of aspect ratio 2, 3, 4 and 5, grid sizes of 19×14, 21×14, 29×14 and 34×14 are used respectively.

4.8 List of the constants and their values

C_1	1.44	C_2	1.92	Constants used in 'k' and 'ϵ' Transport Equations
σ_k	0.90	σ_ϵ	1.30	Values are from Nakayama et al.[2]
C'	0.0185	C_k'	0.552	L Y model constants-from Nakayama et al.[2]
C_D	0.09			Near wall constant from Zhou[52]
C_5	0.08	C_6	0.08	Constants of model I and model II
a_1	2.7573	a_2	-4.2053	Constants used in Reynolds stress functions Obtained from Brundrett and Baines[7]
a_3	1.1751	a_4	1.4563	
a_5	-0.0291	a_6	-0.0744	
a_7	0.01	a_8	1.9638	
a_9	-2.3596	a_{10}	-1.1175	
a_{11}	2.7006	a_{12}	0.7935	
a_{13}	1.8457	a_{14}	2.2926	

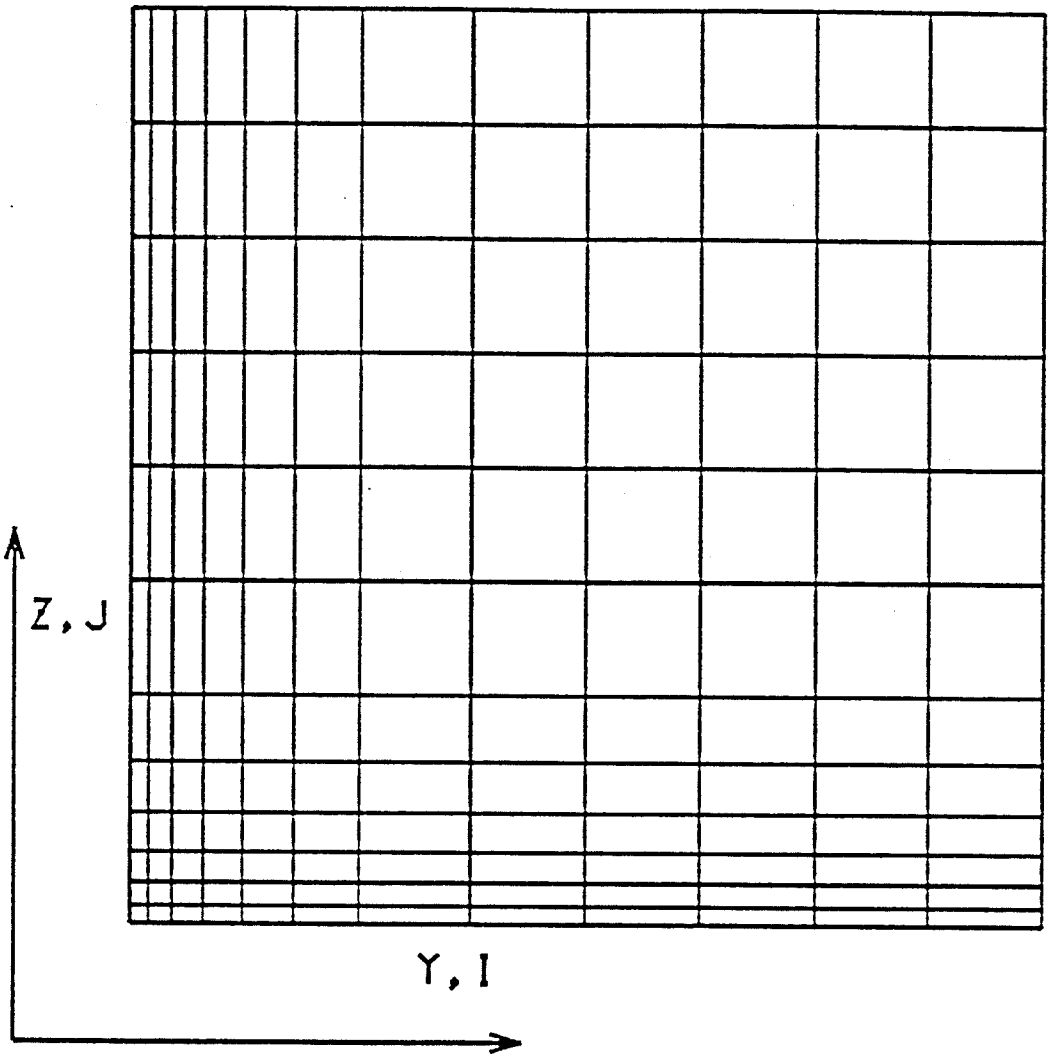

Figure 4.1: Grid structure used to suit Vorticity source method in square cross section.

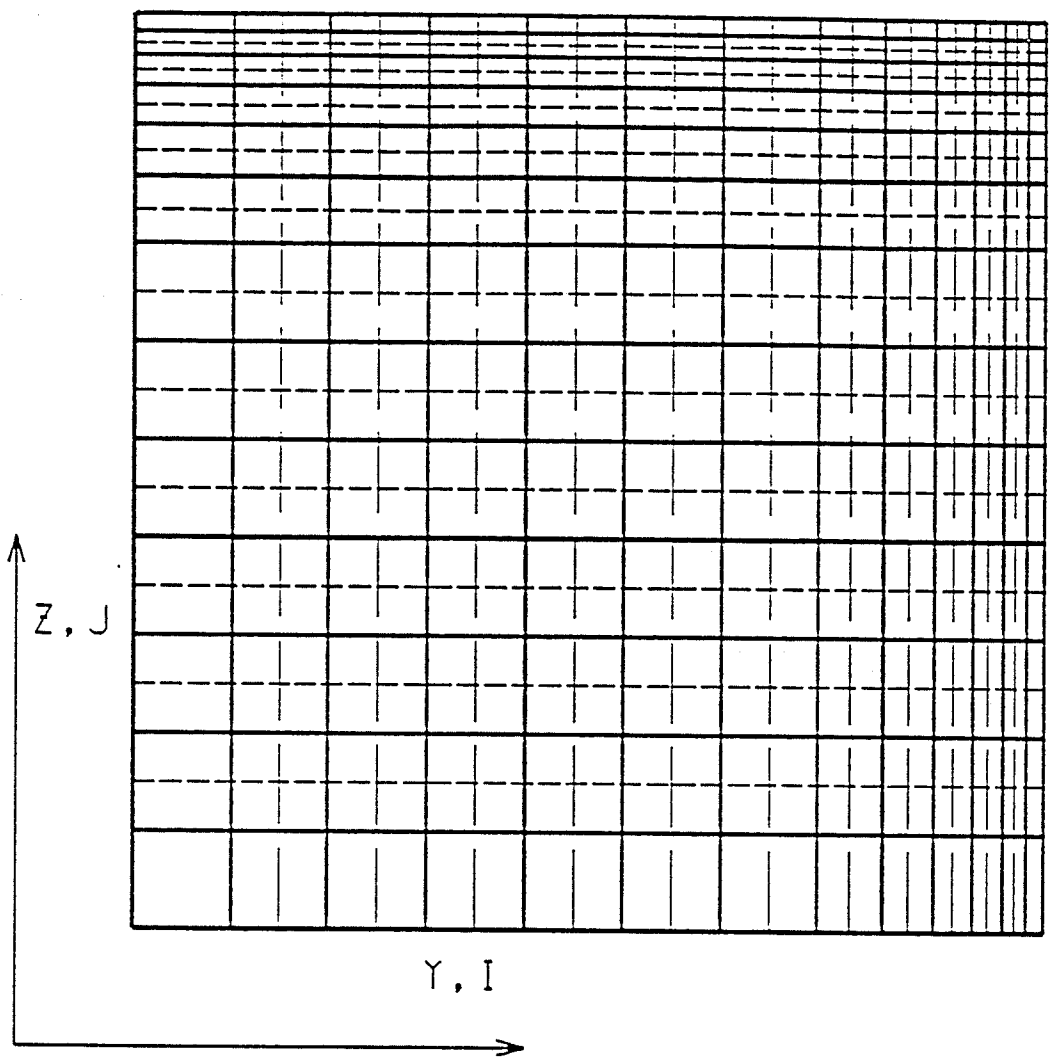

Figure 4.2: Typical grid structure designed to suit Primitive variable scheme in square cross section.

- — Main grid
- - - - Wgrid
- - - - Vgrid

Chapter 5

Results and Discussion

A computer program in FORTRAN language(listed in Appendix A) was written to test the model formulated to predict turbulent flow in a square duct and in rectangular ducts of various aspect ratios. It was run on the AMDAHL main frame using MVS/TSO and also on a UNIX SUN/SPARC workstation. As mentioned earlier, the program was initially run without secondary flows and the output was stored as input to the overall run with secondary flows. All the important parameters are plotted either using contour plots or using X-Y graphs. Wherever possible these plots are compared with the experimental data as well as with the output of previous models.

In all the contour diagrams, it is to be noted that the solid lines represent the wall or solid boundaries and the dotted lines represent the boundaries between the symmetric flow segments. Predictions involving model I using the vorticity source term method are presented in the third quadrant. Predictions of the rest of the models involved are given in the first quadrant.

5.1 Model I

Model I, based on Vorticity Source Method is formulated in Chapter 3. Governing transport equations involved are discretized as described in Zhou[52].

Model I,expressed algebraically through the equation(3.53), is used for calculating the vorticity source term values, only at those nodes that are lying immediately

adjacent to the walls. This is done in accordance with observation that the maximum vorticity generation occurs near the solid walls. This model when used to predict the values of vorticity source terms, assigned maximum values to the grid points near the sharp corner as expected since the secondary flow generation is mainly due to the presence of the sharp corner. For other nodes, vorticity source terms are assigned based on an exponential interpolation. Multitude of values were tried as the constants of exponentiation. Based on this a set of numerical predictions were obtained for a square duct. These predictions were compared with the prediction, obtained without any assumption of the vorticity source terms in the interior nodes. But they were found to be essentially the same. Hence it was decided to assign zero values of vorticity source to the interior nodes without imposing any artificial interpolated values.

For the node, that lies at the intersection of these two string of nodes no vorticity source value is applied. This is in accordance with the experimental observation,on the presence of zero shear stress plane along the corner bisector. Artificial sign conversion was applied on the wall shear stress along the vertical wall to obtain counter- rotating secondary flow cells.

5.1.1 Square duct

Model I was applied to a turbulent flow in a square duct. Due to the symmetry of the flow, only the flow in the third quadrant was considered. Predicted results are plotted in Figs. 5.1 and 5.2.

Fig. 5.1 compares the predicted secondary flow streamlines with the experimental data of Hoagland[5] and Zhou's[52] prediction with LY model using VSM. Predictions are for a flow at Re=150,000. Typical maximum value of the secondary flow generated is approximately 1.7% of the bulk velocity. General shape of the predicted secondary flow cells matches with the experimental data. But the centre of the flow cell is pushed away from the corner by a distance that is one and one quarter times the

corresponding distance from the experimental data. In the same figure a comparison is made with Zhou's[52] prediction. Model I's prediction is comparable to that of Zhou's. It may be seen that the distance of the centre of secondary flow cell in Zhou's prediction is also farther away from the corner by a factor of approximately 1.1 times compared to that of the experimental data. In the experimental data secondary flow streamlines penetrate towards the corner deeply and the orientation of the secondary flow cells is towards the corner. Orientations of the secondary flow cells are towards the centre of the duct in both the predictions(model I and Zhou[52]). With both predictions, the penetration towards corner is also not deep. This penetration may be improved by the inclusion of gradients of Reynolds stress $\overline{vw}$ in the vorticity source term.

Fig. 5.2 compares the normalised axial velocity U/U_B isovels of the experimental data of Leutheusser[6] and those of the predictions using model I. This is for a flow in a square duct at Re=83,000. The distortion of the axial velocity isovels along the corner bisector is less in the prediction of model I, when compared with the experimental data. The bulges in the contours of the experimental data, near the corner bisector,are absent in the predicted result. This implies that the secondary flows are not strong enough, yet at 1.7% maximum, it could not have been much stronger. Predicted values compare well near the centre of the duct.

5.1.2 Rectangular duct

Model I was tried in the rectangular duct with an aspect ratio of 3. The program converged. But the vorticity generated was higher than that of the experimental data. Fig. 5.3 compares the normalised wall shear stress profile of the model I with the experimental data of Leuthuesser[6]. Wall shear stress predicted by the model I did not have the sensitive variation in its profile as possesed by its experimental counterpart.

5.1.3 Summary

Thus the model I, tried with the VSM,produces a symmetric prediction in a square duct. Its prediction in square duct is comparable to other models. It differed from the experimental data in the degree of distortion of the axial velocity contours along the corner bisector. In rectangular duct of aspect ratio 3, its performance fell short of experimental data.

5.2 Model I A

Attempts were made to improve the model I. As an effort towards improvement of model I, model I A was developed. As stated earlier this prediction scheme extends the definition of vorticity source term to the entire flow region. It is based on the experimental data of Brundrett and Baines[7] and is applied with VSM. This model has been defined in Chapter 3 by the equation(3.60). Numerical discretization and the solution methodology is the same as that employed by Zhou[52].

This model has been applied to a flow at Re=75,000, in a square duct. But it produced asymmetric prediction in a square duct. However it encouraged the idea of extending the Reynolds stress definition over the whole flow domain and lead the path towards a further refined model II.

5.3 Model II

The idea of extending the definition of vorticity source to the entire flow region lead to the development of model II. Model II is based on the experimental data of Brundrett and Baines[7]and is defined mathematically in Chapter 3, by the equations(3.79) to(3.86). Finite difference discretization of the equations are carried out as shown in Chapter 4. It has been tested numerically using PVM.

Model II has been tested in a square duct and various rectangular ducts with different aspect ratios. Because of the symmetry of the flow,only the flow in the first

quadrant was considered. The prediction in the square duct has no major assumption. It assumes the corner bisector to be the plane of zero shear stress, which is in accordance with many experimental observations. In the rectangular duct,the scheme assumes that values to the Reynolds stress terms be assigned only to the nodes that lie in the square region $S2 \times S2$, in the corner. For the rest of the region, the flow is taken to resemble the flow between parallel plates. This assumption may not hold strong for flows in ducts with aspect ratio close to unity,like 2 or 2.5.

5.3.1 Convergence Experience

When model II was tested numerically,using PVM, initial attempts resulted in the divergence of the program at the early stages. In order to obtain convergence, scanning direction is corrected to carry out iterations from boundaries, so as to quicken the flow of information from the boundaries. But this did not produce any appreciable change in the prediction. Later it was found necessary to heavily under-relax the cross sectional velocity-momentum equations. When this was tried in a square duct,the program finally converged. But asymmetric flow patterns were predicted. A thorough analysis of the working of the program made the author realise the importance of applying changes to the cross sectional velocities simultaneously at the end of one complete iteration, rather than correcting them within an iteration immediately after any change in their values. This is needed since the source terms for these parameters vary dynamically. After these steps, it became possible to test the model II, thoroughly in many ducts.

5.3.2 Square duct

Figs. 5.4 to 5.10 compare the predictions of model II in a square duct with the experimental data. In Fig. 5.4 secondary flow streamlines of the prediction with model II are compared with the experimental data of Hoagland[5] for a flow at Re=150,000. Typical maximum value of the secondary flow predicted is approximately 1.45% of

the bulk velocity. Distance of the centre of the flow cell from the corner is approximately 1.15 times longer in the prediction, than that of the experimental data. But the orientation of the flow cell is towards the corner of the duct, as in the case of the experimental data. Penetration of the secondary flow towards the corner is reasonable, though it is not as deep as that of the experimental data. Flow cells in the prediction are symmetric.

In Fig. 5.5 isovels of the axial velocity, normalised with the bulk velocity, are given for a flow at Re=83,000. It compares the prediction of model II with the experimental data of Leutheusser[6] and the prediction of Nakayama et al.[2] (using LY model with PVM). Near the centre of the duct,model II predicts very close to the experimental data. Along the corner bisector the distortion in the axial velocity profile is distinct, though not as high as that of the experimental data. Model II underpredicts along the corner bisector to a maximum of 4%. In the rest of the flow domain, the prediction of model II is close to that of the experimental data with a maximum difference of 2%. This accuracy of prediction appears to be reasonable when considering the probable accuracy of measurement of the experimental data. At this stage it can be said that model II's prediction is as good as that of Nakayama et al.[2]. A more detailed comparison is provided in the latter part of this chapter.

Fig. 5.6 compares the prediction of model II with the experimental data of Launder and Ying[1], for a flow at Re=215,000. The parameter involved is the normalised axial velocity (U/U_B) at various elevations along the vertical axis. At the centre of the duct prediction match closely with the experimental data. As one moves towards the wall,prediction overshoots the experimental data initially,to drop down to the experimental values finally. Prediction falls within 2% tolerance for approximately 75% of the cross section,that lies close to the centre of the duct. But near the wall this deviation goes upto 5.5%.

In Fig. 5.7 normalised wall shear stress (τ_w/τ_{av}) of the prediction of model II

is compared with the experimental data of Leuthuesser[6] for a flow at Re=34,000. Model II's prediction matches with the experimental data, within a tolerance of approximately 4.5%. Prediction also displays the bump in the wall shear stress profile distinctively.

Fig. 5.8 compares the distributions of normalised turbulent kinetic energy k/u_τ^2, of the model II's prediction with the experimental data of Brundrett and Baines[7]. Model II underpredicts almost all across the flow domain.Reason for this notable deviation from the experimental data is not known.

Fig. 5.9 shows contours of secondary velocity $[(\overline{v^2} + \overline{w^2})^{1/2} * 100/U_B]$, of the prediction using model II and the experimental data of Launder and Ying[1], for a flow at Re=75,000. Secondary velocity predicted is slightly less than the experimental observation, especially adjacent to the corner bisector. Otherwise, the general matching appears to be satisfactory. In the prediction,the point where the maximum secondary velocity occurs is farther from the corner than that in the experimental data. This is consistent with the earlier observation on the distance of the centre of the flow cells from the corner, in which this distance is observed to be longer in the predictions than that of the experimental data.

Fig. 5.10 compares (V/u_τ) profiles of model II's prediction with the experimental data of Launder and Ying[1]. This is for a flow at Re=215,000. There is a considerable deviation with the experimental data, near the wall at $(1 - y/s1) = 0.2$. In the prediction, width of the secondary flow along the corner bisector, is wider than its experimental counterpart. This discrepancy is also observed with the predictions of other prevalent models as shown in [52]. Prediction matches with the experimental data near the centre of the duct.

5.3.3 Rectangular duct

Fig. 5.11 compares the secondary flow streamlines of the prediction of model II with the experimental data of Hoagland[5] for a rectangular duct with an aspect ratio of 2. This is for a flow at Re=34,000. Secondary flow generated in the prediction is less than that of the experimental data. In prediction the larger flow cell is observed to be more dominant. The distance of the centre of the larger flow cell from the corner is 4% longer than its experimental counterpart. Compared to the deviation in the square duct this deviation is relatively less. In square duct,the corresponding variation is approximately 11% more. Shape of the predicted curve varies from the experimental data,especially with its lack of penetration towards the corner.

Figs. 5.12 to 5.15 compare the prediction of model II with experimental data for flows in a rectangular duct with an aspect ratio of 3. In Fig. 5.12 secondary flow streamlines of model II are compared with the experimental data of Hoagland at Re=60,000. The smaller flow cell of the prediction is more dominant in the near corner zone. Distance of the centre of the larger flow cell from the corner is approximately 20% longer than its experimental counterpart. Penetration towards the corner is less than the experimental observation.

Fig. 5.13 compares the isovels of normalised axial velocity (U/U_C) of the prediction of model II with that of Nakayama et al.[2] and the experimental data of Leutheusser[6]. This is for a flow at Re=56,000. Model II predicts close to the experimental data. It shows a maximum deviation of approximately 4% along the corner bisector near the wall. This value compares well with a nearly equal percentage of deviation in the square duct along the corner bisector. The general shape of the contours predicted with model II, matches with that of the experimental data. The isovel near the wall differs slightly from that of the experimental data in that the bulge in the contour is shifted away from the wall. This may be due to the presence of a stronger, dominating smaller cell in the near corner region. Fine tuning of the

turbulent model coefficients may improve the prediction in the near corner zone.

In Fig. 5.14 the profile of normalised wall shear stress(along the wider side of the duct)of the prediction with model II and that of Nakayama et al.[2], are compared with that of the experimental observations of Leutheusser[6], for a flow at Re=56000. Model II's predicted profile displays a peak near the corner, to be followed by a dip as one moves towards the centre of the duct. This variation resembles that of the experimental data. But the place where this peak in the profile appears, is approximately 5% farther away from the corner. Other than that, the predicted profile of the model II, matches with the experimental data with a maximum deviation of approximately 6%. Comparison with the prediction of[2] is done in the latter part of this chapter. In Fig. 5.15 the wall shear stress profile,along the shorter side of model II is compared with the experimental data of Leutheusser[6]. The peak and the dip in the profile of the experimental data are reproduced by the prediction. But the deviation from the experimental data is close to 9%. Deviation is less near the corner.

5.3.4 Summary

Thus to summarise,model II in general, predicts close to the experimental data in the square duct flow. Along the corner bisector, a maximum deviation occurs of the order of approximately 4%. In the remaining domain of the square duct, the predictions fall within 2% of the corresponding experimental data.

In rectangular ducts, model II is compared with experimental data for ducts with aspect ratios of 2 and 3. In the rectangular duct with an aspect ratio of 2, the location of the centre of the centre of the secondary flow cell is close to the experimental data. But the shapes of flow cells differ from their experimental counterparts. Model II in a $3:1$ duct produces a prediction that has a maximum deviation of 5% from the experimental data. This maximum deviation occurs in the near corner region and

along the corner bisector. As mentioned earlier, this may be due to the dominance of the smaller flow cell in the near corner region and may be improved by fine tuning the model contstants.

5.4 Model II vs LY

In this section the prediction of model II is compared with that of Nakayama et al.[2], who applied LY model in combination with PVM.

5.4.1 Square duct

Fig. 5.16 compares secondary flow streamlines of prediction of model II with that of Nakayama et al.[2]. The prediction is for a flow at Re=83,000. No experimental data is available for this Reynolds number flow. Distance of the centre of the flow cell from the corner has almost the same value in both cases. Secondary flow cell in model II's prediction shows orientation towards the corner as does the experimental data(for Re=150,000). With[2], the orientation is slightly towards the centre of the duct. Secondary flow generated is slightly less in model II's prediction.

In Fig. 5.5 isovels of normalised axial velocity of model II are compared with that of [2], for a flow at Re=83000. Both predictions look similar. Both underpredict along the corner bisector, with [2]'s prediction differing by approximately 3% as against the 4% deviation of model II's prediction from the experimental data. Near the centre of the duct [2]'s prediction difffers by about 1.1% from the experimental data.

5.4.2 Rectangular duct

Fig. 5.17 compares the secondary flow streamline of model II's prediction with that of Nakayama et al.[2], for a flow at Re=56,000, in a rectangular duct of aspect ratio 3. With model II, smaller cell dominates the flow near the corner. Distance of the centre of the larger cell from the corner is almost the same in both the predictions. This distance is approximately 1.2% longer than the corresponding distance of the

experimental data, at a slightly higher Reynolds number of 60,000. Maximum value of $(\psi/U_B D_h) \times 10^3$ with model II is approximately 14% less compared to [2].

In Fig. 5.13 normalised axial velocity distributions of model II's prediction are compared with that of [2], for a flow at at Re=56,000. Along the corner bisector, model II overpredicts to a maximum deviation of about 4% as against a maximum deviation of of about 5.5% of [2]. Along the y-axis, near the centre of the duct [2] overpredicts by nearly 4%. Near the corner isovels, [2] has nearly the same shape as that of the experimental data.

In Fig. 5.14 the normalised wall shear stress along the wider side of the duct is displayed for the predictions of model II and [2] along with the experimental data of Leutheusser[6]. Maximum deviation from the experimental data is approximately 5% for [2] versus about 6% for model II. With model II, a bump in the profile occurs at a point nearly 5% farther away from the corner, when compared with the experimental data. The corresponding value with [2] is about $2\frac{1}{2}\%$. Both predictions display a peak that is followed by a dip, as seen with the experimental data.

5.4.3 Summary

In general model II predicts turbulent flows in square and rectangular ducts, as good as Nakayama et al.[2] whose prediction scheme involves LY model and PVM. For the square duct, both schemes underpredicts along the corner bisectors. Distances of the secondary flow cell(larger one in case of rectangular duct) from the corner are almost equal with both the predictions,though they differ from the corresponding experimental values. In the case of axial velocity isovels in a 3 : 1 duct, model II predicts better than [2]. In wall shear stress profile, both the schemes overshoot the experimental value near the corner. Degree of overshooting is slightly less with [2]. Overall, it can be concluded that model II predicts on a par with Nakayama et al.[2] for square and rectangular ducts.

5.5 Other predictions

Fig. 5.18 shows the secondary velocity vector diagrams for a flow in square duct. Figure in the top indicates the flow at Re=83,000 whereas bottom one is for a flow at Re=150,000. Near the corner along the wall, secondary flow is almost at right angle to the walls of the duct. After some distance it becomes parallel to the wall. This may be due to the fact that the secondary flow is influenced by the gradient of the wall shear stress. Fig. 5.19 shows secondary velocity diagram for a flow in a rectangular duct with an aspect ratio of 3 : 1. Here too the flow near the corner along the walls of the duct, is almost perpendicular to the walls. This tendency is similar to the one observed with the flow in square duct.

In Fig. 5.20 the normalised axial velocity isovels and secondary flow streamlines are provided for a flow in a rectangular duct with an aspect ratio of 4 : 1. This is for a flow at Re=20,000. No experimental data is available for this condition. Axial velocity isovels display the distortion along the corner bisectors distinctively. General pattern matches with the experimental data available for other rectangular ducts. Same thing can be said about the secondary flow cells predicted. Centre of the larger flow cell is definitely close to the corner. Fig. 5.21 shows similar flow patterns for a flow in a 5 : 1 duct at Re=20,000. Comments made on the predictions of 4 : 1 duct apply here as well.

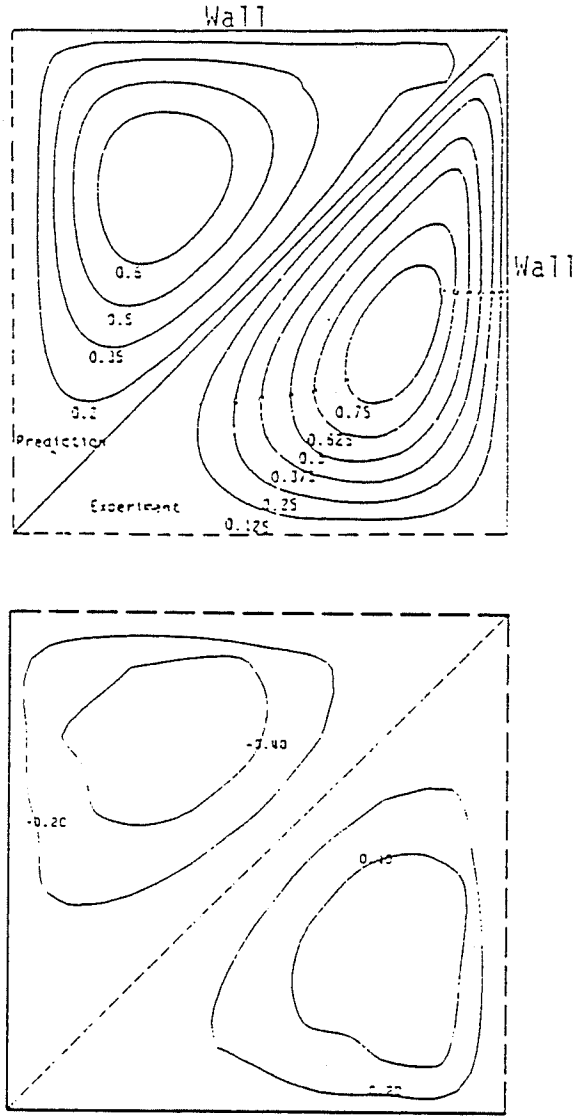

Figure 5.1: Comparison of secondary flow streamlines $(\psi/U_c D_h) \times 10^3$ for a square duct at Re=150,000.

- Top:
  - Upper triangle:Zhou's[52]prediction with LY model using VSM
  - Lower triangle:Experimental data of Hoagland[5]
- Bottom:Prediction with model I

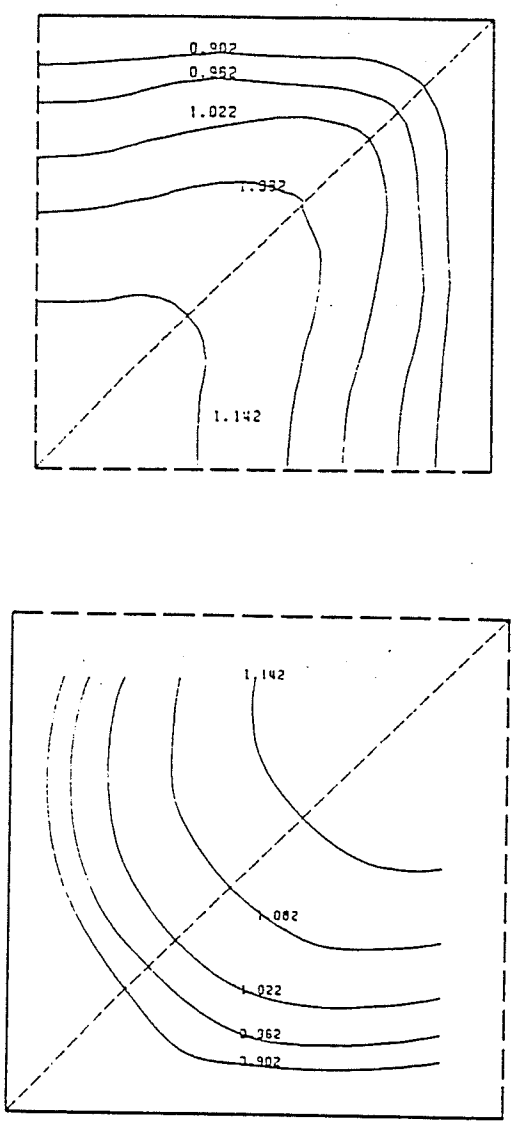

Figure 5.2: Comparison of normalised axial velocity(U/U_B)in a square duct at Re=83,000

- Top:Experimental data of Leutheusser[6]
- Bottom:Prediction with model I

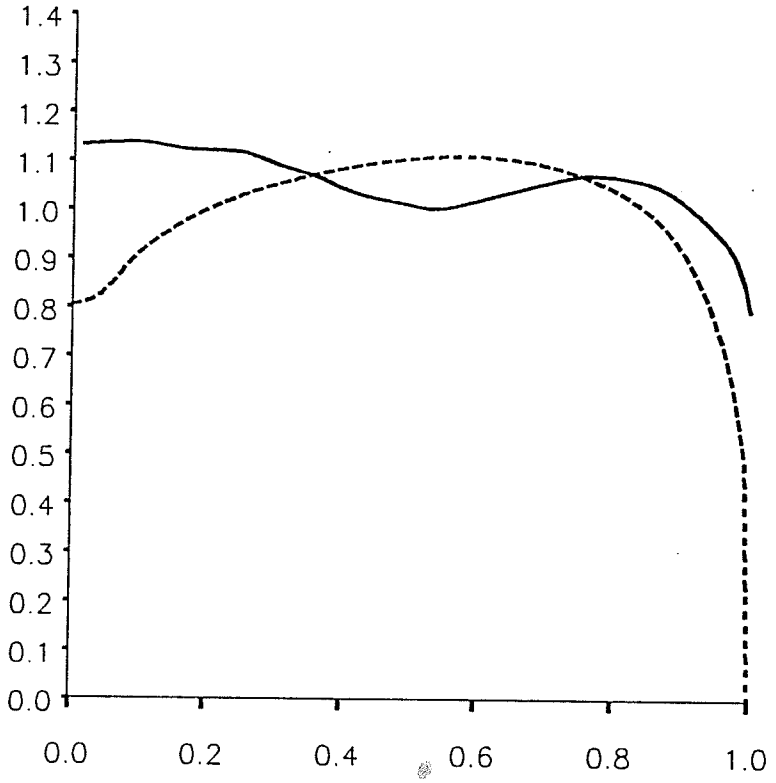

Figure 5.3: Comparison of normalised wall shear stress profile for a 3 : 1 rectangular duct along the wider side, at Re=56,000.

- - - - - - Experimental data of Leutheusser[6]
- — — — Prediction with model I

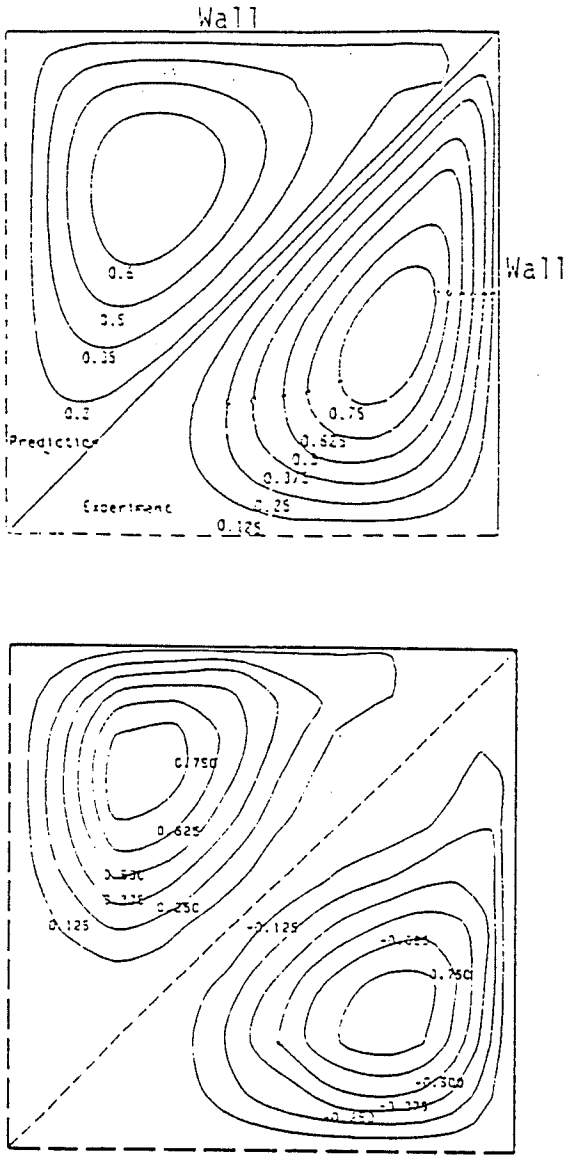

Figure 5.4: Comparison of secondary flow streamlines $(\psi/U_c D_h) \times 10^3$ for a square duct at Re=150,000.

- Top:LY model with VSM by Zhou[52]/ Experimental data of Hoagland[5]
- Bottom:Prediction with model II

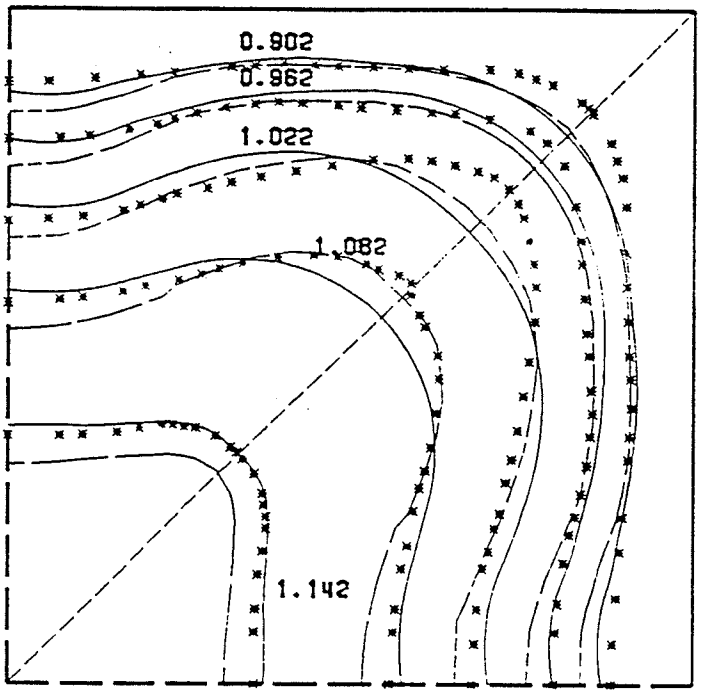

Figure 5.5: Comparison of mean velocity field (U/U_B) for a square duct at Re=83,000

- * * * * * Experimental data of Leutheusser(6).
- - - - - Prediction of Nakayama etal.[2]
- —— Prediction with model II

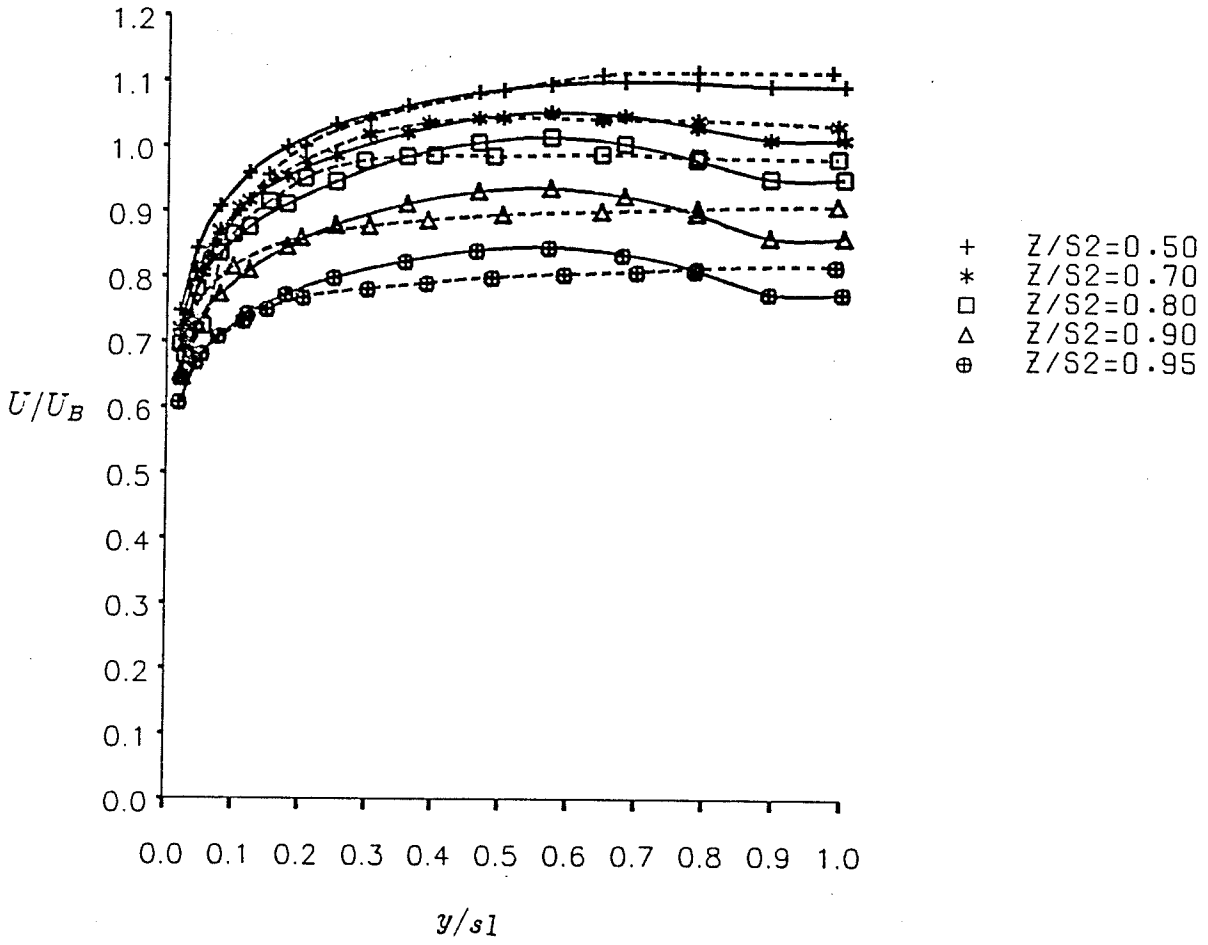

Figure 5.6: U/U_B profiles for a flow in a square duct at Re=215,000

- - - - - Experimental data of Launder and Ying[1]

——— Prediction with model II

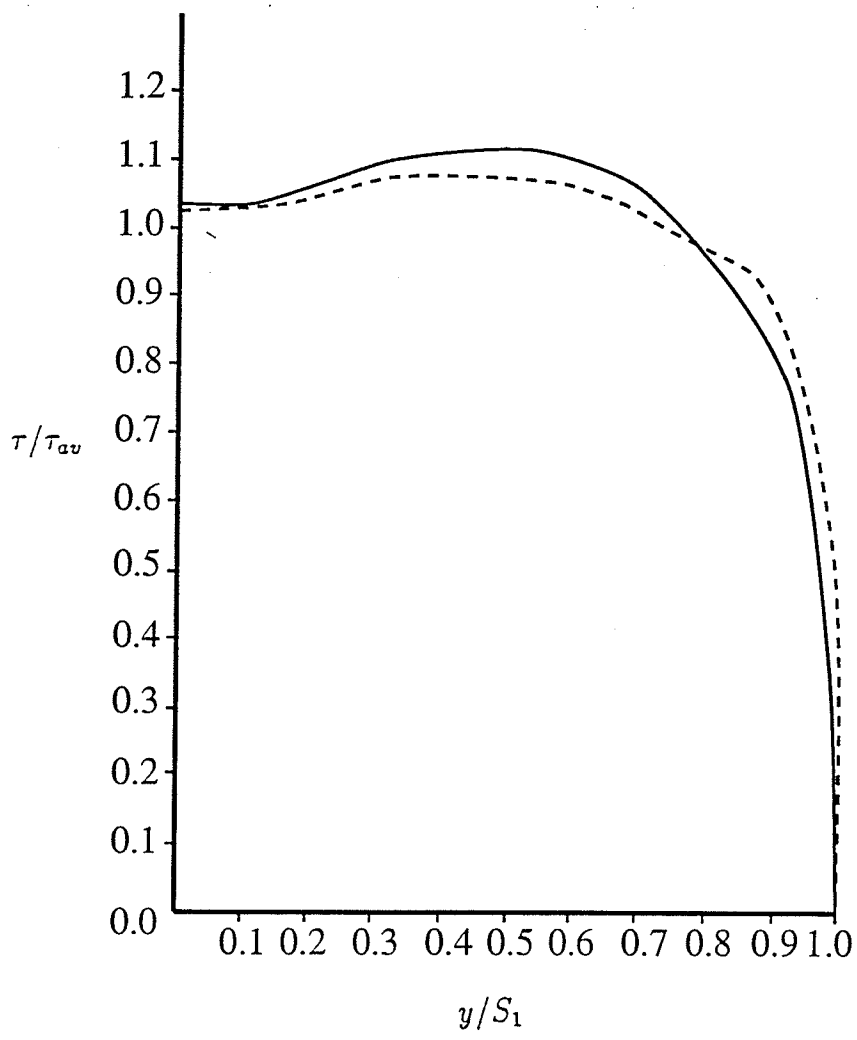

Figure 5.7: Comparison of wall shear stress profile (τ/τ_{av}) for a square duct at Re=34,000.

- —— Prediction with model II
- - - - - Experimental data of Leutheusser[6]

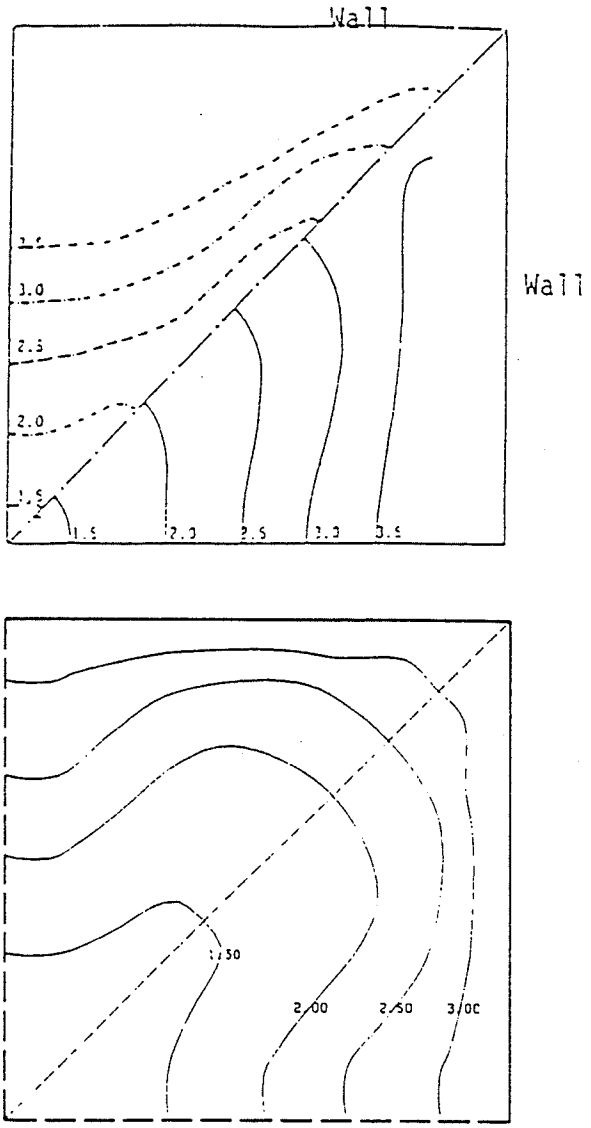

Figure 5.8: Comparison of k^+ contours in a square duct at Re=83,000.

- Top:
  - Upper triangle:Experimental data of Brundrett and Baines(7).
  - Lower triangle:Prediction of Zhou(54)using LY model and VSM
- Bottom:Prediction with model II

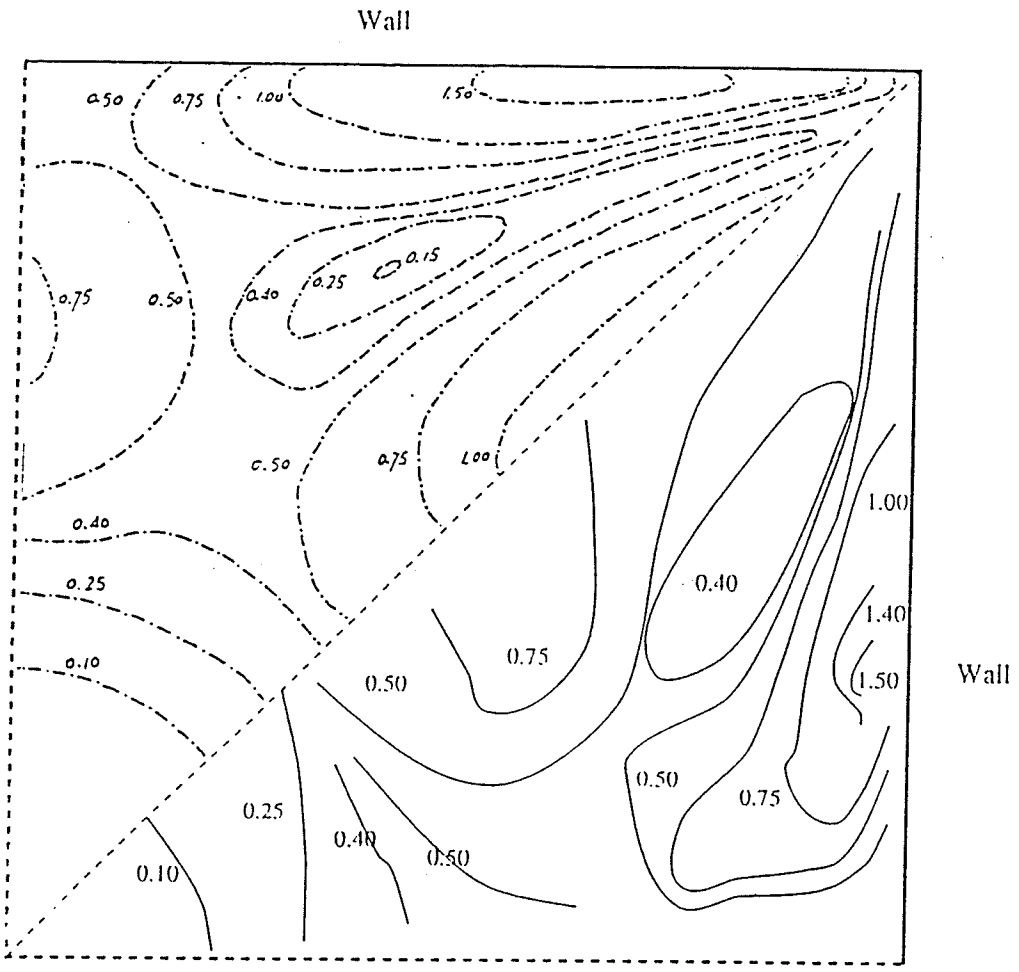

Figure 5.9: Contours of $(\overline{V}_{sec}/U_B) * 100$ in a square duct at Re=75,000

- Upper triangle:Experimental data of Hoagland[5]
- Lower triangle:Prediction with model II

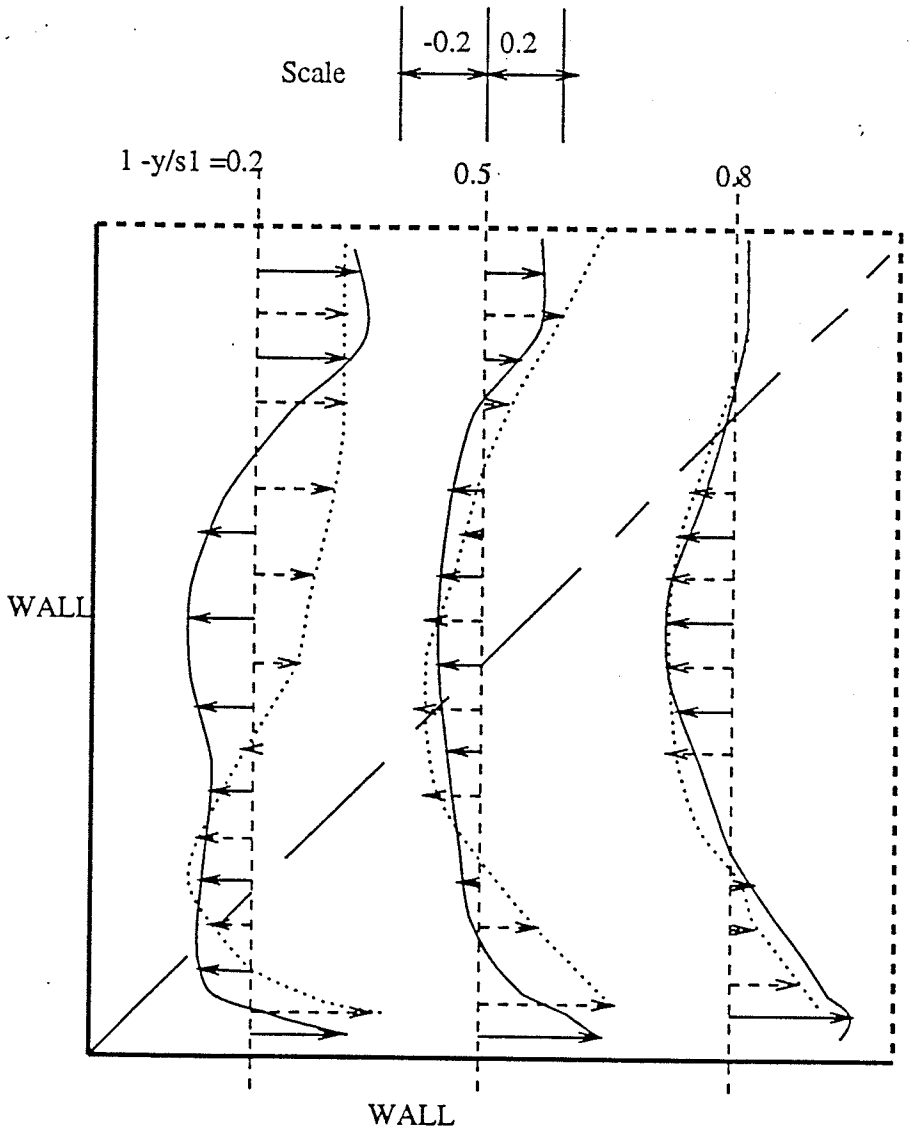

Figure 5.10: U/u_τ profiles for a flow in a square duct at Re=215,000

- - - - - Experimental data of Launder and Ying[1]
- —— Prediction with model II

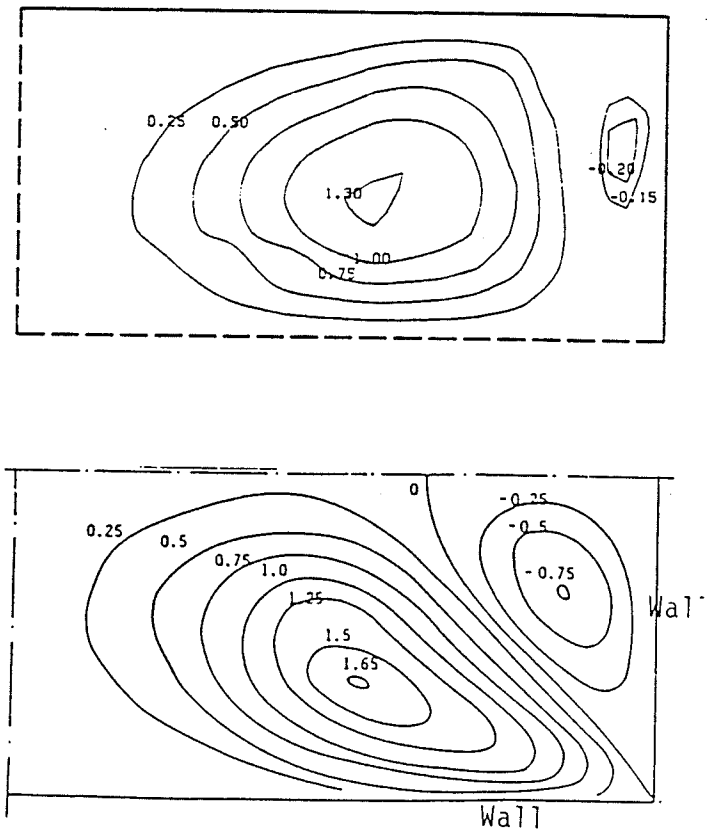

Figure 5.11: Comparison of secondary flow streamlines $(\dot{\psi}/\rho U_c D_h) \times 10^3$ in a 2:1 duct at Re=34,000.

- Top:Prediction with model II
- Bottom:Experimental data of Hoagland[5]

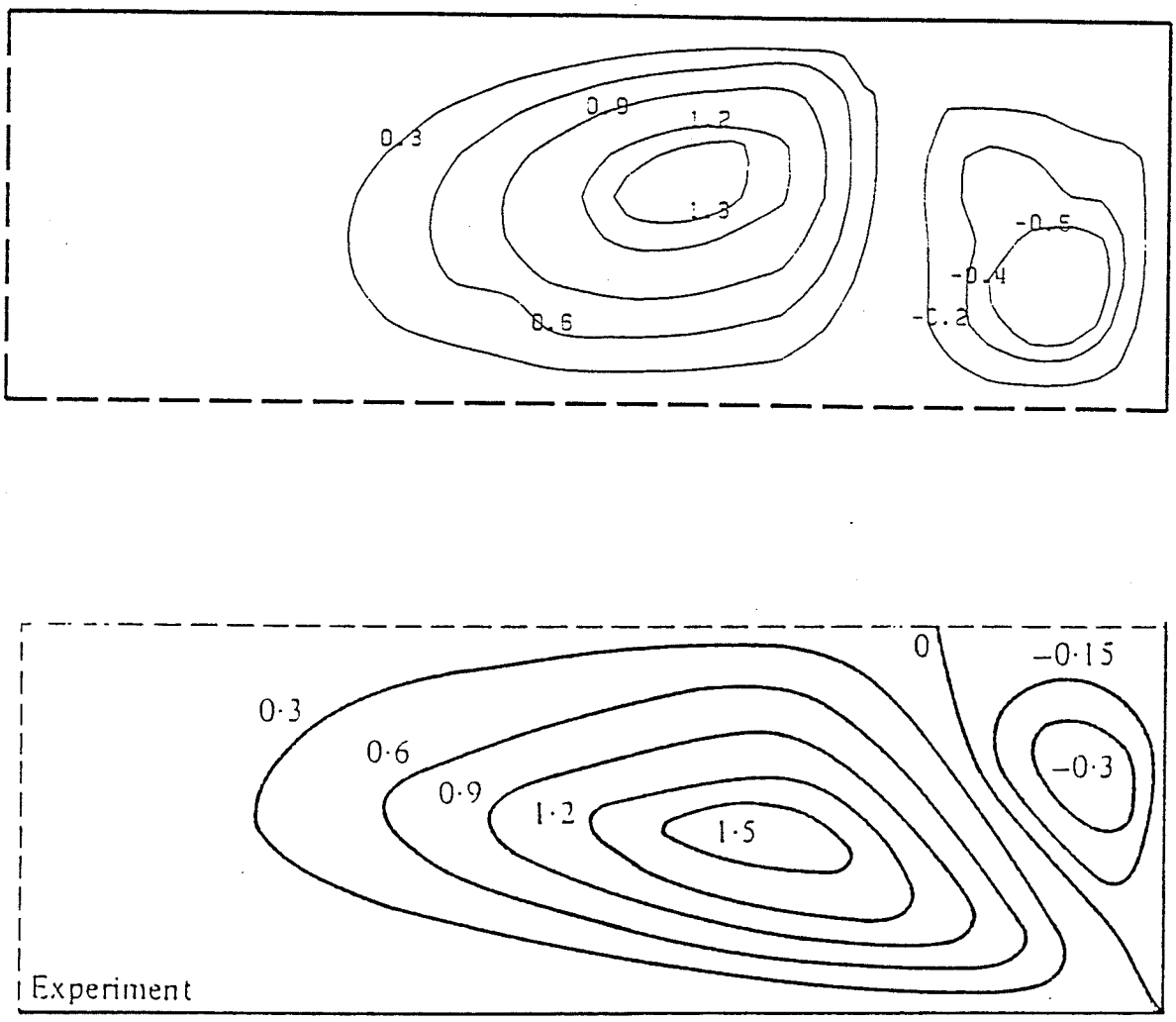

Figure 5.12: Comparison of secondary flow streamlines $(\psi/U_B D_h) \times 10^3$ in a 3:1 duct at Re=60,000.

- Top:Prediction with model II
- Bottom:Experimental data of Hoagland[5]

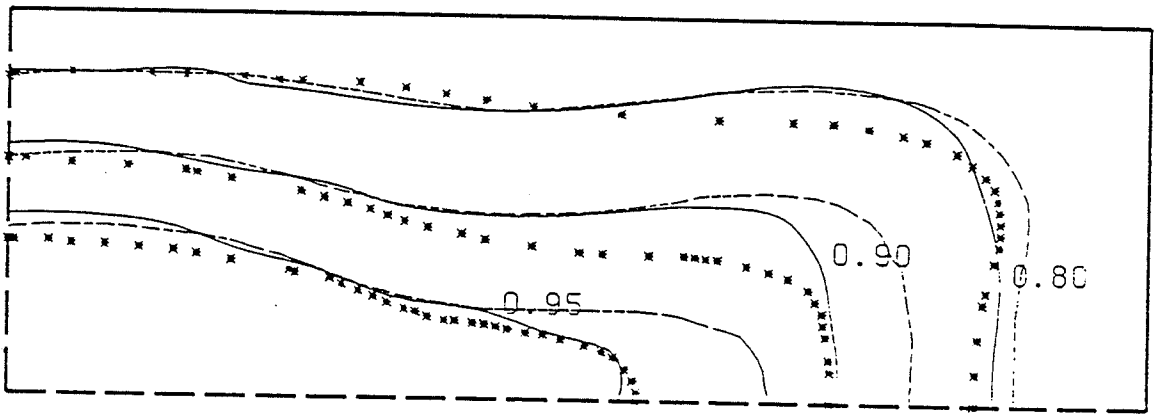

Figure 5.13: Comparison of mean velocity field (U/U_B) for a 3 : 1 duct at Re=56,000

- * * * * * Experimental data of Leutheusser[6]
- - - - - Prediction of Nakayama etal.[2]
- —— Prediction with model II

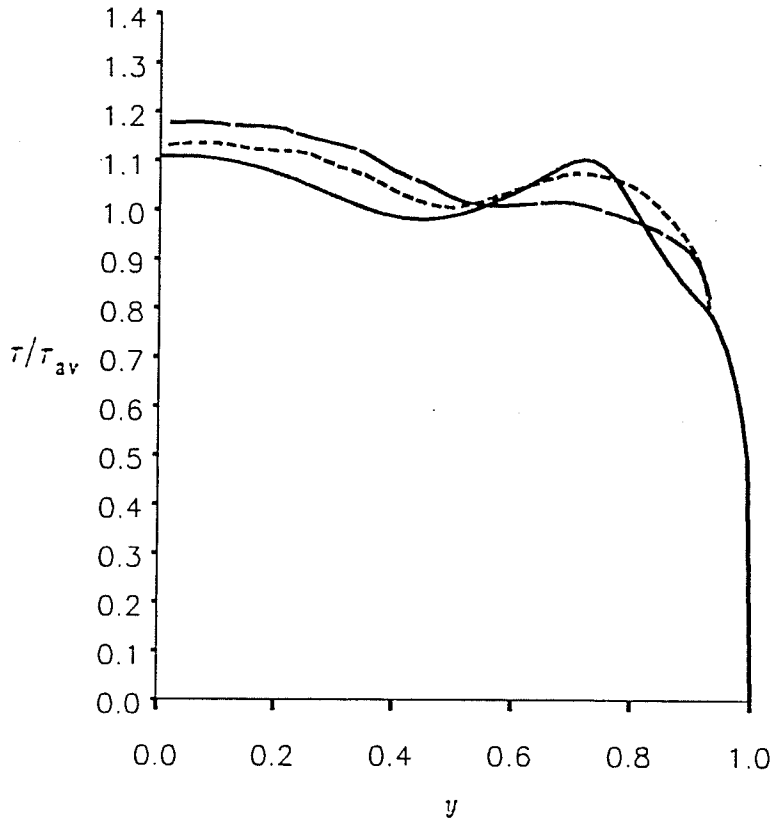

Figure 5.14: Wall shear stress (τ/τ_{av}) profile along the wider side of a 3:1 duct at Re=56,000.

- – – – Experimental data of Leutheusser[6]
- - - - - Nakayama et al.[2]
- ——— Prediction with model II

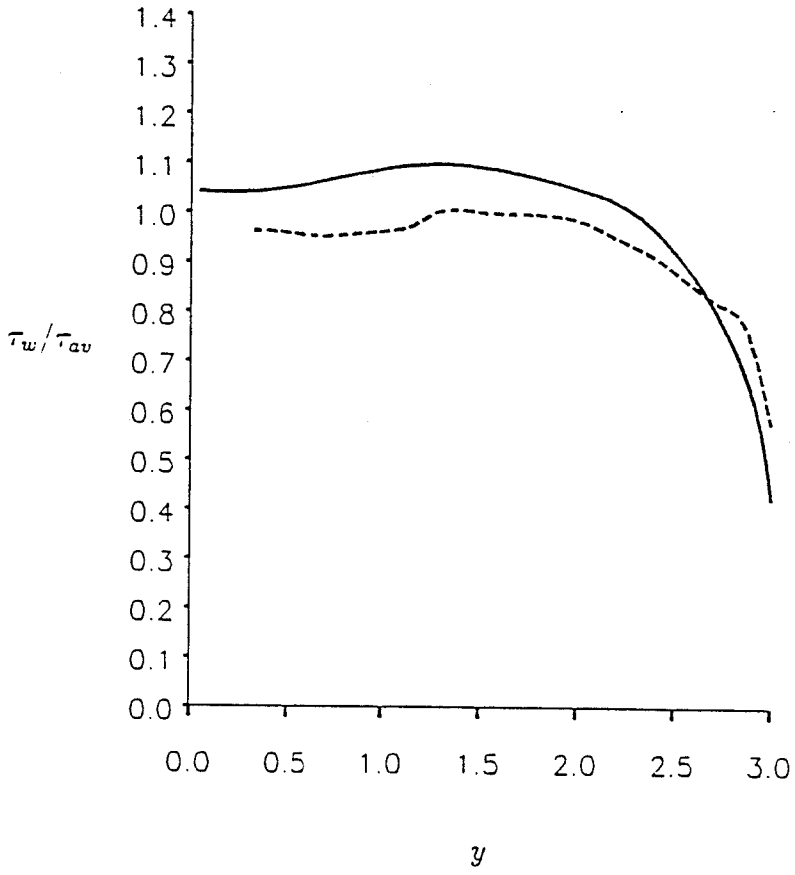

Figure 5.14: Wall shear stress distribution (τ/τ_{av}) for a 3:1 duct, along the shorter side at Re=56,000.

- - - - - Experimental data of Leutheusser[6]
- —— Prediction with model II

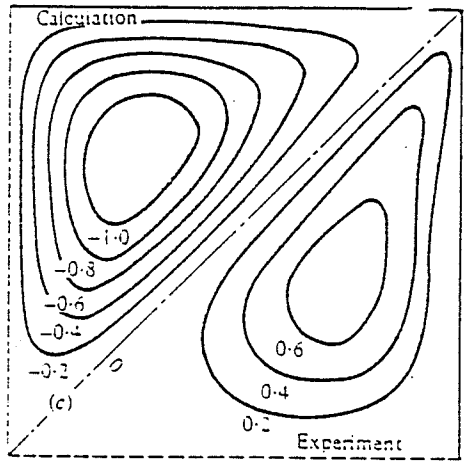

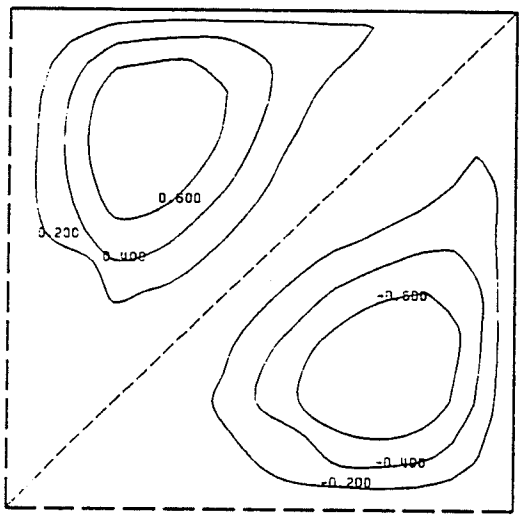

Figure 5.16: Secondary flow streamlines in a square duct

- Top
  - Upper Triangle:Nakayama etal.[2]at Re=83,000
  - Lower Triangle:Experimental data of Gessner and Jones[14] at Re=150,000
- Bottom:Prediction with model II at Re=83,000

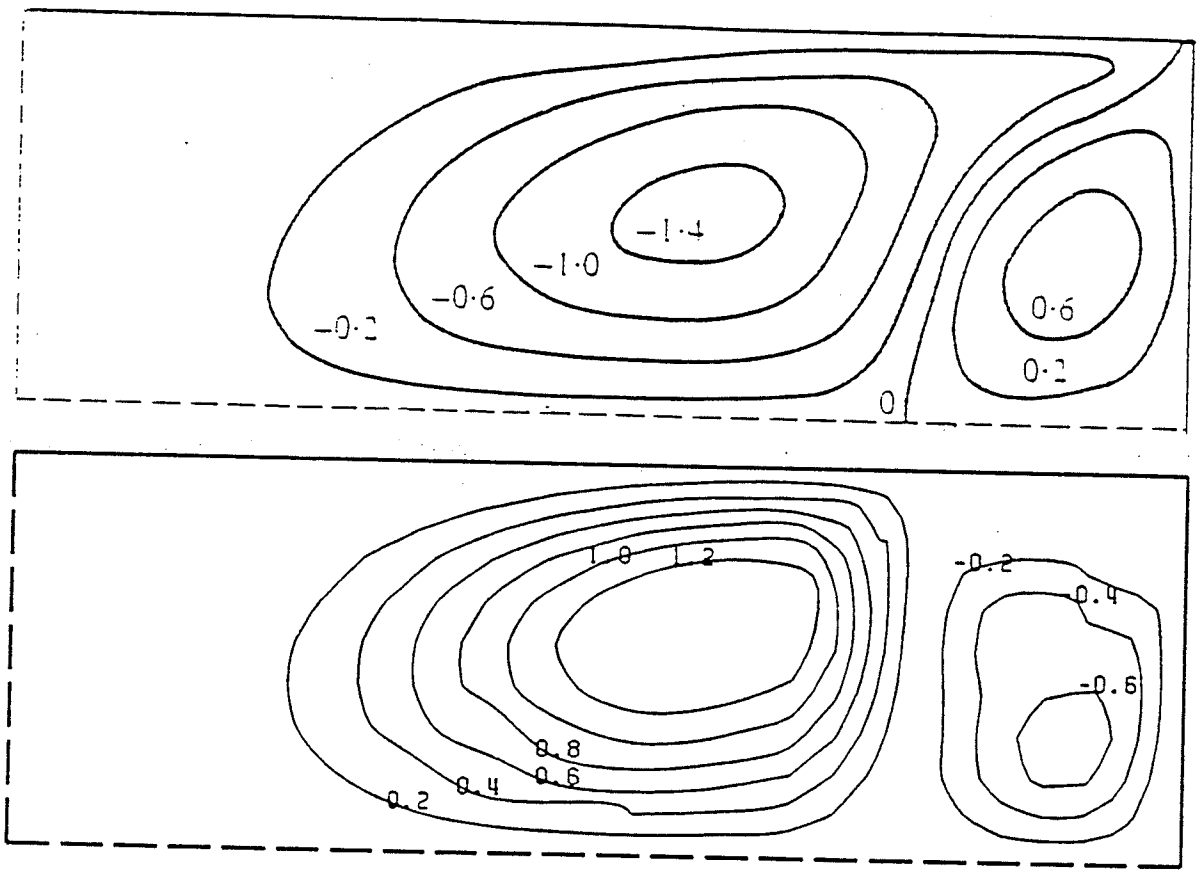

Figure 5.17: Secondary flow streamlines $(\psi/U_B D_h) \times 10^3$ of a 3:1 rectangular duct at Re=56,000.

- Top:Nakayama etal.[2]
- Bottom:Prediction with model II

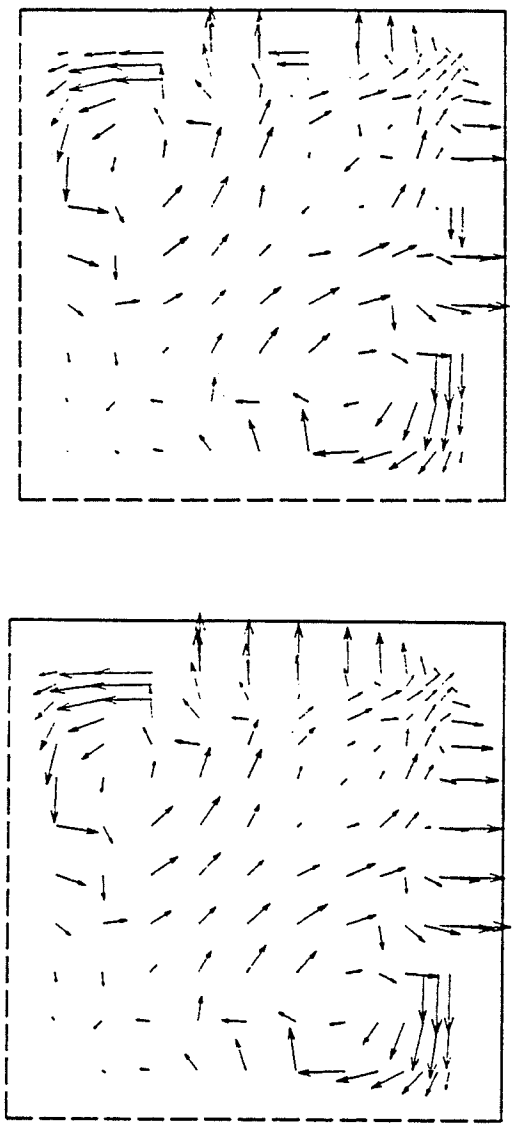

Figure 5.18: Secondary velocity vector diagram of model II in a square duct.

- Top:Re=83,000
- Bottom:Re=150,000

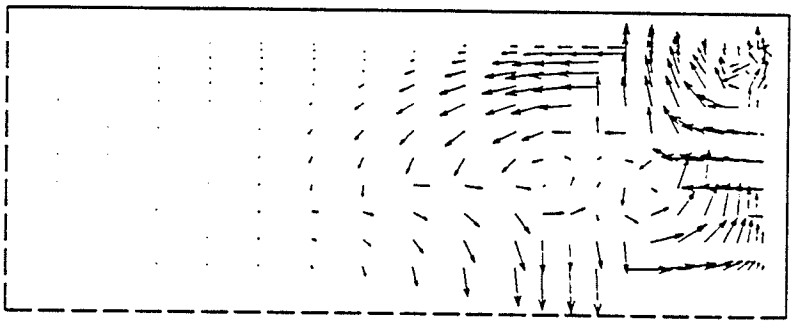

Figure 5.19: Secondary velocity vector diagram of model II in a 3:1 duct at Re=56,000.

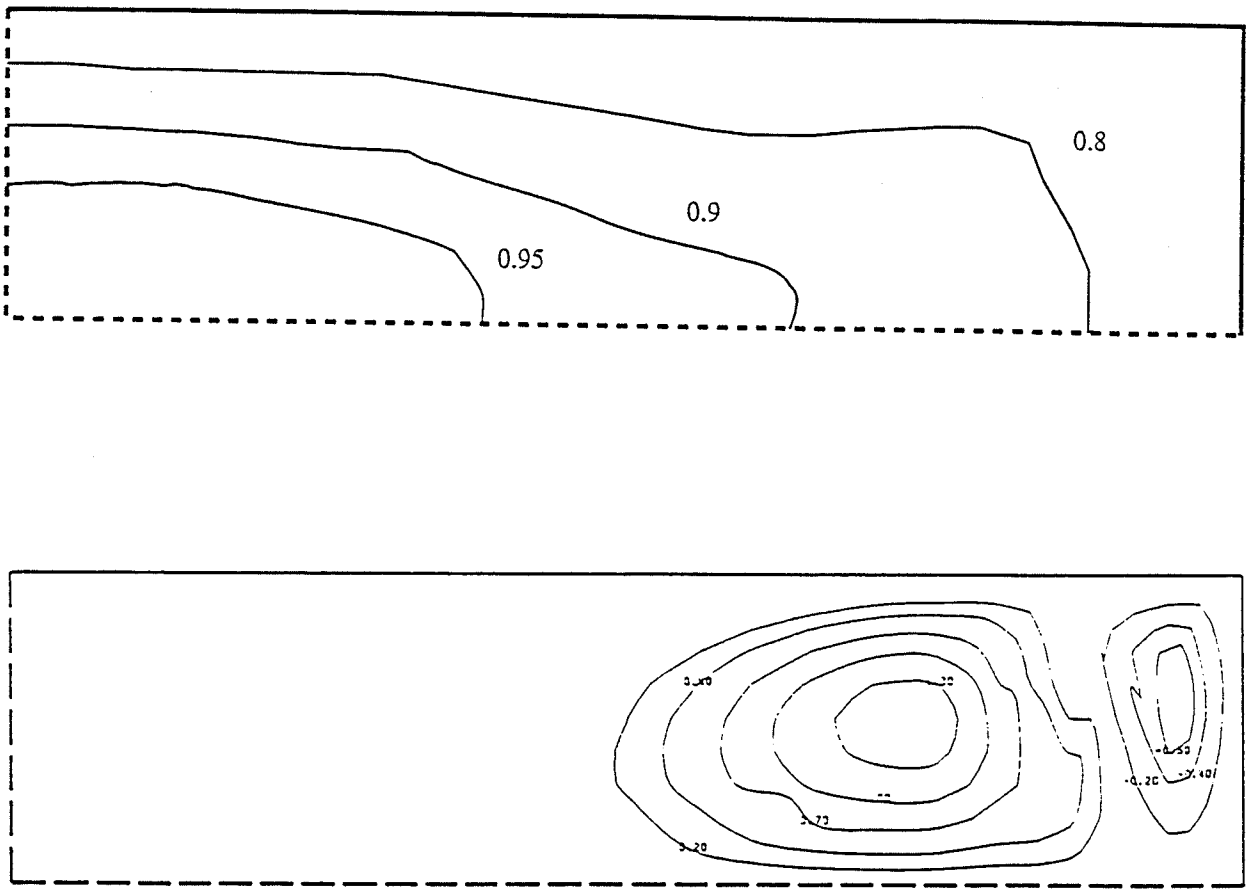

Figure 5.20: Mean velocity field prediction with model II for a 4:1 duct at Re=20,000.

- Top:(U/U_c) isovels
- Bottom:Secondary flow streamlines $(\psi/U_B D_h) \times 10^3$

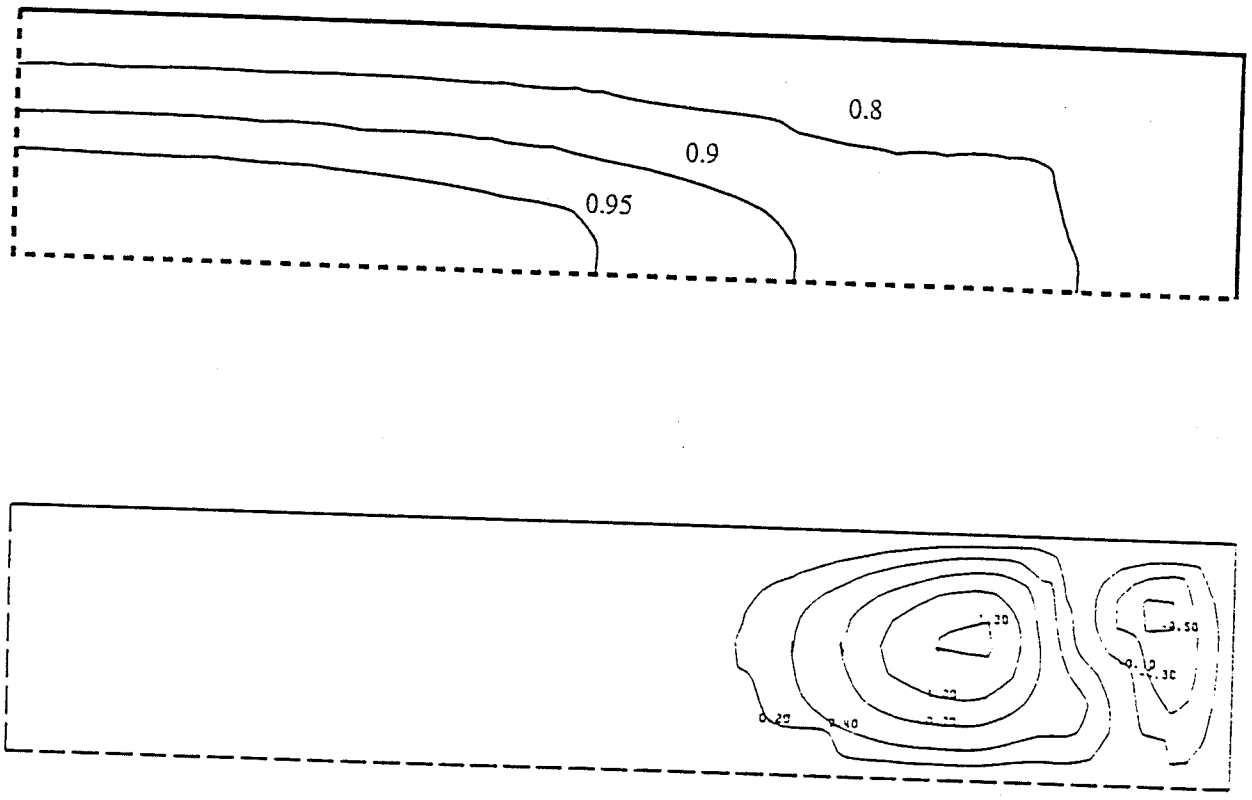

Figure 5.21: Predictions with model II for a 5:1 duct at Re=20,000.

- Top:(U/U_c)prediction.
- Bottom:Secondary flow streamline $(\psi/U_B D_h) \times 10^3$ prediction.

Chapter 6

Conclusions

Thus three different models, based on wall shear stress are proposed. These models have been tried numerically. Model I and model I A,had been tried with Vorticity Stream Function Method. Model II was tried with SIMPLE algorithm and Primitive Variable Method in a square duct and various rectangular ducts of many aspect ratios. Predicted results are plotted and then compared with the experimental data and the predictions of other established models. Main parameters compared, are secondary velocities, axial velocity and wall shear stress. Normalised turbulent kinetic energy is also compared.

Model I produced symmetrical predictions in a square duct. Though its predictions are comparable to the prevalent models, it did not produce sufficient distortion along the corner bisector. Model I A is a transitional one which leads the way to a further developed model, model II. For the square duct, model II underpredicts along the corner bisector by a maximum of approximately 4%. However in the rest of the zone its prediction matches the experimental data within a 2% deviation. It is also successful in producing the sensitive variation along the profile of many parameters. Its wall shear stress prediction falls within a tolerance of about $5\frac{1}{2}\%$ with the experimental data. In rectangular ducts, it generated predictions that match with the experimental data, with a maximum deviation of approximately 4%. Secondary flow cells generated stay close to the corner.

Model II also compares well with the established LY model, tried by Nakayama et al.[2] with PVM. For the square duct, model II predicts accurately in the core region. Near the corner however, [2] predicts better. For rectangular ducts, the model II predictions are better than [2] as far as the axial velocity is concerned. But [2] predicts better wall shear stress profiles. So it can be stated that model II predicts about as well as the prediction scheme of [2].

Overall the predictions of model II match with the experimental data, with a maximum deviation of approximately 4% to 6%. It is also fair to conclude that model II's predictions are on a par with the predictions of established models, for e.g. the Launder and Ying[1]'s model. Thus model II provides a numerical scheme which can serve as an alternative to the Launder and Ying[1] model in predicting turbulent flows in square and rectangular ducts.

Since model II used the same set of empirical constants in all the ducts considered, there appears to be a high probability that model II can be applied for turbulent flows through ducts of other non-circular cross sections such as triangular and trapezoidal. This can be tested in future works. Performance of model II can also be improved further by way of fine tuning the model constants.

References

[1] Launder, B.E.and Ying, W.M. 1973 Prediction of flow and heat transfer in ducts of square cross section. *Proc. Instrn. Mech. Engrs.*, 187, 455-461

[2] Nakayama, A., Chow, W.L.and Sharma, D. 1983 Calculation of fully developed turbulent flows in ducts of arbitrary cross section. *J. Fluid Mech.*, 128, 199-217

[3] Seale, W.J. 1982 Turbulence generated secondary flows in ducts of non-circular cross section. *J. of Mechanical Engineering Sciences*, 24, No.3, 119-127

[4] Perkins, H.J. 1970 The formation of streamwise vorticity in turbulent flow. *J. Fluid Mech.*, 44, 721-40

[5] Hoagland, L.C. 1960 Fully developed turbulent flow in straight rectangular ducts. *Ph.D Thesis, M.I.T.*

[6] Leutheusser, H.J. 1963 Turbulent flow in rectangular ducts. *J. Hydraul. Div. A. S. C. E.* 89(HY3), 1-19

[7] Brundrett, E. and Baines, W.D. 1964 Production and diffusion of vorticity in duct flow. *J. Fluid Mech.*, 19, 375-394

[8] Aly, A.M.M., Trupp, A.C.,and Gerrard, A.D. 1978 Measurements and prediction of fully developed turbulent flow in an equilateral triangular duct. *J. Fluid Mech.*, 85, 57-83

[9] Nikuradse, J. 1926 Untersuchungen uber die geschwindikeits verteitung in turbulenten stromungen. *Ph.D., Thesis. Gottingen*

[10] Prandtl, L. 1926 *Proc. Secon. Int. Congr. of Applied Mech.*, p71, et seq Zurich

[11] Einstein, H.A, and Li, H. 1958 *American Geophysical Union*, 39, 1085-1088

[12] Hinze, J.O. 1967 *Phys.Fluids*, Suppl. 10. S122-S125

[13] Townsend, A.A. 1956 *The stucture of turbulent shear flow.* Cambridge University Press

[14] Gessner, F.B. and Jones, J.B. 1965 On some aspects of fully developed turbulent flow in rectangular channels. *J. Fluid Mech.*, 23, 689-713

[15] Launder, B.E. and Ying, W.M. 1972 Secondary flows in ducts of square section. *J. Fluid Mech.*, 54, 289-95

[16] Launder, B.E. and Singham, J.R. 1971 The prediction of fully developed flow in non-circular ducts. *Symp. Internal Flow, Univ.of Salford*, Paper 12

[17] Wilson, N.W., Azad, R.S. and Trupp, A.C. 1971 Analysis of the effect of secondary flows on the longitudinal velocity distribution in square ducts. *Symp. Internal Flows, Univ.of Salford*, Paper 11

[18] Gerard, R. 1974 Finite element solution for flow in non-circular conduits. *Proc. A.S.C.E.*, 100, (HY3), 425-441

[19] Tracy, H.J. 1965 Turbulent flow in a three dimensional channel. *J. of the Hydraulics Division, Proc.A.S.C.E.*, 91, (HY6), 9-35

[20] Hinze, J.O. 1973 Experimental investigation of secondary currents in the turbulent flow through a straight conduit. *Appl. Sci. Res.*, 28, 453-465

[21] Kjellstrom, B. 1971 Studies of turbulent flow parallel to a rod bundle of triangular array. *AB Atomenergi Rep.* AE-RV-196, Sweden

[22] Trupp, A.C.and Azad, R.S. 1975 The structure of turbulent flow in triangular array rod bundles. *Nuclear Eng. Design*, 32, No.1, 47-84

[23] Lyall, H.G. 1971 Measurement of flow distribution and secondary flow in ducts composed of two square interconnected sub channels. *Symp. Internal Flows, Univ. of Salford*, Paper 33,E16-E23

[24] Kacker, S.C. 1973 Some aspects of fully developed turbulent flow in non-circular ducts. *J. Fluid Mech.*, 57, 583-602

[25] Rowe, D.S. 1973 Measurements of turbulent velocity intensity and scale in rod bundle flow channels. *BNWL*, Rep. 1736, UC-80, Battelle

[26] Carajilescov, P and Todreas, N.E. 1976 Experimental study of axial turbulent flows in an interior subchannel of a bare rod bundles. *Trans.A.S.M.E., J. Heat Transfer*, 98, 262-68

[27] Rehme, K. 1977 Experimentelle untersuchungen der turbulenten stromung in einem wandkanal eines stabbundles. *Kenforschungszentrum, KFK* 2441

[28] Seale, W.J. 1982 Measurements and prediction of turbulent flow in a simulated rod bundle. *J. Fluid Mech.*, 123, 399-423

[29] Hooper, J.D. and Rehme, K. 1984 Large scale stuctural effects in developed turbulent flow through closely spaced rod arrays. *J. Fluid Mech.*, 145, 305-337

[30] Khalifa, M.M.A. 1987 Measurements and predictions of turbulent flow and heat transfer in trapezoidal ducts. *Ph.D. Thesis, Univ. of Manitoba*

[31] Ahmed, S. and Brundrett, E. 1971 Turbulent flow in non-circular ducts.Part 1. *J. Heat Mass Transfer*, 14, 365-371

[32] Po, J.K. 1975 Developing turbulent flow in the entrance region of a square duct. *M.Sc. Thesis, University of Washington*

[33] Melling, A. and Whitelaw, J.H. 1976 Turbulent flow in a rectangular duct. *J. Fluid Mech.*, 78, 289-315

[34] Lund, E.G. 1977 Mean flow and turbulent characteristics in near corner region of a square duct. *M.Sc. Thesis, University of Washington*

[35] Rodi, W. 1980 *Turbulence models and their applications in hydraulics, State of art review.* International Association for Hydraulics Research, Delft, The Netherlands

[36] Hirata, M, Tanaka, H, Tokyo, J, Kawamura, H, Kasagi, N, Ibaraki-Ken, J 1982 Heat transfer in turbulent flows. *Procdgs. of Seventh International Heat Transfer Conf.*, 1, 31-58

[37] Deissler, R.G. and Taylor, M.F. 1958 Analysis of turbulent flow and heat transfer in non-circular ducts. *NACA Tech. Note 4384*

[38] Rapier, A.C. and Redman, J.D. 1964 The calculation of velocity in rod clusters. *UKAEA Report TRG 838*

[39] Bender, D.J., Switick, D.M. and Field, J.H. 1967 Turbulent velocity distribution in a rod bundle. *G.E.A.P. 5411*

[40] Ibragimov, M.Kh. et al. 1966 Calculation of tangential stresses at the wall of a channel and the velocity distribution in the turbulent flow of a fluid. *Soviet Atomic Energy*, 21, 731-739

[41] Meyder, R. 1975 Turbulent velocity and temperature distribution in the central sub-channel of rod bundles. *Nuclear Eng. Design*, 35, 181-189

[42] Ramm, H. and Johannesen, K. 1975 A phenomenological turbulence model and its application to heat transport in infinite rod arrays with axial turbulent flow. *J. Heat Trans. A.S.M.E-97*, 75-HT-MM, 231-237

[43] Nijsing, R. 1972 Heat exchange and heat exchangers with liquid metals. *AGARD- LS- 57- 72*

[44] Hanjelic, K. and Launder, B.E. 1972 A Reynolds stress model of turbulence and its application to asymmetric boundary layers. *J. Fluid Mech.*, 52, 609-638

[45] Naot, D., Shavit, A. and Wolfshtein, M. 1974 Numerical calculation of Reynolds stresses in a square duct with secondary flow. *Warme-und-Stoff-ubertragung*, 7, 151-161

[46] Reece, G.J. 1976 A generalized Reynolds stress model of turbulence. *Ph.D. Thesis, University of London*

[47] Carajilescov, P. and Todreas, N.E. 1975 Experimental and analytical study of axial turbulent flow in an interior sub-channel of a bare-rod-bundle. *Trans. A.S.M.E* 75-WA/ HT-51

[48] Tatchell, D.G. 1975 Convection processes in confined three dimensional boundary layers. *Ph.D. Thesis, University of London*

[49] Gessner, F.B. and Emery, A.F. 1976 A Reynolds stress model for turbulent corner flows Part I. *J. Fluid Eng.*, 98, 261-268

[50] Alshamani, K.M.M. 1978 Correlation among turbulent shear stress,turbulent kinetic energy and axial turbulent intensity. *AIAA J.*, 16, 859-861

[51] Alshamani, K.M.M. 1979 Relationship between turbulent intensities in turbulent pipe and channel flows. *Aero J.*, 83, 159-161

[52] Zhou, Z. 1985 A comparison of turbulent flow predictions for rectangular ducts using five vorticity source models. *M.Sc. Thesis, University of Manitoba*

[53] Gosman, A.D, Pun, W.M, Runchal, A.K, Spalding, D.B. and Wolfshtein, M. 1969 *Heat and mass transfer in recirculating flows*, Academic Press, London

[54] Patankar, S.V.and Spalding, D.B. 1972 A calculation procedure for heat,mass and momentum transfer in 3-D parabolic flows. *Int. J. Heat Mass Trans.*, 15, 1787-1806

[55] Caretto, L.S, Curr, R.M.and Spalding, D.B. 1972 Two numerical procedures for three dimensional recirculating flows. *Computer Methods in Applied Mechanics and Engineering*, 1, 39-57

[56] Launder, B.E., Reece, G.J.and Rodi, W. 1975 Progress in the development of a Reynolds stress turbulence closure. *J. Fluid Mech.*, 68, 537-566

[57] Gosman, A.D.and Rapley, C.W. 1980 Fully developed flow in passages of arbitrary cross section. *Recent Advances in Numerical Methods in Fluids*, Pineridge Press Ltd.

[58] Scarborough, J.B. 1958 *Numerical mathematical analysis*, 4th edition, John Hopkins Press, Baltimore

[59] Patankar, S.V. 1980 *Numerical Heat Transfer.* Hemisphere Publishing Corporation, NY

[60] Gessner, F.B. and Po, J.K. 1976 A Reynolds stress model for turbulent corner flows, Part 2: Comparison between theory and experimemt. *J. Fluids Engineering*, 98, 269-277

[61] Naot, D.and Rodi, W. 1982 Numerical simulation of secondary currents in a channel flow. *J. Hydraul. Div. A.S.C.E.* 108 (HY8), 948-968

Appendix A

Computer Programming

FORTRAN Variable Explanation

ALITE	Maximum number of iterations allowed
AMU	μ
AMUT	μ_t
CAPA	κ
CD	C_D
CDASH	C'
CDASHK	C'_k
CKO	$C_{k,o}$
DEQ	Hydraulic diameter of the duct
DGPTY	Distance between the main grid points in y direction
DGPTZ	Distance between the main grid points in z direction
EALPHA	Under relaxation factor for ϵ equation
ECOUNT	Convergence criterion for ϵ
NGPY	Number of grid points in y direction of main grid
NGPZ	Number of grid points in z direction of main grid
PALPHA	Under relaxation factor for p
PC	Pressure correction variables
PCALPH	Under relaxaton factor for p'
PRCOUN	Convergence criterion for p
PRIME	Logical switch for running the program with or without secondary flows.
PSI	Streamfunction,Ψ
RE	Reynolds number of the flow
RHO	Density of the fluid,ρ
S1,S2	Dimensions of the duct quadrant

SIGMAE	σ_ϵ
SIGMAK	σ_k
TED	Turbulent dissipation rate,ϵ
TKALPH	Under relaxation factor for k
TKCOUN	Convergence factor for k
TKE	Turbulent Kinetic Energy,k
TOTITR	Number of iterations executed
TOWV,TOWW	Wall shear stresses
UALPHA	Under relaxation factor for U
UB,UBAV	Bulk velocity of the flow in axial direction
UCOUNT	Convergence criterion for U
UFV,UFW	Frictional velocities
VCHK	Convergence criterion for corrected V
VCOUNT	Under relaxation factor of V
VDGPTY	Distance between V grid points in y direction
VO	Old value of V stored in the previous iteration
VY	Grid point location of Vgrid in y direction
VYDEL	Grid width in y direction of V grid
WCHK	Convergence criterion for corrected W
WCOUNT	Under relaxation factor of W
WDGPTZ	Distance between V grid points in y direction
WO	Old value of W stored in the previous iteration
WZ	Grid point location of Wgrid in z direction
WZDEL	Grid width in z direction of W grid
YDEL	Grid width in the y direction for Main grid
YGB	Locations of Main grid boundaries in y direction
ZDEL	Grid width in the z direction for Main grid

ZGB	Locations of Main grid boundaries in z direction

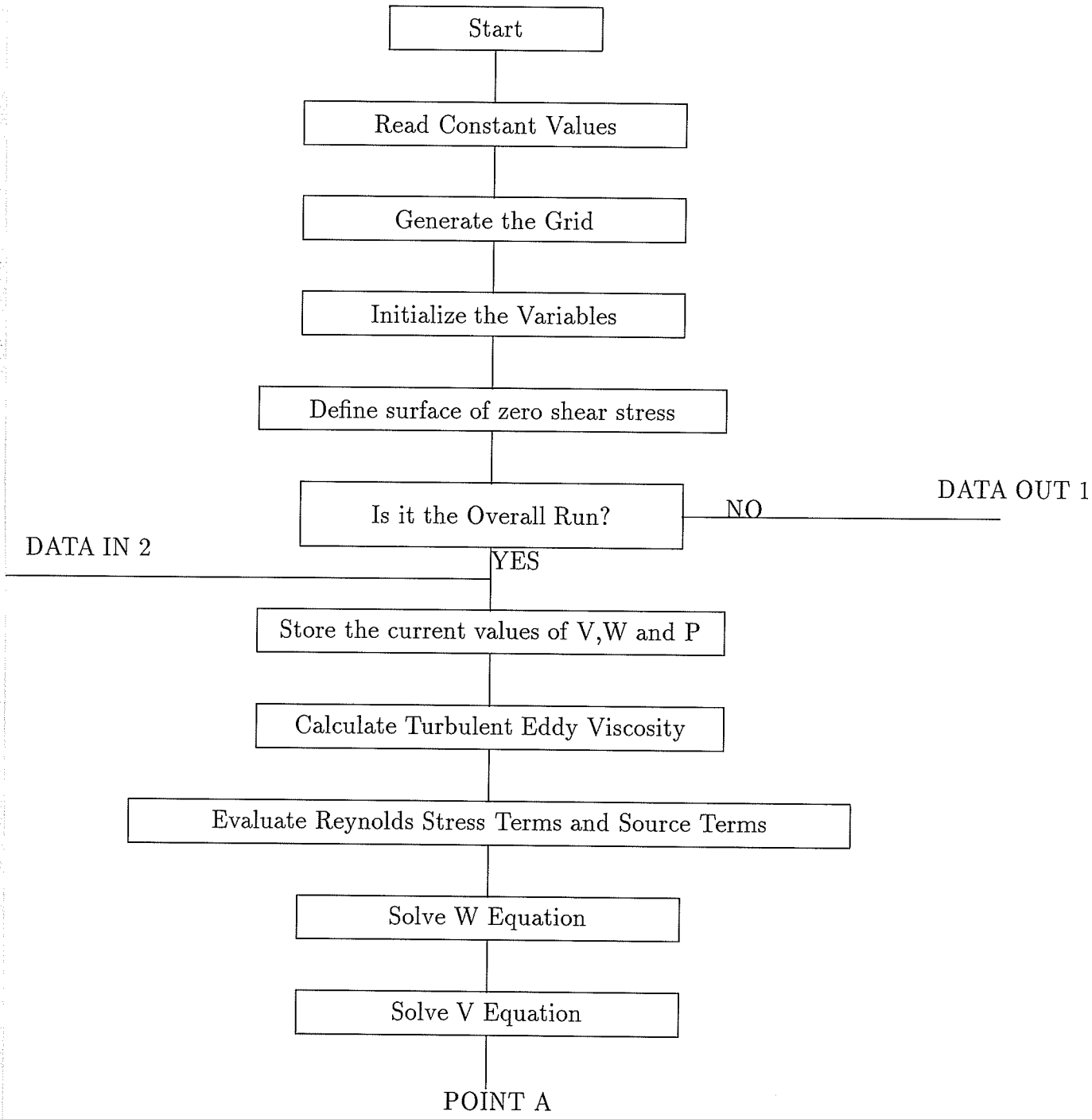

Flowchart for the Computer program

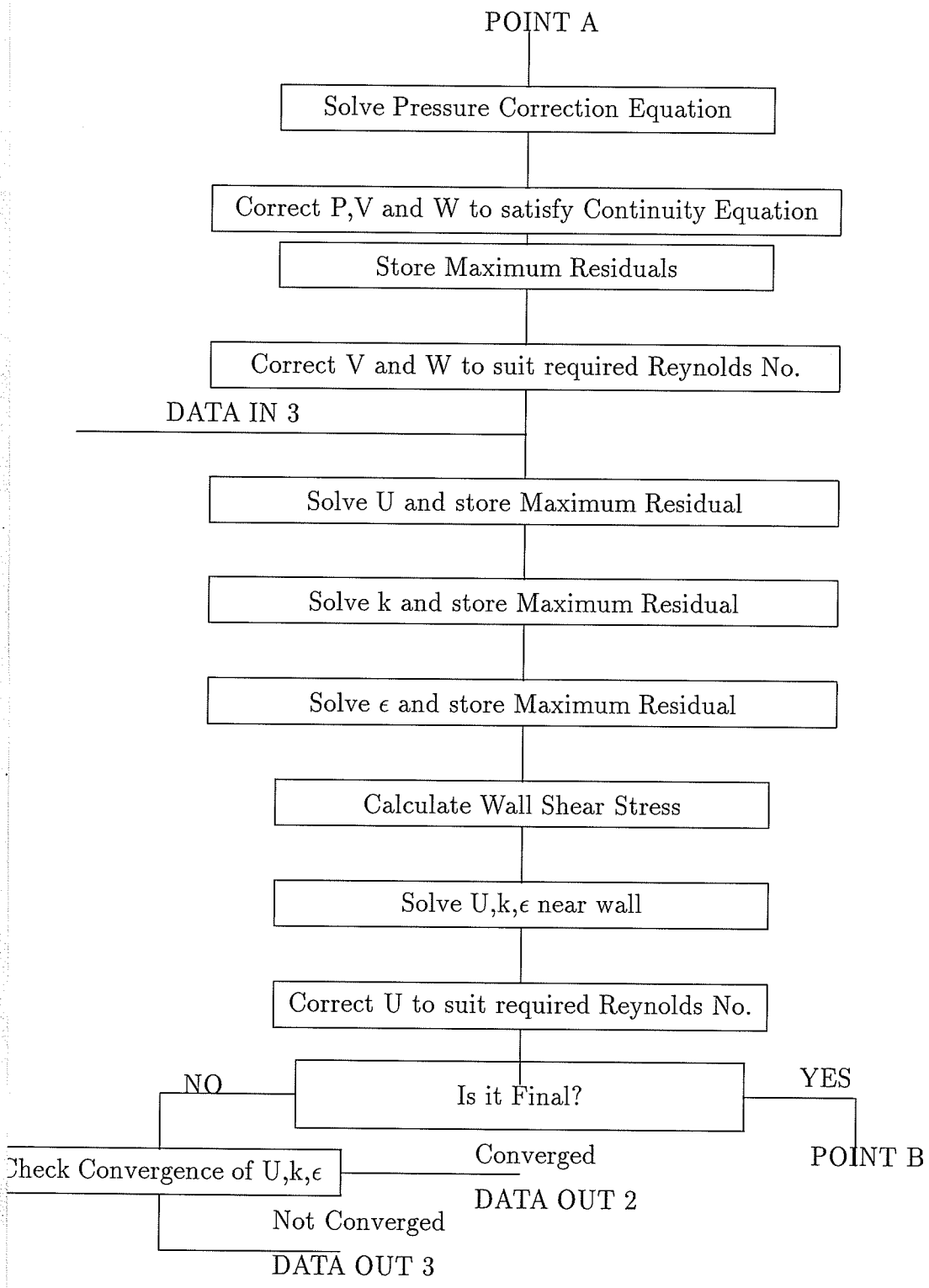
POINT A
Solve Pressure Correction Equation
Correct P,V and W to satisfy Continuity Equation
Store Maximum Residuals
Correct V and W to suit required Reynolds No.
DATA IN 3
Solve U and store Maximum Residual
Solve k and store Maximum Residual
Solve ϵ and store Maximum Residual
Calculate Wall Shear Stress
Solve U,k,ϵ near wall
Correct U to suit required Reynolds No.
NO
Is it Final?
YES
Check Convergence of U,k,ϵ
Converged
DATA OUT 2
POINT B
Not Converged
DATA OUT 3

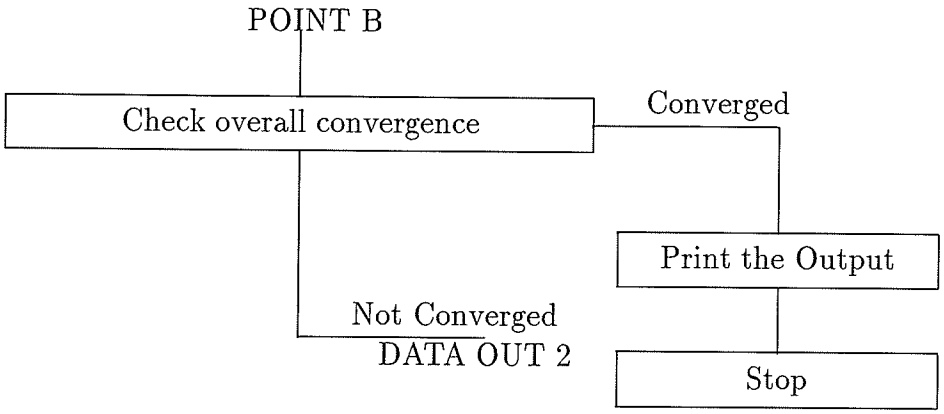
POINT B
Check overall convergence
Converged
Print the Output
Not Converged
DATA OUT 2
Stop

```
//MEYYAPP JOB ',,,I=10,T=01,L=05',CLASS=1
// EXEC WATFIV,REGION=3000K
//GO.SYSIN DD *
$JOB  WATFIV   MEYYAPP,NOEXT
C!!!!!!!!!!!!!!!!!!!!!!!!!!!!!!!!!!!!!!!!!!!!!!!!!!!!!!
C                                                     !
C     PRIMITIVE VARIABLE METHOD RECT DUCT 3:1         !
C                                                     !
C!!!!!!!!!!!!!!!!!!!!!!!!!!!!!!!!!!!!!!!!!!!!!!!!!!!!!!
      IMPLICIT REAL*8(A-H,O-Z)
      COMMON/SET1/NGPY,NGPZ,MY1
      COMMON/SET2/ALITE,COUNT,PRIME
      COMMON/SET3/DGPTY(30),YDEL(30)
      COMMON/SET4/ZGB(30),AMU,RHO
      COMMON/SET5/W(24,14),V(24,14),Z(30)
      COMMON/SET6/P(24,14),Y(30),YGB(30)
      COMMON/SET7/VO(24,14),VALPHA
      COMMON/SET8/DGPTZ(30),ZDEL(30)
      COMMON/SET10/WO(24,14)
      COMMON/SET11/WALPHA,PALPHA
      COMMON/SET13/PCDIFF,PCALPH
      COMMON/SET14/MZ1,MY2,MZ2,MZ3,MY3
      COMMON/SET15/PC(24,14)
      COMMON/SET17/WAPP(24,14),VAPP(24,14),VSOUR(24,14),WSOUR(24,14),C6
      COMMON/SET19/ VY(30),VDGPTY(30),VYDEL(30)
      COMMON/SET20/ WZ(30),WDGPTZ(30),WZDEL(30)
      COMMON/SET22/TKE(24,14),TED(24,14),U(24,14)
      COMMON/SET23/CD,CDASHK,CDASH
      COMMON/SET24/C1,C2,SIGMAK,SIGMAE,CAPA,B,CKO
      COMMON/SET25/AMUT(24,14),TOWV(24),TOWW(14),UFV(24),UFW(14)
      COMMON/SET26/DUY1(24,14),DUZ1(24,14),PRDN(24,14),VP(24,14)
      COMMON/SET27/UDIFF,TKDIFF,EDIFF,DPDX,UALPHA,TKALPH,EALPHA
      COMMON/SET28/UCOUNT,TKCOUN,ECOUNT,TOTITR,UB
      COMMON/SET29/GV(24,14),GW(24,14)
      DIMENSION YY(24),ZZ(14),ZNOSHR(24),YNOSHR(14)
      DIMENSION GRADY(24),GRADZ(14),TWY(24),TWZ(14),PO(24,14)
      DIMENSION TV(24),TW(14),TVG(24),TWG(14),PSI(24,14)
      DIMENSION ZNSV(24),ZNSVG(24),YNSW(14),YNSWG(14),TT(10)
C!!!!!!!!!!!!!!!!!!!!!!!!!!!!!!!!!!!!!!!!!!!!!!!!!!!!!!
C                                                     !
C                                                     !
C               GETTING THE INPUT DATA                !
C                                                     !
C                                                     !
C!!!!!!!!!!!!!!!!!!!!!!!!!!!!!!!!!!!!!!!!!!!!!!!!!!!!!!
      PRIME=2.0
      RE=60000.0
      C6=0.08
      ALITE=1000.0
      AMU=0.00001817
      RHO=1.2047
      CD=0.09
      CKO=0.915
      CDASHK=0.552
      CDASH=0.0185
      C1=1.44
      C2=1.92
      SIGMAK=0.9
      SIGMAE=1.3
      CAPA=0.41
      B=5.0
      A=2.44
      E=5.0
      PRCOUN=0.001
      WCOUNT=0.0001
      VCOUNT=0.0001
      PCCOUN=0.001
      UCOUNT=0.0001
      TKCOUN=0.0001
      ECOUNT=0.0001
      WALPHA=0.05
      VALPHA=0.05
      PCALPH=1.0
      UALPHA=1.0
      TKALPH=0.5
      EALPHA=0.5
      PALPHA=0.5
      VCHK=0.001
      WCHK=0.001
      S2=0.0762
C!!!!!!!!!!!!!!!!!!!!!!!!!!!!!!!!!!!!!!!!!!!!!!!!!!!!!!!!!!!!
      N=3
C!!!!!!!!!!!!!!!!!!!!!!!!!!!!!!!!!!!!!!!!!!!!!!!!!!!!!!!!!!!!
      NGPZ=14
      X1=1.3
      S1=N*S2
      NGPY=NGPZ+(N-1)*5
      GRSPG1=(S2*3/4)/7
      GRSPG2=S2/5
      MY1=NGPY+1
      MZ1=NGPZ+1
      Y(NGPY)=S1
      Z(NGPZ)=S2
      X2=((X1-1)*S2)/(4.0*(X1**(NGPZ/2-1)-1))
      TT(1)=X2
      DO 612 I=2,8
      TT(I)=TT(I-1)*X1
  612 CONTINUE
      DO 613 I=2,7
      K=NGPY+1-I
      Y(K)=Y(K+1)-TT(I-1)
  613 CONTINUE
      DO 615 I=8,NGPZ
      K=NGPY+1-I
      Y(K)=Y(K+1)-GRSPG1
  615 CONTINUE
      DO 630 I=MZ1,NGPY
      K=NGPY+1-I
      Y(K)=Y(K+1)-GRSPG2
  630 CONTINUE
      DO 614 J=2,7
      K=NGPZ+1-J
      Z(K)=Z(K+1)-TT(J-1)
  614 CONTINUE
      DO 631 J=8,NGPZ
      K=NGPZ+1-J
      Z(K)=Z(K+1)-GRSPG1
  631 CONTINUE
      Y(1)=0.0
      Z(1)=0.0
C     WRITE(6,110)(Y(I),I=1,NGPY)
  110 FORMAT(4(5X,6D11.4,/))
C     WRITE(6,111)(Z(J),J=1,NGPZ)
  111 FORMAT(2(5X,6D11.4,/),5X,2D11.4)
C     GO TO 100
C
C
C
```

```
C!!!!!!!!!!!!!!!!!!!!!!!!!!!!!!!!!!!!!!!!!!!!!!!!!!!!!!!!!!
C                                                         !
C  CALCULATING THE FIXED PARAMETERS OF THE MAIN GRID      !
C                                                         !
C!!!!!!!!!!!!!!!!!!!!!!!!!!!!!!!!!!!!!!!!!!!!!!!!!!!!!!!!!!
      MY2=NGPY-1
      MY3=NGPY-2
      DO 12 I=2,MY3
      YGB(I)=(Y(I)+Y(I+1))/2.0
   12 CONTINUE
      YGB(1)=Y(1)
      YGB(MY2)=Y(NGPY)
      Y(NGPY+1)=Y(NGPY)+(Y(NGPY)-Y(NGPY-1))
      DO 10 I=1,NGPY
      DGPTY(I)=Y(I+1)-Y(I)
   10 CONTINUE
      DO 11 I=2,MY2
      YDEL(I)=YGB(I)-YGB(I-1)
   11 CONTINUE
      YDEL(1)=0.0
      YDEL(NGPY)=0.0
      MZ2=NGPZ-1
      MZ3=NGPZ-2
      DO 16 I=2,MZ3
      ZGB(I)=(Z(I)+Z(I+1))/2.0
   16 CONTINUE
      ZGB(1)=Z(1)
      ZGB(MZ2)=Z(NGPZ)
      Z(NGPZ+1)=Z(NGPZ)+(Z(NGPZ)-Z(NGPZ-1))
      DO 48 I=1,NGPZ
      DGPTZ(I)=Z(I+1)-Z(I)
   48 CONTINUE
      DO 19 I=2,MZ2
      ZDEL(I)=ZGB(I)-ZGB(I-1)
   19 CONTINUE
      ZDEL(1)=0.0
      ZDEL(NGPZ)=0.0
      DO 876 I=1,MZ2
      WZ(I)=ZGB(I)
  876 CONTINUE
      DO 878 I=1,MZ3
      WDGPTZ(I)=WZ(I+1)-WZ(I)
  878 CONTINUE
      DO 879 I=1,MZ2
      WZDEL(I)=Z(I+1)-Z(I)
  879 CONTINUE
      DO 872 I=1,MY2
      VY(I)=YGB(I)
  872 CONTINUE
      DO 880 I=1,MY3
      VDGPTY(I)=VY(I+1)-VY(I)
  880 CONTINUE
      DO 871 I=1,MY2
      VYDEL(I)=Y(I+1)-Y(I)
  871 CONTINUE
      DO 501 J=1,NGPZ
      DO 501 I=1,NGPY
      VP(I,J)=YDEL(I)*ZDEL(J)
  501 CONTINUE
      ROWCMU=RHO*CD**0.25
      ANU=AMU/RHO
      AREA=4.0*S1*S2
      CLWTPR=4.0*(S1+S2)
      DEQ=4.0*AREA/CLWTPR
      UBAV=RE*AMU/(RHO*DEQ)
      UB=UBAV
      TOWAVW=0.15
      DPDX=4.0*TOWAVW/DEQ
      UFAVW=DSQRT(TOWAVW/RHO)
      ZPLUS=RHO*UFAVW*DABS(Z(NGPZ)-Z(MZ2))/AMU
      DO 66 I=1,MY2
      TOWV(I)=TOWAVW
      UFV(I)=UFAVW
   66 CONTINUE
      DO 75 J=1,MZ2
      TOWW(J)=TOWAVW
      UFW(J)=UFAVW
   75 CONTINUE
      TOWV(NGPY)=0.0
      TOWW(NGPZ)=0.0
      UFV(1)=0.0
      UFW(1)=0.0
C!!!!!!!!!!!!!!!!!!!!!!!!!!!!!!!!!!!!!!!!!!!!!!!!!!!!!!!!!!
C                                                         !
C          INITIALIZING THE VARIABLES                     !
C                                                         !
C!!!!!!!!!!!!!!!!!!!!!!!!!!!!!!!!!!!!!!!!!!!!!!!!!!!!!!!!!!
      DO 899 I=1,NGPY
      DO 899 J=1,NGPZ
      U(I,J)=0.0
      V(I,J)=0.0
      W(I,J)=0.0
      P(I,J)=0.0
      PC(I,J)=0.0
      TKE(I,J)=0.0
      TED(I,J)=0.0
      PSI(I,J)=0.0
      VSOUR(I,J)=0.0
      WSOUR(I,J)=0.0
      AMUT(I,J)=0.0
      GV(I,J)=0.0
      GW(I,J)=0.0
  899 CONTINUE
C     READ(12,*)U,TKE,TED,DPDX
      READ(11,*)U,TKE,TED,V,W,P,PC,DPDX,TOWV,TOWW
C     DO 641 I=1,MY2
C     DO 641 J=1,MZ2
C     IF(Y(I).GE.(S1-S2))GO TO 639
C     TKE(I,J)=TKE(I,J)*RHO/TOWW(J)
C     GO TO 641
C639  IF(J.GT.I)GO TO 642
C     TKE(I,J)=TKE(I,J)*RHO/TOWW(J)
C     GO TO 641
C642  TKE(I,J)=TKE(I,J)*RHO/TOWV(I)
C641  CONTINUE
C     WRITE(3,797) TKE
C     WRITE(6,797)((TKE(I,J),I=1,NGPY),J=1,NGPZ)
  797 FORMAT(4(6D11.4,/))
C     GO TO 100
C     GO TO 8105
C     GO TO 333
C     GO TO 2222
C     DO 901 I=1,MY2
C     DO 901 J=1,MZ2
C     TKE(I,J)=0.1
C     TED(I,J)=0.3
C     U(I,J)=UBAV
C901  CONTINUE
```

```
C      DO 250 I=1,MY2
C      IF(TKE(I,MZ3).LE.0.0)TKE(I,MZ3)=0.0
C      RWMUK=ROWCMU*DSQRT(TKE(I,MZ3))
C      ZDPLS=RWMUK*(Z(NGPZ)-Z(MZ3))/AMU
C      IF(ZDPLS .LE. 0.0) ZDPLS=ZPLUS
C      UPLS4 = A *DLOG(ZDPLS) + E
C      TOWV(I) =RWMUK*U(I,MZ3) / UPLS4
C 250 CONTINUE
C      TOWV(NGPY)=0.0
C      DO 251 J=1,MZ2
C      IF(TKE(MY3,J).LE.0.0)TKE(MY3,J)=0.0
C      RWMUK=ROWCMU*DSQRT(TKE(MY3,J))
C      ZDPLS=RWMUK*(Y(NGPY)-Y(MY3))/AMU
C      IF(ZDPLS.LE.0.0) ZDPLS=ZPLUS
C      UPLS4=A*DLOG(ZDPLS)+E
C      TOWW(J)=RWMUK*U(MY3,J)/UPLS4
C 251 CONTINUE
C      TOWW(NGPZ)=0.0
  570 FORMAT(/,7(1X,D11.4))
      TOTITR=0.0
      DO 6031 I=2,MY2
      YY(I)=(Y(I)-Y(I-1))/(Y(I+1)-Y(I))
 6031 CONTINUE
      DO 6032 J=2,MZ2
      ZZ(J)=(Z(J)-Z(J-1))/(Z(J+1)-Z(J))
 6032 CONTINUE
      SCEIL=S1-S2
      DO 6008 I=1,NGPY
      IF((SCEIL-Y(I)).LT.0.0001)GO TO 6009
      ZNOSHR(I)=Z(NGPZ)
      GO TO 6008
 6009 DO 6007 J=1,NGPZ
      IF(DABS(Z(J)-(Y(I)-SCEIL)).GT.0.0001)GO TO 6007
      ZNOSHR(I)=S2-Z(J)
      YNOSHR(J)=ZNOSHR(I)
      GO TO 6008
 6007 CONTINUE
 6008 CONTINUE
      DO 7049 J=2,MZ2
      GRADZ(J)=((YNOSHR(J+1)-YNOSHR(J))*ZZ(J)+(YNOSHR(J)-
     *YNOSHR(J-1))/ZZ(J))/(Z(J+1)-Z(J-1))
 7049 CONTINUE
      DO 7050 I=2,MY2
      GRADY(I)=((ZNOSHR(I+1)-ZNOSHR(I))*YY(I)+(ZNOSHR(I)-
     *ZNOSHR(I-1))/YY(I))/(Y(I+1)-Y(I-1))
 7050 CONTINUE
      GRADZ(1)=(YNOSHR(2)-YNOSHR(1))/DGPTZ(1)
      GRADY(1)=(ZNOSHR(2)-ZNOSHR(1))/DGPTY(1)
C!!!!!!!!!!!!!!!!!!!!!!!!!!!!!!!!!!!!!!!!!!!!!!!!!!!!!!!!!!!!!!!!
C                                                                     !
C        MAIN ITERATION LOOP STARTS HERE                              !
C                                                                     !
C!!!!!!!!!!!!!!!!!!!!!!!!!!!!!!!!!!!!!!!!!!!!!!!!!!!!!!!!!!!!!!!!
 125  PDIFF=0.0
      PCDIFF=0.0
      VDIFF=0.0
      WDIFF=0.0
      DO 9423 J=1,MZ2
      DO 9450 I=1,NGPY
      WO(I,J)=W(I,J)
 9450 CONTINUE
 9423 CONTINUE
      DO 9923 J=1,NGPZ
      DO 9950 I=2,MY2
      VO(I,J)=V(I,J)
 9950 CONTINUE
 9923 CONTINUE
      DO 9323 J=1,NGPZ
      DO 9350 I=1,NGPY
      PO(I,J)=P(I,J)
 9350 CONTINUE
 9323 CONTINUE
C!!!!!!!!!!!!!!!!!!!!!!!!!!!!!!!!!!!!!!!!!!!!!!!!!!!!!!!!!!!!!!!!
C                                                                     !
C   TURB.VISCOSITY AT THE MAIN GRID POINTS AND AT THE                 !
C        GRID BOUNDARIES ARE CALCULATED                               !
C                                                                     !
C!!!!!!!!!!!!!!!!!!!!!!!!!!!!!!!!!!!!!!!!!!!!!!!!!!!!!!!!!!!!!!!!
      ITR=0
 8103 ITR=ITR+1
      DO 6100 J=1,MZ2
      DO 6101 I=1,MY2
      IF(TED(I,J).NE.0.0)GO TO 6102
      AMUT(I,J)=0.0
      GO TO 6101
 6102 AMUT(I,J)=CD*RHO*TKE(I,J)**2/TED(I,J)
 6101 CONTINUE
 6100 CONTINUE
      DO 9001 J=1,MZ2
      DO 9002 I=1,MY2
      FXE=(Y(I+1)-VY(I))/DGPTY(I)
      IF((AMUT(I,J).NE.0.0).AND.(AMUT(I+1,J).NE.0.0))GO TO 401
      GV(I,J)=0.0
      GO TO 402
 401  GV(I,J)=AMUT(I,J)*AMUT(I+1,J)/(AMUT(I,J)*FXE+
     $AMUT(I+1,J)*(1.0-FXE))
      IF(I.EQ.1)GV(I,J)=AMUT(I,J)
      IF(I.EQ.MY2)GV(I,J)=AMUT(I+1,J)
 402  FXN=(Z(J+1)-WZ(J))/DGPTZ(J)
      IF((AMUT(I,J).NE.0.0).AND.(AMUT(I,J+1).NE.0.0))GO TO 403
      GW(I,J)=0.0
      GO TO 9002
 403  GW(I,J)=AMUT(I,J)*AMUT(I,J+1)/(AMUT(I,J)*FXN+
     $AMUT(I,J+1)*(1.0-FXN))
      IF(J.EQ.1)GW(I,J)=AMUT(I,J)
      IF(J.EQ.MZ2)GW(I,J)=AMUT(I,J+1)
 9002 CONTINUE
 9001 CONTINUE
C!!!!!!!!!!!!!!!!!!!!!!!!!!!!!!!!!!!!!!!!!!!!!!!!!!!!!!!!!!!!!!!!
C                                                                     !
C     SOURCE TERMS FOR V AND W EQNS.ARE CALCULATED                    !
C                                                                     !
C!!!!!!!!!!!!!!!!!!!!!!!!!!!!!!!!!!!!!!!!!!!!!!!!!!!!!!!!!!!!!!!!
      DO 4100 J=1,MZ2
      DO 4100 I=1,MY2
      IF(I.NE.1)GO TO 4107
      DUY1(I,J)=0.0
      GO TO 4108
 4107 DUY1(I,J)=((U(I+1,J)-U(I,J))*YY(I)+(U(I,J)-U(I-1,J))/YY(I))/
     $(Y(I+1)-Y(I-1))
 4108 IF(J.NE.1)GO TO 4109
      DUZ1(I,J)=0.0
      GO TO 4100
 4109 DUZ1(I,J)=((U(I,J+1)-U(I,J))*ZZ(J)+(U(I,J)-U(I,J-1))/ZZ(J))/
     $(Z(J+1)-Z(J-1))
 4100 CONTINUE
      DO 849 J=2,MZ2
      TWZ(J)=((DSQRT(TOWW(J+1))-DSQRT(TOWW(J)))*ZZ(J)+(DSQRT(TOWW(J))-
```

```
     *DSQRT(TOWW(J-1)))/ZZ(J))/(Z(J+1)-Z(J-1))
  849 CONTINUE
      DO 848 I=2,MY2
      TWY(I)=((DSQRT(TOWV(I+1))-DSQRT(TOWV(I)))*YY(I)+(DSQRT(TOWV(I))-
     *DSQRT(TOWV(I-1)))/YY(I))/(Y(I+1)-Y(I-1))
  848 CONTINUE
      TWY(1)=(DSQRT(TOWV(1))-DSQRT(TOWV(2)))/(Y(2)-Y(1))
      TWZ(1)=(DSQRT(TOWW(1))-DSQRT(TOWW(2)))/(Z(2)-Z(1))
      DO 811 I=2,MY3
      TV(I)=(TOWV(I)+TOWV(I+1))/2.0
      TVG(I)=(DSQRT(TOWV(I+1))-DSQRT(TOWV(I)))/VYDEL(I)
      ZNSV(I)=(ZNOSHR(I+1)+ZNOSHR(I))/2.0
  811 ZNSVG(I)=(ZNOSHR(I+1)-ZNOSHR(I))/VYDEL(I)
      DO 802 J=2,MZ3
      TW(J)=(TOWW(J)+TOWW(J+1))/2.0
      TWG(J)=(DSQRT(TOWW(J+1))-DSQRT(TOWW(J)))/WZDEL(J)
      YNSW(J)=(YNOSHR(J+1)+YNOSHR(J))/2.0
  802 YNSWG(J)=(YNOSHR(J+1)-YNOSHR(J))/WZDEL(J)
      DO 5031 J=1,MZ2
      DO 5031 I=2,MY3
      IF((I.EQ.2).AND.(J.EQ.2))GO TO 5032
      IF(Y(I).GE.(S1-YNOSHR(J)))GO TO 5032
      ZV=(S2-Z(J))/ZNSV(I)
      FF1=2.7573 * ZV**3 - 4.2053 * ZV**2 + 1.1751 * ZV + 1.4563
      FF2=8.2719 * ZV**2 - 8.4106 * ZV + 1.1751
      FF3= -0.05822 * ZV - 0.0744
      FF4= -2.0 * DSQRT(DABS(TV(I))) * TVG(I) * FF1 +
     $ TV(I) * ZV * ZNSVG(I) * FF2 / ZNSV(I)
      FF5= -TV(I) * FF3 / ZNSV(I)
      VSOUR(I,J)=(FF4 + FF5 - (P(I+1,J)-P(I,J)) / VYDEL(I)) *
     $ VYDEL(I) * ZDEL(J)
      GO TO 5031
 5032 YV=(S1-VY(I))/YNOSHR(J)
      FF1=5.8914 * YV**2 - 4.7192 * YV - 1.1175
      FF2= -0.02911 * YV**2 - 0.0744 * YV + 0.001
      FF3= -0.05822 * YV - 0.0744
      FF4= -TOWW(J) * FF1 / YNOSHR(J)
      FF5= -2.0 * DSQRT(TOWW(J)) * TWZ(J) * FF2 + TOWW(J) * YV *
     $ GRADZ(J) * FF3 / YNOSHR(J)
      VSOUR(I,J)=(FF4 + FF5 - (P(I+1,J)-P(I,J)) / VYDEL(I)) *
     $ VYDEL(I) * ZDEL(J)
 5031 CONTINUE
      DO 5033 J=2,MZ3
      DO 5033 I=1,MY2
      IF(Y(I).GT.(S1-YNOSHR(J)))GO TO 5034
      ZV=(S2-WZ(J))/ZNOSHR(I)
      FF1=5.8914 * ZV**2 - 4.7192 * ZV - 1.1175
      FF2= -0.02911 * ZV**2 - 0.0744 * ZV + 0.001
      FF3= -0.05822 * ZV - 0.0744
      FF4= -TOWV(I) * FF1 / ZNOSHR(I)
      FF5= -2.0 * DSQRT(DABS(TOWV(I))) * TWY(I) * FF2 +
     $ TOWV(I) * ZV * GRADY(I) * FF3 / ZNOSHR(I)
      WSOUR(I,J)=(FF4 + FF5 - (P(I,J+1)-P(I,J)) / WZDEL(J)) *
     $ YDEL(I) * WZDEL(J)
      GO TO 5033
 5034 YV=(S1-Y(I))/YNSW(J)
      FF1=2.7573 * YV**3 - 4.2053 * YV**2 + 1.1751 * YV + 1.4563
      FF2=8.2719 * YV**2 - 8.4106 * YV + 1.1751
      FF3= -0.05822 * YV - 0.0744
      FF4= -2.0 * DSQRT(TW(J)) * TWG(J) * FF1
     $ + TW(J) * YV * YNSWG(J) * FF2 / YNSW(J)
      FF5= -TW(J) * FF3 / YNSW(J)
      WSOUR(I,J)=(FF4 + FF5 - (P(I,J+1)-P(I,J)) / WZDEL(J)) *
     $ YDEL(I) * WZDEL(J)
 5033 CONTINUE
      DO 1041 J=1,MZ2
      DO 1041 I=1,9
 1041 VSOUR(I,J)=0.0
      DO 1042 J=2,MZ3
      DO 1042 I=1,11
 1042 WSOUR(I,J)=0.0
      IF(PRIME.EQ.1.0)GO TO 8100
      IF(TOTITR.GT.100.0)VALPHA=0.06
      IF(TOTITR.GT.100.0)WALPHA=0.06
      CALL WGRID
      CALL VGRID
      CALL PCGRID
 1233 FORMAT(1X,'PC(I,J):')
  770 FORMAT(1X,7D11.4,/,1X,5D11.4)
      TOTITR=TOTITR+1.0
C!!!!!!!!!!!!!!!!!!!!!!!!!!!!!!!!!!!!!!!!!!!!!!!!!!!!!!!!!!!!!!!!!!!!!
C                                                                     !
C          CORRECTING P,V & W VALUES                                  !
C                                                                     !
C!!!!!!!!!!!!!!!!!!!!!!!!!!!!!!!!!!!!!!!!!!!!!!!!!!!!!!!!!!!!!!!!!!!!!
      PFDIF=0.0
      DO 405 J=2,MZ2
      DO 406 I=2,MY2
      P(I,J)=P(I,J)+PALPHA*PC(I,J)
      IF(PO(I,J).EQ.0.0)GO TO 406
      DIF=DABS(P(I,J)-PO(I,J))
      IF(DABS(DIF).GT.PFDIF)PFDIF=DIF
  406 CONTINUE
  405 CONTINUE
      VCDIF=0.0
      WCDIF=0.0
      DO 410 J=1,MZ2
      DO 411 I=2,MY3
      IF(VAPP(I,J).EQ.0.0)GO TO 4110
      V(I,J)=V(I,J)+(ZDEL(J)*(PC(I,J)-PC(I+1,J)))/VAPP(I,J)
 4110 IF(VO(I,J).LE.1.0D-10)GO TO 411
      DIF=DABS(V(I,J)-VO(I,J))
      IF(DABS(DIF).GT.VCDIF)VCDIF=DIF
  411 CONTINUE
  410 CONTINUE
      DO 412 J=2,MZ3
      DO 413 I=1,MY2
      IF(WAPP(I,J).EQ.0.0)GO TO 4130
      W(I,J)=W(I,J)+(YDEL(I)*(PC(I,J)-PC(I,J+1)))/WAPP(I,J)
 4130 IF(WO(I,J).LE.1.0D-10)GO TO 413
      DIF=DABS(W(I,J)-WO(I,J))
      IF(DABS(DIF).GT.WCDIF)WCDIF=DIF
  413 CONTINUE
  412 CONTINUE
      DO 6084 J=2,MZ3
      DO 6084 I=1,MY2
      W(I,J)=W(I,J)*UBAV/UB
 6084 CONTINUE
      DO 5084 J=1,MZ2
      DO 5084 I=2,MY3
      V(I,J)=V(I,J)*UBAV/UB
 5084 CONTINUE
 8100 CALL UGRID
      CALL KGRID
      CALL EGRID
      DO 6021 I=1,MY2
      IF(TKE(I,MZ3).LE.0.0)TKE(I,MZ3)=0.0
      RWMUK=ROWCMU*DSQRT(TKE(I,MZ3))
```

```
      ZDPLS=RWMUK*(Z(NGPZ)-Z(MZ3))/AMU
      IF(ZDPLS .LE. 0.0) ZDPLS=ZPLUS
      UPLS4 = A *DLOG(ZDPLS) + E
      TOWV(I) =RWMUK*U(I,MZ3) / UPLS4
 6021 CONTINUE
      TOWV(NGPY)=0.0
      DO 6022 J=1,MZ2
      IF(TKE(MY3,J).LE.0.0)TKE(MY3,J)=0.0
      RWMUK=ROWCMU*DSQRT(TKE(MY3,J))
      ZDPLS=RWMUK*(Y(NGPY)-Y(MY3))/AMU
      IF(ZDPLS.LE.0.0) ZDPLS=ZPLUS
      UPLS4=A*DLOG(ZDPLS)+E
      TOWW(J)=RWMUK*U(MY3,J)/UPLS4
 6022 CONTINUE
      TOWW(NGPZ)=0.0
C!!!!!!!!!!!!!!!!!!!!!!!!!!!!!!!!!!!!!!!!!!!!!!!!!!!!!!!!!!!!!!
C                                                             !
C       CALCULATE AVERAGE WALL SHEAR STRESSES                 !
C                                                             !
C!!!!!!!!!!!!!!!!!!!!!!!!!!!!!!!!!!!!!!!!!!!!!!!!!!!!!!!!!!!!!!
 2222 SUMW = 0.0
      DO 28 I=2,NGPY
      TOWM = (DABS(TOWV(I)) + DABS(TOWV(I-1))) / 2.0
      SUMW = SUMW + TOWM * (Y(I) - Y(I-1))
   28 CONTINUE
      TAV1=SUMW/S1
      SUMM=0.0
      DO 72 J=2,NGPZ
      TOWM=(TOWW(J)+TOWW(J-1))/2.0
      SUMM=SUMM+TOWM*(Z(J)-Z(J-1))
   72 CONTINUE
      TAV2=SUMM/S2
c     DO 233 I=1,NGPY
c233  TOWV(I)=TOWV(I)/TAV1
c     WRITE(6,110)(TOWV(I),I=1,NGPY)
c     DO 234 J=1,NGPZ
c234  TOWW(J)=TOWW(J)/TAV2
c     WRITE(6,111)(TOWW(J),J=1,NGPZ)
c     GO TO 100
      TOWAVW =(SUMW+SUMM)/(S1+S2)
      UFAVW =DSQRT(DABS(TOWAVW/RHO))
      DPDX = 4.0 * TOWAVW / DEQ
      DO 29 I=1,MY2
      UFV(I)=DSQRT(DABS(TOWV(I))/RHO)
      TKE(I,MZ2) = UFV(I) * UFV(I) / DSQRT(CD)
      TED(I,MZ2) = UFV(I) * UFV(I) * UFV(I) / (CAPA * (Z(NGPZ)-Z(MZ2)))
      ZPLUSP = UFV(I) * (Z(NGPZ)-Z(MZ2)) / ANU
      IF(ZPLUSP.EQ.0.0)GO TO 29
      U(I,MZ2) = UFV(I) * (A * DLOG(ZPLUSP) + E)
   29 CONTINUE
      DO 92 J=1,MZ2
      UFW(J)=DSQRT(DABS(TOWW(J))/RHO)
      TKE(MY2,J)=UFW(J)*UFW(J)/DSQRT(CD)
      TED(MY2,J)=UFW(J)*UFW(J)*UFW(J)/(CAPA*(Y(NGPY)-Y(MY2)))
      ZPLUSQ=UFW(J)*(Y(NGPY)-Y(MY2))/ANU
      IF(ZPLUSQ.EQ.0.0)GO TO 92
      U(MY2,J)=UFW(J)*(A*DLOG(ZPLUSQ)+E)
   92 CONTINUE
C!!!!!!!!!!!!!!!!!!!!!!!!!!!!!!!!!!!!!!!!!!!!!!!!!!!!!!!!!!!!!!
C                                                             !
C        AVERAGE BULK VELOCITY CALCULATION                    !
C                                                             !
C!!!!!!!!!!!!!!!!!!!!!!!!!!!!!!!!!!!!!!!!!!!!!!!!!!!!!!!!!!!!!!
  333 CONTINUE
      UCENTR=U(1,1)
C     DO 334 J=1,NGPZ
C     DO 334 I=1,NGPY
C334  U(I,J)=U(I,J)/UCENTR
C     WRITE(8,*)U
C     REWIND 8
C     WRITE(6,783)((U(I,J),I=1,MY2,2),J=1,NGPZ)
C     GO TO 100
      DO 84 J=1,MZ2
      DO 84 I=1,MY2
      U(I,J)=U(I,J)*UBAV/UB
   84 CONTINUE
      IF(PRIME.GT.1.0)GO TO 8105
      IIII=ITR/100
      IIII=IIII*100
      IF(ITR.NE.IIII)GO TO 97
      WRITE(6,2004)ITR,UDIFF,TKDIFF,EDIFF
 2004 FORMAT(1X,'ITR=',I5,'UDIFF=',D11.4,
     $'TKDIFF=',D11.4,'EDIFF=',D11.4)
      WRITE(6,1200)
      WRITE(6,783)((U(I,J),I=1,MY2,2),J=1,NGPZ)
      WRITE(6,1201)
      WRITE(6,770)((TKE(I,J),I=1,MY2,2),J=1,NGPZ)
      WRITE(6,1202)
      WRITE(6,770)((TED(I,J),I=1,MY2,2),J=1,NGPZ)
   97 IF((UDIFF.LT.1.D-04).AND.(TKDIFF.LT.1.D-04).AND.(EDIFF.LT.1.D-04))
     $GO TO 116
      IF(ITR.LT.1000)GO TO 8103
  116 CONTINUE
      WRITE(6,1200)
      WRITE(6,783)((U(I,J),I=1,MY2,2),J=1,NGPZ)
      WRITE(6,1201)
      WRITE(6,770)((TKE(I,J),I=1,MY2,2),J=1,NGPZ)
      WRITE(6,1202)
      WRITE(6,770)((TED(I,J),I=1,MY2,2),J=1,NGPZ)
 1200 FORMAT(2X,'U(I,J):')
 1201 FORMAT(2X,'TKE(I,J):')
 1202 FORMAT(2X,'TED(I,J):')
      WRITE(12,*)U,TKE,TED,DPDX
      REWIND 12
      GO TO 100
 8105 DO 6123 J=2,MZ2
      DO 6124 I=2,MY2
      VC=(V(I,J)+V(I,J-1)+V(I-1,J)+V(I-1,J-1))/4.0
      PSI(I,J)=VC*DGPTZ(J-1)+PSI(I,J-1)
 6124 CONTINUE
 6123 CONTINUE
      REY=UB*RHO*DEQ/AMU
      SUM=0.0
      DO 888 J=1,NGPZ
      DO 888 I=1,NGPY
  888 SUM=SUM+U(I,J)*YDEL(I)*ZDEL(J)
      UB = SUM*4.0/AREA
C     WRITE(6,168)UB
C     DO 336 I=1,NGPY
C     DO 336 J=1,NGPZ
C336  PSI(I,J)=PSI(I,J)*1000.0/(UB * DEQ)
      WRITE(6,110)((PSI(I,J),I=1,NGPY),J=1,NGPZ)
      GO TO 100
      III=TOTITR/100
      III=III*100
      IF(TOTITR.NE.III)GO TO 6125
      WRITE(6,169)TOTITR,PFDIF,VCDIF,WCDIF,PCDIFF
C
```

```
  169 FORMAT(1X,'TOTITR:',F7.3,1X,'PFDIF:',D11.4,1X,'VCDIF:',D11.4,1X,
     $'WCDIF:',D11.4,1X,'PCDIFF:',D11.4)
      WRITE(6,170)UDIFF,TKDIFF,EDIFF
  170 FORMAT(1X,'UDIFF:',D11.4,1X,'TKDIFF:',D11.4,1X,'EDIFF:',D11.4)
 1010 CONTINUE
 6125 IF(TOTITR.EQ.1400)GO TO 102
      IF((VCDIF.GT.VCHK).OR.(WCDIF.GT.WCHK).OR.(PFDIF.GT.PRCOUN).OR.
     $(UDIFF.GT.UCOUNT).OR.(TKDIFF.GT.TKCOUN).OR.(EDIFF.GT.ECOUNT))
     $GO TO 125
C!!!!!!!!!!!!!!!!!!!!!!!!!!!!!!!!!!!!!!!!!!!!!!!!!!!!!!!!!!!!!!!!!!!
C                                                                      !
C                        OUT PUT                                       !
C                                                                      !
C!!!!!!!!!!!!!!!!!!!!!!!!!!!!!!!!!!!!!!!!!!!!!!!!!!!!!!!!!!!!!!!!!!!
 102  WRITE(6,168)UB
 168  FORMAT(1X,'BULK VELOCITY:',F10.6)
      WRITE(11,*)U,TKE,TED,V,W,P,PC,DPDX,TOWV,TOWW
      REWIND 11
      WRITE(6,195)TOTITR
 195  FORMAT(1X,'NO.OF MAIN ITERATIONS=',F7.3)
      WRITE(6,169)TOTITR,PFDIF,VCDIF,WCDIF,PCDIFF
      WRITE(6,170)UDIFF,TKDIFF,EDIFF
      WRITE(6,110)((U(I,J),I=1,NGPY),J=1,NGPZ)
      WRITE(6,110)((TKE(I,J),I=1,NGPY),J=1,NGPZ)
      WRITE(6,110)((TED(I,J),I=1,NGPY),J=1,NGPZ)
      WRITE(6,110)((V(I,J),I=1,NGPY),J=1,NGPZ)
      WRITE(6,110)((W(I,J),I=1,NGPY),J=1,NGPZ)
      WRITE(6,110)((P(I,J),I=1,NGPY),J=1,NGPZ)
      WRITE(6,110)((PC(I,J),I=1,NGPY),J=1,NGPZ)
      WRITE(6,110)(TOWV(I),I=1,NGPY)
      WRITE(6,110)(TOWW(J),J=1,NGPZ)
 100  STOP
      END
C!!!!!!!!!!!!!!!!!!!!!!!!!!!!!!!!!!!!!!!!!!!!!!!!!!!!!!!!!!!!!!!!!!!
C                                                                      !
C           WGRID CALCULATIONS START                                   !
C                                                                      !
C!!!!!!!!!!!!!!!!!!!!!!!!!!!!!!!!!!!!!!!!!!!!!!!!!!!!!!!!!!!!!!!!!!!
      SUBROUTINE WGRID
      IMPLICIT REAL*8(A-H,O-Z)
      COMMON/SET1/NGPY,NGPZ,MY1
      COMMON/SET3/DGPTY(30),YDEL(30)
      COMMON/SET4/ZGB(30),AMU,RHO
      COMMON/SET5/W(24,14),V(24,14),Z(30)
      COMMON/SET6/P(24,14),Y(30),YGB(30)
      COMMON/SET11/WALPHA,PALPHA
      COMMON/SET14/MZ1,MY2,MZ2,MZ3,MY3
      COMMON/SET17/WAPP(24,14),VAPP(24,14),VSOUR(24,14),WSOUR(24,14),C6
      COMMON/SET20/ WZ(30),WDGPTZ(30),WZDEL(30)
      COMMON/SET22/TKE(24,14),TED(24,14),U(24,14)
C!!!!!!!!!!!!!!!!!!!!!!!!!!!!!!!!!!!!!!!!!!!!!!!!!!!!!!!!!!!!!!!!!!!
C                                                                      !
C              ITERATIONS  START HERE                                  !
C                                                                      !
C!!!!!!!!!!!!!!!!!!!!!!!!!!!!!!!!!!!!!!!!!!!!!!!!!!!!!!!!!!!!!!!!!!!
      DO 24 J=2,MZ3
      DO 20 II=2,NGPY
      I=NGPY+1-II
      GEW=AMU
      VE1=(V(I,J+1)+V(I,J))/2.0
      FE1=RHO*VE1*WZDEL(J)
      PE1=(RHO*VE1*DGPTY(I))/GEW
      CALL NE(FE1,PE1,AE1,WZDEL(J),DGPTY(I),GEW)
      IF(I.NE.1)GO TO 2020
      AW1=0.0
      FW1=0.0
      SS1=-W(I+1,J)
      GO TO 2021
 2020 VW1=(V(I-1,J+1)+V(I-1,J))/2.0
      GWW=AMU
      FW1=RHO*VW1*WZDEL(J)
      PW1=(RHO*VW1*DGPTY(I-1))/GWW
      CALL SW(FW1,PW1,AW1,WZDEL(J),DGPTY(I-1),GWW)
      SS1=W(I-1,J)
 2021 GNW=AMU
      WN1=(W(I,J+1)+W(I,J))/2.0
      FN1=RHO*WN1*YDEL(I)
      PN1=(RHO*WN1*WDGPTZ(J))/GNW
      CALL NE(FN1,PN1,AN1,YDEL(I),WDGPTZ(J),GNW)
      GSW=AMU
      WS1=(W(I,J)+W(I,J-1))/2.0
      FS1=RHO*WS1*YDEL(I)
      PS1=(RHO*WS1*WDGPTZ(J-1))/GSW
      CALL SW(FS1,PS1,AS1,YDEL(I),WDGPTZ(J-1),GSW)
      BI=C6*WSOUR(I,J)
      WAPP(I,J)=AE1+AW1+AN1+AS1+FE1-FW1+FN1-FS1
 890  IF(WAPP(I,J).LT.1.0D-15)WAPP(I,J)=0.0
      IF(WAPP(I,J).EQ.0.0)GO TO 20
      WI=(AE1*W(I+1,J)+AW1*SS1+AN1*W(I,J+1)+AS1*W(I,J-1)+BI)/WAPP(I,J)
 702  W(I,J)=W(I,J)+WALPHA*(WI-W(I,J))
  20  CONTINUE
  24  CONTINUE
  99  RETURN
      END
C!!!!!!!!!!!!!!!!!!!!!!!!!!!!!!!!!!!!!!!!!!!!!!!!!!!!!!!!!!!!!!!!!!!
C                                                                      !
C           VGRID CALCULATIONS START                                   !
C                                                                      !
C!!!!!!!!!!!!!!!!!!!!!!!!!!!!!!!!!!!!!!!!!!!!!!!!!!!!!!!!!!!!!!!!!!!
      SUBROUTINE VGRID
      IMPLICIT REAL*8(A-H,O-Z)
      COMMON/SET1/NGPY,NGPZ,MY1
      COMMON/SET4/ZGB(30),AMU,RHO
      COMMON/SET5/W(24,14),V(24,14),Z(30)
      COMMON/SET6/P(24,14),Y(30),YGB(30)
      COMMON/SET7/VO(24,14),VALPHA
      COMMON/SET8/DGPTZ(30),ZDEL(30)
      COMMON/SET10/WO(24,14)
      COMMON/SET14/MZ1,MY2,MZ2,MZ3,MY3
      COMMON/SET17/WAPP(24,14),VAPP(24,14),VSOUR(24,14),WSOUR(24,14),C6
      COMMON/SET19/ VY(30),VDGPTY(30),VYDEL(30)
      COMMON/SET22/TKE(24,14),TED(24,14),U(24,14)
C!!!!!!!!!!!!!!!!!!!!!!!!!!!!!!!!!!!!!!!!!!!!!!!!!!!!!!!!!!!!!!!!!!!
C                                                                      !
C              ITERATIONS START HERE                                   !
C                                                                      !
C!!!!!!!!!!!!!!!!!!!!!!!!!!!!!!!!!!!!!!!!!!!!!!!!!!!!!!!!!!!!!!!!!!!
      DO 24 JJ=2,NGPZ
      J=NGPZ+1-JJ
      DO 20 I=2,MY3
      GEV=AMU
      VE2=(V(I+1,J)+V(I,J))/2.0
      FE2=RHO*VE2*ZDEL(J)
      PE2=(RHO*VE2*VDGPTY(I))/GEV
      CALL NE(FE2,PE2,AE2,ZDEL(J),VDGPTY(I),GEV)
      GWV=AMU
      VW2=(V(I,J)+V(I-1,J))/2.0
      FW2=RHO*VW2*ZDEL(J)
```

```
      PW2=(RHO*VW2*VDGPTY(I-1))/GWV
      CALL SW(FW2,PW2,AW2,ZDEL(J),VDGPTY(I-1),GWV)
      GNV=AMU
      WN2=(WO(I+1,J)+WO(I,J))/2.0
      FN2=RHO*WN2*VYDEL(I)
      PN2=(RHO*WN2*DGPTZ(J))/GNV
      CALL NE(FN2,PN2,AN2,VYDEL(I),DGPTZ(J),GNV)
      IF(J.NE.1)GO TO 2003
      AS2=0.0
      FS2=0.0
      SM2=-V(I,J+J)
      GO TO 2004
 2003 WS2=(WO(I+1,J-1)+WO(I,J-1))/2.0
      GSV=AMU
      FS2=RHO*WS2*VYDEL(I)
      PS2=(RHO*WS2*DGPTZ(J-1))/GSV
      CALL SW(FS2,PS2,AS2,VYDEL(I),DGPTZ(J-1),GSV)
      SM2=V(I,J-1)
 2004 BI=C6*VSOUR(I,J)
      VAPP(I,J)=AE2+AW2+AN2+AS2+FE2-FW2+FN2-FS2
      IF(VAPP(I,J).LT.1.0D-15)VAPP(I,J)=0.0
      IF(VAPP(I,J).EQ.0.0)GO TO 20
      VI=(AE2*V(I+1,J)+AW2*V(I-1,J)+AN2*V(I,J+1)+AS2*SM2+BI)/VAPP(I,J)
  702 V(I,J)=V(I,J)+VALPHA*(VI-V(I,J))
   20 CONTINUE
   24 CONTINUE
   99 RETURN
      END
C!!!!!!!!!!!!!!!!!!!!!!!!!!!!!!!!!!!!!!!!!!!!!!!!!!!!!!!!!!!!!!!!!!!
C                                                                       !
C       PRESSURE CORRECTION CALCULATIONS START                          !
C                                                                       !
C!!!!!!!!!!!!!!!!!!!!!!!!!!!!!!!!!!!!!!!!!!!!!!!!!!!!!!!!!!!!!!!!!!!
      SUBROUTINE PCGRID
      IMPLICIT REAL*8(A-H,O-Z)
      COMMON/SET1/NGPY,NGPZ,MY1
      COMMON/SET3/DGPTY(30),YDEL(30)
      COMMON/SET4/ZGB(30),AMU,RHO
      COMMON/SET5/W(24,14),V(24,14),Z(30)
      COMMON/SET6/P(24,14),Y(30),YGB(30)
      COMMON/SET8/DGPTZ(30),ZDEL(30)
      COMMON/SET13/PCDIFF,PCALPH
      COMMON/SET14/MZ1,MY2,MZ2,MZ3,MY3
      COMMON/SET15/PC(24,14)
      COMMON/SET17/WAPP(24,14),VAPP(24,14),VSOUR(24,14),WSOUR(24,14),C6
C!!!!!!!!!!!!!!!!!!!!!!!!!!!!!!!!!!!!!!!!!!!!!!!!!!!!!!!!!!!!!!!!!!!
C                                                                       !
C       PRESSURE CORRECTION ITERATIONS START                            !
C                                                                       !
C!!!!!!!!!!!!!!!!!!!!!!!!!!!!!!!!!!!!!!!!!!!!!!!!!!!!!!!!!!!!!!!!!!!
  632 ASUM=0.0
      DO 24 J=2,MZ2
      DO 20 I=2,MY2
      IF(I.EQ.MY2)GO TO 403
      IF(VAPP(I,J).NE.0.0)GO TO 6118
      CE=0.0
      GO TO 403
 6118 CE=ZDEL(J)**2.0/VAPP(I,J)
  403 IF(I.EQ.2)GO TO 404
      IF(VAPP(I-1,J).NE.0.0)GO TO 6119
      CW=0.0
      GO TO 404
 6119 CW=ZDEL(J)**2.0/VAPP(I-1,J)
  404 IF(J.EQ.MZ2)GO TO 415
      IF(WAPP(I,J).NE.0.0)GO TO 6120
      CN=0.0
      GO TO 415
 6120 CN=YDEL(I)**2.0/WAPP(I,J)
  415 IF(J.EQ.2)GO TO 405
      IF(WAPP(I,J-1).NE.0.0)GO TO 6121
      CS=0.0
      GO TO 405
 6121 CS=YDEL(I)**2.0/WAPP(I,J-1)
  405 BI=(V(I-1,J)-V(I,J))*ZDEL(J)+(W(I,J-1)-W(I,J))*YDEL(I)
      IF(J.EQ.2)CS=0.0
      IF(I.EQ.2)CW=0.0
      IF(I.EQ.MY2)CE=0.0
      IF(J.EQ.MZ2)CN=0.0
      CP=CE+CW+CN+CS
      IF(CP.EQ.0.0)GO TO 20
      PCI=(CE*PC(I+1,J)+CW*PC(I-1,J)
     $+CN*PC(I,J+1)+CS*PC(I,J-1)+BI)
     $/CP
      DIF=DABS(PCI-PC(I,J))
  703 IF(DABS(DIF).GT.DABS(PCDIFF))PCDIFF=DIF
  702 PC(I,J)=PC(I,J)+PCALPH*(PCI-PC(I,J))
   20 CONTINUE
   24 CONTINUE
  100 RETURN
      END
C!!!!!!!!!!!!!!!!!!!!!!!!!!!!!!!!!!!!!!!!!!!!!!!!!!!!!!!!!!!!!!!!!!!
C                                                                       !
C           UGRID CALCULATIONS START                                    !
C                                                                       !
C!!!!!!!!!!!!!!!!!!!!!!!!!!!!!!!!!!!!!!!!!!!!!!!!!!!!!!!!!!!!!!!!!!!
      SUBROUTINE UGRID
      IMPLICIT REAL*8(A-H,O-Z)
      COMMON/SET1/NGPY,NGPZ,MY1
      COMMON/SET3/DGPTY(30),YDEL(30)
      COMMON/SET4/ZGB(30),AMU,RHO
      COMMON/SET5/W(24,14),V(24,14),Z(30)
      COMMON/SET6/P(24,14),Y(30),YGB(30)
      COMMON/SET8/DGPTZ(30),ZDEL(30)
      COMMON/SET14/MZ1,MY2,MZ2,MZ3,MY3
      COMMON/SET22/TKE(24,14),TED(24,14),U(24,14)
      COMMON/SET23/CD,CDASHK,CDASH
      COMMON/SET24/C1,C2,SIGMAK,SIGMAE,CAPA,B,CKO
      COMMON/SET25/AMUT(24,14),TOWV(24),TOWW(14),UFV(24),UFW(14)
      COMMON/SET26/DUY1(24,14),DUZ1(24,14),PRDN(24,14),VP(24,14)
      COMMON/SET27/UDIFF,TKDIFF,EDIFF,DPDX,UALPHA,TKALPH,EALPHA
      COMMON/SET28/UCOUNT,TKCOUN,ECOUNT,TOTITR,UB
      COMMON/SET29/GV(24,14),GW(24,14)
C!!!!!!!!!!!!!!!!!!!!!!!!!!!!!!!!!!!!!!!!!!!!!!!!!!!!!!!!!!!!!!!!!!!
C                                                                       !
C             ITERATIONS  START HERE                                    !
C                                                                       !
C!!!!!!!!!!!!!!!!!!!!!!!!!!!!!!!!!!!!!!!!!!!!!!!!!!!!!!!!!!!!!!!!!!!
      UDIFF=0.0
      DO 24 JJ=3,NGPZ
      J=NGPZ+1-JJ
      DO 20 II=3,NGPY
      I=NGPY+1-II
      GEU=AMU+GV(I,J)
      FE=RHO*V(I,J)*ZDEL(J)
      PE=(RHO*V(I,J)*DGPTY(I))/GEU
      CALL NE(FE,PE,AE,ZDEL(J),DGPTY(I),GEU)
      IF(I.NE.1)GO TO 207
      AW=0.0
```

```
      FW=-RHO*V(I+1,J)*ZDEL(J)
      RR1=0.0
      GO TO 208
 207  GWU=AMU+GV(I-1,J)
      RR1=U(I-1,J)
      FW=RHO*V(I-1,J)*ZDEL(J)
      PW=(RHO*V(I-1,J)*DGPTY(I-1))/GWU
      CALL SW(FW,PW,AW,ZDEL(J),DGPTY(I-1),GWU)
 208  GNU=AMU+GW(I,J)
      FN=RHO*W(I,J)*YDEL(I)
      PN=(RHO*W(I,J)*DGPTZ(J))/GNU
      CALL NE(FN,PN,AN,YDEL(I),DGPTZ(J),GNU)
      IF(J.NE.1)GO TO 209
      AS=0.0
      FS=-RHO*W(I,J+1)*YDEL(I)
      RR2=0.0
      GO TO 210
 209  GSU=AMU+GW(I,J-1)
      RR2=U(I,J-1)
      FS=RHO*W(I,J-1)*YDEL(I)
      PS=(RHO*W(I,J-1)*DGPTZ(J-1))/GSU
      CALL SW(FS,PS,AS,YDEL(I),DGPTZ(J-1),GSU)
 210  BI=DPDX*VP(I,J)
 890  UAP=AE+AW+AN+AS
      IF(UAP.LT.1.0D-10)GO TO 20
      UI=(AE*U(I+1,J)+AW*
     $RR1+AN*U(I,J+1)+AS*RR2+BI)
     $/UAP
      DIF=DABS(UI-U(I,J))/U(I,J)
 703  IF(DABS(DIF).GT.DABS(UDIFF))UDIFF=DIF
 702  U(I,J)=U(I,J)+UALPHA*(UI-U(I,J))
  20  CONTINUE
  24  CONTINUE
      U(1,1)=((U(2,1)+(U(2,1)-U(3,1))*DGPTY(1)/DGPTY(2)) + (U(1,2)
     $ +(U(1,2)-U(1,3))*DGPTZ(1)/DGPTZ(2))) / 2.0
  99  RETURN
      END
C!!!!!!!!!!!!!!!!!!!!!!!!!!!!!!!!!!!!!!!!!!!!!!!!!!!!!!!!!!!!!!!
C                                                             !
C             KGRID CALCULATIONS START                        !
C                                                             !
C!!!!!!!!!!!!!!!!!!!!!!!!!!!!!!!!!!!!!!!!!!!!!!!!!!!!!!!!!!!!!!!
      SUBROUTINE KGRID
      IMPLICIT REAL*8(A-H,O-Z)
      COMMON/SET1/NGPY,NGPZ,MY1
      COMMON/SET3/DGPTY(30),YDEL(30)
      COMMON/SET4/ZGB(30),AMU,RHO
      COMMON/SET5/W(24,14),V(24,14),Z(30)
      COMMON/SET6/P(24,14),Y(30),YGB(30)
      COMMON/SET8/DGPTZ(30),ZDEL(30)
      COMMON/SET14/MZ1,MY2,MZ2,MZ3,MY3
      COMMON/SET22/TKE(24,14),TED(24,14),U(24,14)
      COMMON/SET23/CD,CDASHK,CDASH
      COMMON/SET24/C1,C2,SIGMAK,SIGMAE,CAPA,B,CKO
      COMMON/SET25/AMUT(24,14),TOWV(24),TOWW(14),UFV(24),UFW(14)
      COMMON/SET26/DUY1(24,14),DUZ1(24,14),PRDN(24,14),VP(24,14)
      COMMON/SET27/UDIFF,TKDIFF,EDIFF,DPDX,UALPHA,TKALPH,EALPHA
      COMMON/SET28/UCOUNT,TKCOUN,ECOUNT,TOTITR,UB
      COMMON/SET29/GV(24,14),GW(24,14)
C!!!!!!!!!!!!!!!!!!!!!!!!!!!!!!!!!!!!!!!!!!!!!!!!!!!!!!!!!!!!!!!
C                                                             !
C             ITERATIONS  START HERE                          !
C                                                             !
C!!!!!!!!!!!!!!!!!!!!!!!!!!!!!!!!!!!!!!!!!!!!!!!!!!!!!!!!!!!!!!!
      TKDIFF=0.0
      DO 24 JJ=3,NGPZ
      J=NGPZ+1-JJ
      DO 20 II=3,NGPY
      I=NGPY+1-II
      GEK=AMU+GV(I,J)/SIGMAK
      FE=RHO*V(I,J)*ZDEL(J)
      PE=(RHO*V(I,J)*DGPTY(I))/GEK
      CALL NE(FE,PE,AE,ZDEL(J),DGPTY(I),GEK)
      IF(I.NE.1)GO TO 207
      AW=0.0
      FW=-RHO*V(I+1,J)*ZDEL(J)
      RR1=0.0
      GO TO 208
 207  GWK=AMU+GV(I-1,J)/SIGMAK
      RR1=TKE(I-1,J)
      FW=RHO*V(I-1,J)*ZDEL(J)
      PW=(RHO*V(I-1,J)*DGPTY(I-1))/GWK
      CALL SW(FW,PW,AW,ZDEL(J),DGPTY(I-1),GWK)
 208  GNK=AMU+GW(I,J)/SIGMAK
      FN=RHO*W(I,J)*YDEL(I)
      PN=(RHO*W(I,J)*DGPTZ(J))/GNK
      CALL NE(FN,PN,AN,YDEL(I),DGPTZ(J),GNK)
      IF(J.NE.1)GO TO 209
      AS=0.0
      FS=-RHO*W(I,J+1)*YDEL(I)
      RR2=0.0
      GO TO 210
 209  GSK=AMU+GW(I,J-1)/SIGMAK
      RR2=TKE(I,J-1)
      FS=RHO*W(I,J-1)*YDEL(I)
      PS=(RHO*W(I,J-1)*DGPTZ(J-1))/GSK
      CALL SW(FS,PS,AS,YDEL(I),DGPTZ(J-1),GSK)
 210  PRDN(I,J)=AMUT(I,J)*(DUY1(I,J)**2+DUZ1(I,J)**2)*VP(I,J)
      IF(TKE(I,J).NE.0)GO TO 502
      BI=0.0
      GO TO 503
 502  BI=RHO*TED(I,J)*VP(I,J)/TKE(I,J)
 503  TKEAP=AE+AW+AN+AS
 2035 IF(TKEAP.EQ.0.0)GO TO 20
      TKEI=(AE*TKE(I+1,J)+AW*
     $RR1+AN*TKE(I,J+1)+AS*RR2+PRDN(I,J))/(TKEAP+BI)
      DIF=DABS(TKEI-TKE(I,J))/TKE(I,J)
 703  IF(DABS(DIF).GT.DABS(TKDIFF))TKDIFF=DIF
 702  TKE(I,J)=TKE(I,J)+TKALPH*(TKEI-TKE(I,J))
  20  CONTINUE
  24  CONTINUE
      TKE(1,1)=((TKE(2,1)+(TKE(2,1)-TKE(3,1))*DGPTY(1)/DGPTY(2))
     $ + (TKE(1,2)+(TKE(1,2)-TKE(1,3))*DGPTZ(1)/DGPTZ(2))) / 2.0
  99  RETURN
      END
C!!!!!!!!!!!!!!!!!!!!!!!!!!!!!!!!!!!!!!!!!!!!!!!!!!!!!!!!!!!!!!!
C                                                             !
C             EGRID CALCULATIONS START                        !
C                                                             !
C!!!!!!!!!!!!!!!!!!!!!!!!!!!!!!!!!!!!!!!!!!!!!!!!!!!!!!!!!!!!!!!
      SUBROUTINE EGRID
      IMPLICIT REAL*8(A-H,O-Z)
      COMMON/SET1/NGPY,NGPZ,MY1
      COMMON/SET3/DGPTY(30),YDEL(30)
      COMMON/SET4/ZGB(30),AMU,RHO
      COMMON/SET5/W(24,14),V(24,14),Z(30)
      COMMON/SET6/P(24,14),Y(30),YGB(30)
      COMMON/SET8/DGPTZ(30),ZDEL(30)
```

```
      COMMON/SET14/MZ1,MY2,MZ2,MZ3,MY3
      COMMON/SET22/TKE(24,14),TED(24,14),U(24,14)
      COMMON/SET23/CD,CDASHK,CDASH
      COMMON/SET24/C1,C2,SIGMAK,SIGMAE,CAPA,B,CKO
      COMMON/SET25/AMUT(24,14),TOWV(24),TOWW(14),UFV(24),UFW(14)
      COMMON/SET26/DUY1(24,14),DUZ1(24,14),PRDN(24,14),VP(24,14)
      COMMON/SET27/UDIFF,TKDIFF,EDIFF,DPDX,UALPHA,TKALPH,EALPHA
      COMMON/SET28/UCOUNT,TKCOUN,ECOUNT,TOTITR,UB
      COMMON/SET29/GV(24,14),GW(24,14)
C!!!!!!!!!!!!!!!!!!!!!!!!!!!!!!!!!!!!!!!!!!!!!!!!!!!!!!!!!!!!
C                                                           !
C              ITERATIONS  START HERE                       !
C                                                           !
C!!!!!!!!!!!!!!!!!!!!!!!!!!!!!!!!!!!!!!!!!!!!!!!!!!!!!!!!!!!!
      EDIFF=0.0
      DO 24 JJ=3,NGPZ
      J=NGPZ+1-JJ
      DO 20 II=3,NGPY
      I=NGPY+1-II
      GEE=AMU+GV(I,J)/SIGMAE
      FE=RHO*V(I,J)*ZDEL(J)
      PE=(RHO*V(I,J)*DGPTY(I))/GEE
      CALL NE(FE,PE,AE,ZDEL(J),DGPTY(I),GEE)
      IF(I.NE.1)GO TO 207
      AW=0.0
      FW=-RHO*V(I+1,J)*ZDEL(J)
      RR1=0.0
      GO TO 208
  207 GWE=AMU+GV(I-1,J)/SIGMAE
      RR1=TED(I-1,J)
      FW=RHO*V(I-1,J)*ZDEL(J)
      PW=(RHO*V(I-1,J)*DGPTY(I-1))/GWE
      CALL SW(FW,PW,AW,ZDEL(J),DGPTY(I-1),GWE)
  208 GNE=AMU+GW(I,J)/SIGMAE
      FN=RHO*W(I,J)*YDEL(I)
      PN=(RHO*W(I,J)*DGPTZ(J))/GNE
      CALL NE(FN,PN,AN,YDEL(I),DGPTZ(J),GNE)
      IF(J.NE.1)GO TO 209
      AS=0.0
      FS=-RHO*W(I,J+1)*YDEL(I)
      RR2=0.0
      GO TO 210
  209 GSE=AMU+GW(I,J-1)/SIGMAE
      RR2=TED(I,J-1)
      FS=RHO*W(I,J-1)*YDEL(I)
      PS=(RHO*W(I,J-1)*DGPTZ(J-1))/GSE
      CALL SW(FS,PS,AS,YDEL(I),DGPTZ(J-1),GSE)
  210 IF((TKE(I,J).NE.0.0).OR.(DABS(TKE(I,J)).GT.1.D-10))GO TO 222
      BI=0.0
      S=0.0
      GO TO 223
  222 S=TED(I,J)*C1*PRDN(I,J)/TKE(I,J)
      BI=RHO*TED(I,J)*C2*VP(I,J)/TKE(I,J)
  223 EAP=AE+AW+AN+AS
      IF(EAP.EQ.0.0)GO TO 20
      TEDI=(AE*TED(I+1,J)+AW*
     $RR1+AN*TED(I,J+1)+AS*RR2+S)/(EAP+BI)
      DIF=DABS(TEDI-TED(I,J))/TED(I,J)
  703 IF(DABS(DIF).GT.DABS(EDIFF))EDIFF=DIF
  702 TED(I,J)=TED(I,J)+EALPHA*(TEDI-TED(I,J))
   20 CONTINUE
   24 CONTINUE
      TED(1,1)=((TED(2,1)+(TED(2,1)-TED(3,1))*DGPTY(1)/DGPTY(2))
     $ + (TED(1,2)+(TED(1,2)-TED(1,3))*DGPTZ(1)/DGPTZ(2))) / 2.0
   99 RETURN
      END
C!!!!!!!!!!!!!!!!!!!!!!!!!!!!!!!!!!!!!!!!!!!!!!!!!!!!!!!!!!!!
C                                                           !
C   SUBROUTINE FOR HANDLING LOW(PURE DIFFUSION) AND         !
C                                                           !
C   HIGH PECKLET NUMBERS (NORTH & EAST BOUNDARIES)          !
C                                                           !
C!!!!!!!!!!!!!!!!!!!!!!!!!!!!!!!!!!!!!!!!!!!!!!!!!!!!!!!!!!!!
      SUBROUTINE NE(SF,SP,SA,SDEL,SDGPT,SG)
      IMPLICIT REAL*8(A-H,O-Z)
      IF(DABS(SP).GT.1.0D-7)GO TO 23
      SA=SG*SDEL/SDGPT
      GO TO 26
   23 IF(SP.LT.100.0)GO TO 24
      SA=0.0
      GO TO 26
   24 IF(SP.GT.(-100.0))GO TO 25
      SA=(-1.0)*SF
      GO TO 26
   25 SA=SF/(DEXP(SP)-1.0)
   26 RETURN
      END
C
C
C
C!!!!!!!!!!!!!!!!!!!!!!!!!!!!!!!!!!!!!!!!!!!!!!!!!!!!!!!!!!!!
C                                                           !
C    SUBROUTINE FOR HANDLING LOW(PURE DIFFUSION) AND        !
C                                                           !
C    HIGH PECKLET NUMBERS (SOUTH & WEST BOUNDARIES)         !
C                                                           !
C!!!!!!!!!!!!!!!!!!!!!!!!!!!!!!!!!!!!!!!!!!!!!!!!!!!!!!!!!!!!
      SUBROUTINE SW(SF,SP,SA,SDEL,SDGPT,SG)
      IMPLICIT REAL*8(A-H,O-Z)
      IF(DABS(SP).GT.1.0D-7)GO TO 23
      SA=SG*SDEL/SDGPT
      GO TO 26
   23 IF(SP.LT.100.0)GO TO 24
      SA=SF
      GO TO 26
   24 IF(SP.GT.(-100.0))GO TO 25
      SA=0.0
      GO TO 26
   25 SA=SF*DEXP(SP)/(DEXP(SP)-1.0)
   26 RETURN
      END
$ENTRY
//GO.FT10F001 DD DSN=MEYYAPP.PREC6,DISP=SHR
//GO.FT11F001 DD DSN=MEYYAPP.PREC7,DISP=SHR
//GO.FT12F001 DD DSN=MEYYAPP.PREC8,DISP=SHR
//GO.FT13F001 DD DSN=MEYYAPP.PREC9,DISP=SHR
//GO.FT09F001 DD DSN=MEYYAPP.P360S1,DISP=SHR
//GO.FT08F001 DD DSN=MEYYAPP.ISOVEL2,DISP=SHR
//GO.FT03F001 DD DSN=MEYYAPP.ISOVEL5,DISP=SHR
//GO.FT15F001 DD DSN=MEYYAPP.SVVR33,DISP=SHR
//GO.FT16F001 DD DSN=MEYYAPP.SVVR34,DISP=SHR
*/
```